NASA
National Aeronautics and
Space Administration

jpl

EFFECT OF PULSED CURRENT CHARGING ON THE PERFORMANCE OF NICKEL-CADMIUM CELLS

(FINAL REPORT)

January 1977

Prepared by

Columbia University
Department of Chemical Engineering and
Applied Chemistry
New York, New York 10027

For

Jet Propulsion Laboratory
California Institute of Technology
Pasadena, California 91103

JPL Contract 953970

This report was prepared for the Jet Propulsion Laboratory, California Institute of Technology, sponsored by the NASA under contract NAS 7-100.

FINAL REPORT FOR JPL CONTRACT 953970

EFFECT OF PULSED CURRENT CHARGING ON THE PERFORMANCE OF NICKEL-CADMIUM CELLS

Submitted to

California Institute of Technology
Jet Propulsion Laboratory

Prepared by

A. A. Bedrossian and H. Y. Cheh

Department of Chemical Engineering and Applied Chemistry
Columbia University
New York, New York 10027

1976

ABSTRACT

EFFECT OF PULSED CURRENT CHARGING ON THE PERFORMANCE OF NICKEL-CADMIUM CELLS

AGHAVNI ARTUN BEDROSSIAN

The method used for charging Ni-Cd cells affects significantly the performance of the system. Recent investigations have shown promising results by pulsed current (p-c) charging. However, little information is available concerning the fundamental aspects of the charging process. This work is aimed at a basic understanding of the effect of pulsed current charging on the charge acceptance of Ni-Cd cells in terms of mass transfer, kinetic and structural considerations.

A systematic investigation on the performance of Ni-Cd cells by pulsed current charging was conducted under a variety of well-defined charge-discharge conditions. Experiments were carried out with half cells and film electrodes. The system behavior was studied by charge acceptance, mechanistic and structural measurements.

Under the experimental conditions used in this work, the reactions at the Ni-electrode can be described

by a solid-state mechanism, whereas, the reactions at the Cd-electrode can be explained by a combination of solid-state and dissolution-precipitation mechanism.

From the charge acceptance, x-ray and SEM studies, both Ni- and Cd-electrodes were found to show similar behavior under p-c charging conditions, exhibiting a maximum and a minimum in charge acceptance at identical charging conditions. Their performance showed complex dependence on: self-discharge, type of active material formed, and in the case of Cd, crystal size of the active material. Pulsed current charging was found to reduce irreversibilities from mass transfer limitations resulting in a postponement of gas evolution. This effect was more pronounced in the case of the Cd-electrode. Structural changes and modifications in the active material composition were also observed. In general, an increase in instantaneous p-c density and duty cycle, caused an increase in charge acceptance. However, the effect was not of a significant magnitude.

This investigation also includes a theoretical formulation on the reduction of concentration overpotential under p-c electrolysis. The model was tested with a ferro-ferricyanide system. Excellent agreement was obtained between the theoretically calculated and experimentally determined values.

From the experimental and theoretical findings of this work, the practical importance of p-c charging is evident. Utilizing a p-c of optimum characteristics, a small improvement in charge acceptance, a shorter charging time and power savings can be achieved.

TABLE OF CONTENTS

		Page
ACKNOWLEDGMENTS		ii
INDEX OF TABLES		xi
INDEX OF FIGURES		xiv
Chapter		
I.	INTRODUCTION	1
II.	REVIEW OF LITERATURE	5
	A. The Ni-Cd Battery	5
	B. Electrode Reactions	7
	C. Effect of Pulsed Current on the Performance of Electrochemical Systems	14
	D. Experimental Techniques Used in This Investigation	19
	1. Rotating Disk Electrode	19
	2. Cyclic Voltametry	22
III.	THEORETICAL CALCULATIONS ON THE REDUCTION OF CONCENTRATION OVERPOTENTIAL IN PULSED CURRENT ELECTROLYSIS	24
IV.	EFFECT OF PULSED CURRENT CHARGING ON THE Ni-Cd CELL	33
	A. Mass Transfer	33
	B. Kinetics	34
	C. Structure	35

Chapter Page

V. EXPERIMENTAL APPROACH 36

A. Charge Acceptance Measurements 37

1. Apparatus 37

2. Procedure 39

B. Measurements on the Reduction of Concentration Overpotential 40

1. Apparatus 40

2. Procedure 41

C. Mechanistic Studies 43

1. Limiting Current Measurements 43

a. Apparatus 43

b. Procedure 43

2. Cyclic Sweep Experiments 43

a. Apparatus 43

b. Procedure 47

VI. RESULTS 49

A. Charge Acceptance Measurements 49

B. Measurements on the Reduction of Concentration Overpotential 64

C. Mechanistic Studies 71

1. Limiting Current Measurements 71

2. Cyclic Sweep Experiments 83

D. Structural Studies 95

1. SEM 95

2. TEM 95

3. X-ray Diffraction 109

Chapter		Page
VII.	DISCUSSION	116
	A. Ni-electrode	116
	1. Thermodynamics	116
	2. Mechanistic Considerations	117
	3. Charge Acceptance Measurements	123
	4. Structural Studies	128
	B. Cd-electrode	131
	1. Thermodynamics	131
	2. Mechanistic Considerations	131
	3. Charge Acceptance Measurements	135
	4. Structural Studies	142
	C. Reduction of Concentration Overpotential by Pulsed Current Electrolysis	146
VIII.	CONCLUSIONS	148
IX.	RECOMMENDATIONS	154
X.	BIBLIOGRAPHY	157
XI.	APPENDIX	161
	1. Reduction of Concentration Overpotential by Pulsed Current Electrolysis	161
	A. Theoretical Development	161
	B. Calculations	165
	2. Design of Electronic Circuits	178
	3. Reduction of Concentration Overpotential by Pulsed Current Electrolysis for the Ferro-Ferricyanide System	181
	4. Ni-electrode	196
	A. Thermodynamics	196
	B. Mechanistic Considerations	200

Chapter Page

5. Cd-electrode 204

6. Definition of Terms from the Battery Field Used in the Present Work 205

XII. NOMENCLATURE 206

ACKNOWLEDGMENTS

This work was performed for the Jet Propulsion Laboratory, California Institute of Technology, sponsored by the National Aeronautics and Space Administration under Contract NAS7-100. One of the authors (A.A.B.) would like to acknowledge partial support in the form of a fellowship from the American Association of Women.

The valuable suggestions and technical assistance of Mr. H. Frank of JPL during the course of this work are gratefully acknowledged.

INDEX OF TABLES

Table		Page
1.	Summary of experimental conditions for over-potential measurements of the ferro-ferricyanide system under p-c conditions	44
2.	Charge acceptance of Ni-electrode under d-c charging conditions	52
3.	Charge acceptance of Ni-electrode under p-c charging conditions (active material prepared at 5mA d-c for 20 min.)	53
4.	Charge acceptance of Ni-electrode under p-c charging conditions (active material prepared at 5mA d-c for 30 min.)	55
5.	Cycle life of Ni-electrode under d-c and p-c charging conditions	57
6.	Charge acceptance of Cd-electrode under d-c charging conditions	60
7.	Charge acceptance of Cd-electrode under p-c charging conditions (active material prepared at 5mA d-c for 15 min.)	61
8.	Charge acceptance of Cd-electrode under d-c and p-c charging conditions (active material prepared at 5mA d-c for 30 min.)	63
9.	Self-discharge of Cd-electrode during the off period of the pulse	65
10.	Limiting current densities for the ferro-ferricyanide system at six rotation speeds	66
11.	Diffusion coefficient calculations for the ferro-ferricyanide system, from eqns. (A16) and (A22)	69
12.	Exchange current density of the ferro-ferricyanide system at various rotation speeds, obtained from eqn. (A30)	72
13.	Ferro-ferricyanide system, experimental data and reduction of concentration overpotential during the anodic reaction, under p-c conditions and 1610 rpm	74

Table Page

14. Ferro-ferricyanide system, experimental data and reduction of concentration overpotential during the anodic reaction, under p-c conditions and three rotation speeds 76

15. Ferro-ferricyanide system, experimental data and reduction of concentration overpotential during the cathodic reaction, under p-c conditions and 1610 rpm 78

16. Ferro-ferricyanide system, experimental data and reduction of concentration overpotential during the cathodic reaction, under p-c conditions and three rotation speeds 80

17. Ni-electrode, percent of initial charge accumulated during the eight cycle under d-c charging conditions 125

18. Ni-electrode, percent of initial charge accumulated during the eight cycle under p-c charging conditions 126

19. Cd-electrode, percent of initial charge accumulated during the eight cycle under d-c and p-c charging conditions 140

A1. Instantaneous values of $(\eta_{p-c})_c/(\eta_{d-c})_c$ calculated from eqns. (38) and (39), for $\theta_1/\theta = 0.2$ and $a\theta = 0.5$ 166

A2. Instantaneous values of $(\eta_{p-c})_c/(\eta_{d-c})_c$ calculated from eqns. (38) and (39), for $\theta_1/\theta = 0.4$ and $a\theta = 0.5$ 168

A3. Instantaneous values of $(\eta_{p-c})_c/(\eta_{d-c})_c$ calculated from eqns. (38) and (39), for $\theta_1/\theta = 0.6$ and $a\theta = 0.5$ 170

A4. Instantaneous values of $(\eta_{p-c})_c/(\eta_{d-c})_c$ calculated from eqns. (38) and (39), for $\theta_1/\theta = 0.8$ and $a\theta = 0.5$ 172

A5. Average value of the reduction of concentration overpotential for $a\theta = 0.5$ 177

A6. Ferro-ferricyanide system, overpotential under d-c conditions and 400 rpm 182

Table Page

A7. Ferro-ferricyanide system, overpotential under d-c conditions and 915 rpm 183

A8. Ferro-ferricyanide system, overpotential under d-c conditions and 1610 rpm 184

A9. Ferro-ferricyanide system, overpotential under d-c conditions and 2500 rpm 185

A10. Ferro-ferricyanide system, overpotential under d-c conditions and 3600 rpm 186

A11. Ferro-ferricyanide system, overpotential under d-c conditions and 4950 rpm 187

A12. Activation overpotential of the ferro-ferricyanide system calculated from eqn. (A31) and exchange current density of 5.733 mA/cm^2 191

A13. Values of ln $(i/(1-\exp(-nF\eta/RT))$ for the ferro-ferricyanide system at 400 rpm 193

A14. Values of the diffusion layer thickness and cycle time for the ferro-ferricyanide system at six rotation speeds 195

A15. Values of the activity coefficient and the activity of KOH solution for various molal concentrations 198

INDEX OF FIGURES

Figure		Page
1.	Schematic representation of Romanov and McCulloch type pulsed currents	18
2.	Instantaneous values of $(\eta_{p-c})_c/(\eta_{d-c})_c$ during one complete cycle of the applied p-c with a duty cycle of 0.2 and $a\theta$ of 0.5	29
3.	Average values of the reduction of concentration overpotential as a function of duty cycle and instantaneous p-c density, for $a\theta$ of 0.5 .	31
4.	Apparatus for charge acceptance measurements .	38
5.	Apparatus for measurements of the reduction of concentration overpotential with the ferro-ferricyanide system	42
6.	Apparatus for limiting current measurements .	46
7.	Apparatus for cyclic sweep experiments	48
8.	Typical charge-discharge behavior of the Ni-electrode	50
9.	Typical charge-discharge behavior of the Ni-electrode as a function of fraction of capacity charged	51
10.	Typical charge-discharge behavior of the Cd-electrode	58
11.	Typical charge-discharge behavior of the Cd-electrode as a function of fraction of capacity charged	59
12.	Current-potential plot at six rotation speeds for the ferro-ferricyanide system	67
13.	A plot of current density vs. overpotential at six rotation speeds for the ferro-ferricyanide system under d-c conditions	68
14.	A plot used for evaluating the diffusion coefficients of the ferro-ferricyanide system . .	70

Figure		Page
15.	A plot used for evaluating the transfer coefficients for the ferro-ferricyanide system . . .	73
16.	Theoretical and experimental values of the average reduction of concentration overpotential as a function of duty cycle and instantaneous p-c density	82
17.	Current-potential behavior of the Ni-electrode at five rotation speeds and a sweep rate of 0.4mA/min	84
18.	Current-potential behavior of the Ni-electrode at several sweep rates and 400 rpm	85
19.	Ni-electrode, full sweeps at 400 rpm	86
20.	Current-potential behavior of the Cd-electrode at five rotation speeds and a sweep rate of 0.5mA/min	87
21.	Cyclic potential sweep for the Ni-electrode at three sweep rates	88
22.	Cyclic potential sweep for the Ni-electrode at three sweep rates	89
23.	Cyclic potential sweep for the Ni-electrode at a sweep rate of 1 V/min	90
24.	Cyclic potential sweep for the Ni-electrode at a sweep rate of 1.8 V/hr and conditions similar to those used by MacArthur (33)	91
25.	Cyclic sweep for the Ni-electrode under controlled current conditions and three sweep rates	92
26.	Cyclic potential sweep for the Cd-electrode at 0.1 V/min	93
27.	Cyclic sweep for the Cd-electrode under controlled current conditions and four sweep rates	94
28.	Scanning electron micrographs of Ni-electrodes charged under d-c and variety of p-c conditions, magnification of 3000 x	96
29.	Scanning electron micrographs of Ni-electrodes charged under d-c and variety of p-c conditions, magnification of 10000 x	97

Figure Page

30. Scanning electron micrograph of a Cd-electrode charged with 5mA d-c, montage at magnification of 3000 x 98

31. Scanning electron micrograph of a Cd-electrode charged with 5mA instantaneous p-c, 0.1 duty cycle and 50 Hz frequency, montage at magnification of 3000 x 99

32. Scanning electron micrograph of a Cd-electrode charged with 5mA instantaneous p-c, 0.25 duty cycle and 50 Hz frequency, montage at magnification of 3000 x 100

33. Scanning electron micrograph of a Cd-electrode charged with 5mA instantaneous p-c, 0.5 duty cycle and 50 Hz frequency, montage at magnification of 3000 x 101

34. Scanning electron micrograph of a Cd-electrode charged with 10mA instantaneous p-c, 0.5 duty cycle and 50 Hz frequency, montage at magnification of 3000 x 102

35. Scanning electron micrograph of a Cd-electrode charged with 5mA instantaneous p-c, 0.75 duty cycle and 50 Hz frequency, montage at magnification of 3000 x 103

36. Scanning electron micrographs of Cd-electrodes charged under d-c and variety of p-c conditions, magnification of 10000 x 104

37. Scanning electron micrographs of Cd-electrodes charged under variety of p-c conditions, magnification of 10000 x 105

38. Scanning electron micrographs of Cd-electrodes charged under d-c and variety of p-c conditions, magnification of 30000 x 106

39. Scanning electron micrographs of Cd-electrodes charged under variety of p-c conditions, magnification of 30000 x 107

40. Transmission electron micrographs of Cd-electrodes charged under d-c and p-c conditions, magnification of 26400 x 108

Figure Page

41. X-ray diffraction pattern of a Cd-electrode charged with 5mA d-c 110

42. X-ray diffraction pattern of a Cd-electrode charged with 5mA instantaneous p-c, 0.1 duty cycle and 50 Hz frequency 111

43. X-ray diffraction pattern of a Cd-electrode charged with 5mA instantaneous p-c, 0.25 duty cycle and 50 Hz frequency 112

44. X-ray diffraction pattern of a Cd-electrode charged with 10mA instantaneous p-c, 0.5 duty cycle and 50 Hz frequency 113

45. X-ray diffraction pattern of a Cd-electrode charged with 5mA instantaneous p-c, 0.75 duty cycle and 50 Hz frequency 114

46. X-ray diffraction pattern of a Cd-electrode charged with 5mA d-c, obtained by the powder method 115

47. Mechanism of the reactions occurring at the Ni-electrode 119

48. A plot of $\Delta E_{discharge}$ vs. fraction of capacity discharged for the Ni-electrode 129

49. Mechanism of the reactions occurring at the Cd-electrode 133

50. Effect of charging rate on crystal size for crystallization at a solid-solid interphase and a solid-liquid interphase 137

51. A plot of $\Delta E_{discharge}$ vs. fraction of capacity discharged for the Cd-electrode 141

A1. Schematic diagram of a pulsed current 163

A2. Instantaneous values of $(\eta_p)_c/(\eta_{d-c})_c$ during one complete cycle of the applied p-c, with a duty cycle of 0.4 and $a\theta$ of 0.5 174

A3. Instantaneous values of $(\eta_p)_c/(\eta_{d-c})_c$ during one complete cycle of the applied p-c, with a duty cycle of 0.6 and $a\theta$ of 0.5 175

A4. Instantaneous values of $(\eta_p)_c/(\eta_{d-c})_c$ during one complete cycle of the applied p-c, with a duty cycle of 0.8 and $a\theta$ of 0.5 176

Figure		Page
A5.a)	Schematic diagram of the electronic circuit used for the Time Control unit	179
A5.b)	Schematic diagram of the electronic circuit used for the Operations Control unit	180
A6.	A plot used for evaluating the activity of H_2O in a 6.0 M KOH solution	199
A7.	A plot of i_p vs. $V^{1/2}$ for the Ni-electrode . .	201
A8.	A plot of Ep vs. log V for the Ni-electrode .	203

I

INTRODUCTION

A battery (or a galvanic cell) has the property of converting chemical into electrical energy. Depending on the extent of their rechargeability, batteries are divided in two groups; i) primary--non regenerated for reuse, and ii) secondary (or storage)--readily rechargeable.

The Ni-Cd battery belongs to the group of secondary batteries, where the Ni-electrode forms the positive terminal and the Cd-electrode forms the negative. During discharge the system behaves as a galvanic cell, i.e. a source of electrical energy which is provided by the reduction of the Ni-electrode and oxidation of the Cd-electrode. In the process of charging, the cell behaves as an electrolytic cell, hence utilizing an external current source to oxidize the Ni-electrode and reduce the Cd-electrode.

Alkaline storage batteries, such as the Ni-Cd cell, offer a wide variety of physical design types and performance characteristics. Their versatility is utilized in numerous systems. Some of the most common applications are emergency lighting, stand-by power, electrical switchgear signaling, engine cranking, motive power, portable tools and equipment, photographic

equipment, medical instruments and prosthetic devices, satellites and space probes. A successful secondary battery must meet the following requirements: maximum reversibility in the conversion between chemical and electrical energy, high energy density, long shelf life, immunity to electrical abuse and storage conditions, efficient performance under a variety of conditions and low self-discharge rates.

In view of these applications and requirements, many investigations have been conducted with Ni-Cd batteries, to study the reaction mechanism and active material composition of both electrodes. Studies have also been performed concerning the major factors affecting the system behavior, such as structure of electrodes, electrolyte composition, the rate and depth of discharge and charging techniques. Based on the kinetic studies, several different reaction mechanisms have been proposed in the literature. The most widely accepted ones are the solid-state and the dissolution-precipitation mechanisms. The investigations concerned with charging techniques have been recently concentrated in pulsed current charging. This technique stemmed from the field of pulsed current electrolysis which has been used in the last decade in studies of electrodeposition and evaluation of electro-kinetic parameters. Pulsed electrolysis is known to affect the surface morphology of the electrodeposits and

the reaction rate, and to allow the application of instantaneous current densities higher than those used under direct current conditions. When used for charging secondary batteries, pulsed current has shown some effect on the charge acceptance of the system and the crystal size of the active material. These investigations, however, have been mostly empirical in nature. In addition, because these studies have been performed using commercial batteries with porous plates, little information leading towards an understanding of the basic processes involved in the system, has been obtained. Hence, the results are usually applicable to the particular systems used in these investigations. In view of these difficulties, a more fundamental approach is needed to study the charge-discharge processes of this system under both direct and pulsed current charging conditions.

The present work is aimed at a systematic investigation of the effect of pulsed current charging on the charge acceptance of Ni-Cd cells, with special emphasis on mass transfer, kinetic and structural aspects. Due to the fact that the system contains numerous variables which interact in a complex manner, half cells and film electrodes were chosen for this work. The charge acceptance of both Ni and Cd half cells under a variety of well-defined charge-discharge conditions was measured. The present investigation also incorporates a theoretical

formulation of the effect of pulsing on the reduction of concentration overpotential. This was experimentally verified with a model ferro-ferricyanide system. Mechanistic studies on the electrode reactions were carried out by means of sweep experiments under both controlled current and controlled potential conditions. Limiting current measurements were performed by using a rotating disk electrode. Active material composition and structural modifications at both electrodes, caused by pulsed charging, were studied by means of X-ray diffraction, TEM and SEM.

A literature review is first presented on the electrode reactions including thermodynamic, kinetic and structural aspects, the effect of pulsed current electrolysis on the performance of electrolytic systems and background on experimental techniques utilized in the present work. Development of the theoretical equations for the reduction of concentration overpotential is then presented. The expected effect of pulsed current charging on the three major aspects, mass transfer, kinetics and structure, of the system is discussed. Experimental details concerning the apparatus and procedure used for the various studies are described. The results are then discussed. Finally, conclusions from this work and recommendations for further studies are presented.

II

REVIEW OF LITERATURE

A. The Ni-Cd Battery

Depending on the configuration, capacity and electrode structures, there are several kinds of Ni-Cd batteries. These include the button (20-3000 mAh), cylindrical (450-8000 mAh), and rectangular (1.6-23 Ah), types with sintered and pocket electrodes. These systems have been described and summarized in detail by Falk et al. (25), Vinal (51) and Mantell (35).

The sintered plate cell has electrodes consisting of porous sintered plaques into which the active materials are impregnated. The positive active material is nickel hydrate, while the negative one is cadmium sponge. Both active materials contain additives to improve the performance. The electrolyte is potassium hydroxide with a small amount of lithium hydroxide. A separator which is highly absorbant and chemically inert is used between the two electrodes.

In general the simplified electrode reactions can be represented as follows:

at the positive electrode:

$$Ni(OH)_2 + OH^- \underset{\text{discharge}}{\overset{\text{charge}}{\rightleftharpoons}} NiOOH + H_2O + e^- \qquad (1)$$

at the negative electrode:

$$Cd(OH)_2 + 2e^- \underset{\text{discharge}}{\overset{\text{charge}}{\rightleftharpoons}} Cd + 2OH^- \qquad (2)$$

Therefore the overall cell reaction can be represented as:

$$2Ni(OH)_2 + Cd(OH)_2 \underset{\text{discharge}}{\overset{\text{charge}}{\rightleftharpoons}} 2NiOOH + Cd + 2H_2O \qquad (3)$$

The above equations describe the primary cell reactions. At both electrodes there are secondary reactions which are responsible for hydrogen evolution at the Cd-electrode and oxygen evolution at the Ni-electrode during overcharge, according to:

$$2H_2O + 2e^- \longrightarrow H_2(g) + 2OH^- \qquad (4)$$

and

$$4OH^- \longrightarrow O_2(g) + 2H_2O + 4e^- \qquad (5)$$

The generation of gases is a major problem in sealed Ni-Cd batteries. Although hydrogen is not oxidized at a significant rate at the positive electrode, oxygen can be reduced at the negative electrode and the achievement of its rapid consumption, makes the sealing of Ni-Cd cells possible. For operation in this manner the states of charge of the two electrodes are adjusted prior to sealing, so that the positive electrode becomes fully charged before the negative and as a result oxygen is produced on one electrode and then consumed at the other, before the

evolution of hydrogen becomes possible.

B. Electrode Reactions

The electrode reactions, their mechanism, the thermodynamic aspects, structure and composition of the active materials have been the subject of numerous investigations (3, 8, 10, 12, 14, 19, 24, 27-30, 33, 34, 37, 42, 43, 48 and 50). However, due to the great complexity of the system, different results have been observed depending on the experimental conditions. Consequently a number of expressions for the reversible electrode potential, reaction mechanisms and active material compositions have been proposed. An extensive summary of these studies is presented by Falk et al. (25), Milner and Thomas (38), Briggs (12) and Armstrong et al. (3). It is beyond the scope of this review to include all the different approaches and their corresponding findings. Therefore only the most widely accepted theories for the system will be presented.

Many attempts have been made to predict the reversible electrode potential for the reaction occurring at the Ni-electrode. There is a considerable disagreement in most studies between the experimental and theoretical values (24). It has been practically impossible to observe a truly reversible electrode potential due to the continuous self-discharge existing in the system and the

large double layer capacitances of the electrode associated with the faradaic processes. If the rate of the self-discharge is sufficiently low, then the observed potential may represent a mixture of the reversible nickel oxide and the reversible oxygen electrode potentials. It may also incorporate kinetic factors. Therefore, the long term open circuit potentials are at best mixed potentials and at worst discharge potentials. Based on experimental results MacArthur (33) proposed that the potential of the electrode reaction could be represented as:

$$E_r = E_o - 0.0591 \log \frac{[a_{KOH}]^m}{[a_{H_2O}]^n} \qquad (6)$$

where E_r is the reversible electrode potential, E_o is the standard electrode potential which has a value of 0.411V, m and n are the stoichiometric coefficients in the following reaction:

$$HgO + 2[Red] + mKOH \longrightarrow Hg + 2[Ox] + nH_2O \qquad (7)$$

Most of the investigations which are concerned with the mechanistic aspects of the electrode reaction have been conducted with half cells of the battery. The electrodes used have been of the sintered type. These studies resulted in the identification of two distinct mechanisms, namely the solid-state mechanism and the dissolution-precipitation mechanism, the latter involving intermediate product formation.

Based on potential sweep experiments, with film Ni-electrodes, MacArthur (33 and 34) has proposed a model describing the reactions occurring at the Ni-electrode. However, it should be noted that his representation of the system behavior is greatly simplified and completely neglects phase changes in the solid. Its derivation is based on the assumption that electron transfer through the nickel hydroxide lattice is faster than proton transfer. Hence, the redox reaction $Ni^{+2} \rightleftharpoons Ni^{+3} + e^{-}$ may be regarded as reversible. The model proposes a reaction at the Ni-electrode consisting of the following two steps. First, a proton is released adjacent to the nickel ion site during oxidation. It diffuses to the electrolyte interface, where it reacts with hydroxide ion to form a water molecule in the electrolyte. Second, a proton vacancy is created in the active material lattice, during reduction, which is filled up by the protons diffusing from the electrolyte interface into the lattice. The rate of the reaction is controlled by the rate of proton transfer, since the electrode process is found to be much faster than the rate of diffusion of a proton through a solid phase. Based on this mechanism, the experimentally determined values of the diffusion coefficient of a proton during the oxidation and reduction reactions are 0.33×10^{-9} cm^2/sec and 0.71×10^{-10} cm^2/sec, respectively. The magnitudes of these values are consistent with diffusion through a solid.

Also from the potential sweep experiments with interrupted scans, the formation of a poorly conducting film was observed. A film breakdown was achieved by applying a more cathodic potential.

The active materials corresponding to the state of charge and discharge are established to be NiOOH and $Ni(OH)_2$ respectively. They have been found to exist in four structures, γ and β for the oxidized, and α and β for the reduced species. The structure of $Ni(OH)_2$ has been studied by means of X-ray techniques and infrared spectroscopy, and was found to be of hexagonal layer lattice. The layers consist of Ni^{+2} planes sandwiched between planes of OH^-. There is a detectable difference in the interlayer separation for samples of different age, due to water insertion between layers. No evidence of hydrogen bonding is present. For NiOOH a similar structural arrangement has been observed. In contrast to the $Ni(OH)_2$ structure, there was evidence for the presence of hydrogen bonding in NiOOH. Bode and coworkers (8) have reported that at least two different reactions exist at the Ni-electrode, both of them heterogeneous, based on different reacting materials and yielding different products. For the oxidized material, two distinct states exist for both β-NiOOH and γ-NiOOH, one of which can only be charged, while the other can only be discharged. From their experimental work they found the potential difference between the two states of β-NiOOH to

be 100mV, while that for the γ-NiOOH to be 60mV. Other investigators (14, 24, 33, 34, 42 and 43) have been concerned with the stoichiometric composition of the active materials and have found different active oxygen to nickel ratios, depending on the aging conditions of the electrode. These differences were attributed to oxygen absorption by β-NiOOH as well as by $Ni(OH)_2$.

To summarize the Ni-electrode reactions, consider the following simplified schematic diagram, used by Bode (8):

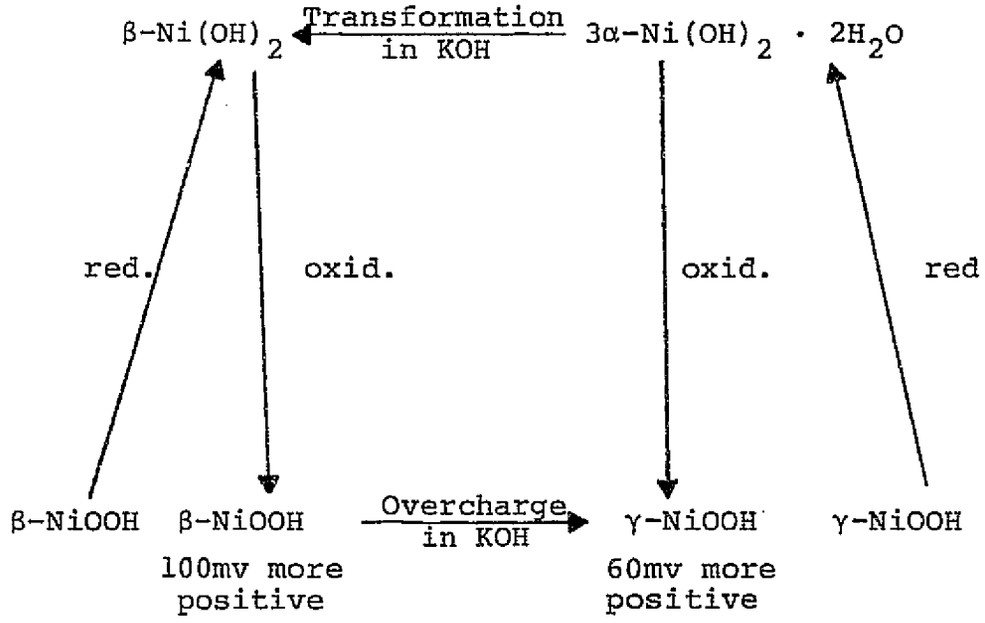

However, phase transformations of nickel hydroxide as proposed by Bode have been challenged by McEwen (37). The latter author showed that the experimental evidence used by Bode to establish this model could be explained by movement of water from the hydroxide lattice.

The reactions at the Cd-electrode have also received a great deal of attention (3, 10, 14, 24, 30, 38, 42 and 43), with special considerations on the cause of premature passivation during discharge.

Evaluation of the thermodynamic equilibrium potential of the Cd-electrode has been relatively easy in comparison to that for the Ni-electrode. The potential of the cadmium electrode with respect to Hg/HgO reference electrode is described by:

$$E_r = -0.906 - \frac{RT}{2F} \ln(a_{H_2O}) \qquad (8)$$

A recent investigation (14) has suggested that the anodic oxidation reaction at the Cd-electrode is most satisfactorily described by the solid state-dissolution precipitation mechanism, which postulates the cause of passivation to be an underlayer of CdO. The proposed reaction model can be described in the following manner. A thin, glassy, nonstoichiometric, continuous layer of CdO is formed on the surface of the Cd-electrode, which is buried beneath the final hydrolysis product ($Cd(OH)_2$). The outer surface of this layer dissolves continuously, complexing and precipitating out as the final product. Cd^{++} penetrate through the CdO underlayer, contributing towards the replacement of the dissolved CdO and also forming a soluble intermediate such as $Cd(OH)_3^-$, which is then precipitated out as the final product. The presence

of CdO has been established through potential measurements and also from the presence of paramagnetic species such as O_2^- and O_3^-.

Using the rotating ring-disk electrode technique, Okinaka (42) detected the formation of dissolved intermediate species during the anodic and cathodic processes of the Cd-electrode. These findings lead him to the conclusion that the dissolution-precipitation mechanism describes the system behavior, while that of solid-state growth is of negligible importance for the experimental conditions employed in his work.

The discharged active material was found to have two different structures; β-$Cd(OH)_2$ - hexagonal and γ-$Cd(OH)_2$ - monoclinic, depending on the discharge conditions, indicating an effect due to different electrolyte concentration and temperature. The electrode reactions can be represented as follows (14);
during discharge:

$$Cd + 3OH^- \longrightarrow Cd(OH)_3^- + 2e^- \qquad (9)$$

$$Cd(OH)_3^- \longrightarrow Cd(OH)_2 + OH^-_{ads} \qquad (10)$$

$$OH^-_{ads} \longrightarrow O^-_{ads} + e^- + H^+ \qquad (11)$$

$$O^-_{ads} \longrightarrow O_{ads} + e^- \qquad (12)$$

$$O_{ads} + O^-_{ads} \longrightarrow O_2^- \qquad \text{at } -10°C \qquad (13)$$

$$O^-_{ads} + 2O_{ads} \longrightarrow O_3^- \qquad \text{at } -40°C \qquad (14)$$

and during charge:

$$Cd(OH)_2 + OH^- \longrightarrow Cd(OH)_3^- \quad (15)$$

$$Cd(OH)_3^- + 2e^- \longrightarrow Cd + 3OH^- \quad (16)$$

In summary a schematic representation of the reactions at the Cd-electrode, based on Casey and Gardner (14), is given below:

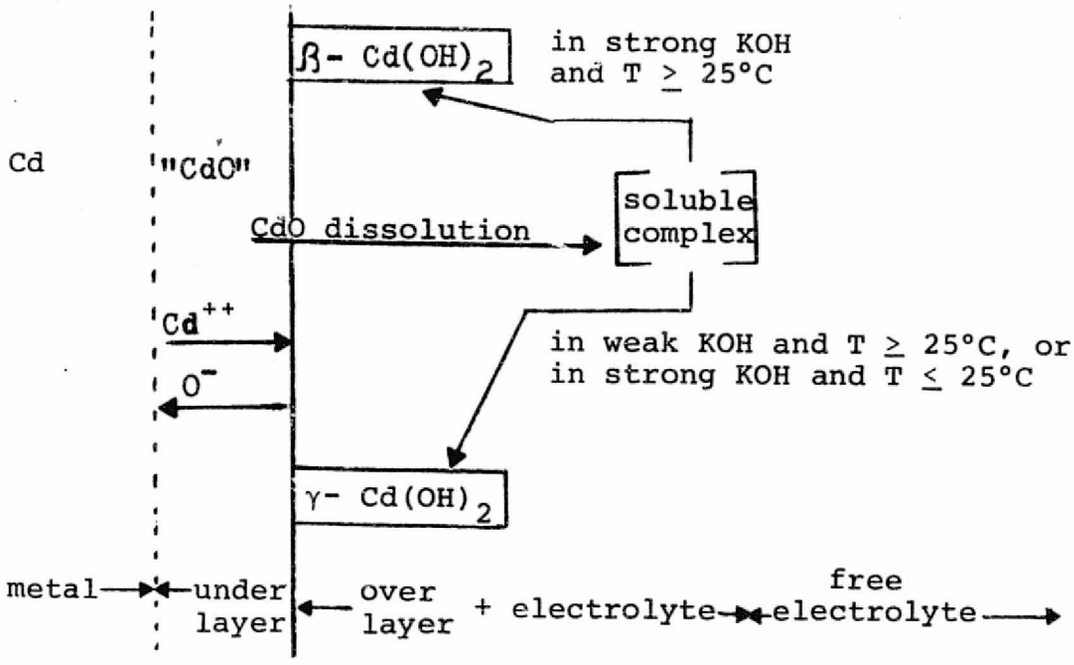

C. Effect of Pulsed Current on the Performance of Electrochemical Systems

In the last decade the approach for studying the different aspects of electrochemical systems, by pulsed electrolysis, has gained a great deal of attention. A mathematical formulation for evaluating kinetic parameters, such as transfer coefficient and exchange current density

in electrochemical systems, based on pulsed current has been derived (44-46 and 49). The effect of pulsed current on mass transfer in electrolytic systems was also derived and experimentally verified (16-18). However, to the best of our knowledge, pulsed current studies conducted with batteries have been mostly exploratory in nature. These experiments have been concerned with complex systems such as commercially available batteries or systems with sintered electrodes. Therefore, the results obtained are usually applicable to the particular set of experimental conditions.

Pulsed electrolysis reduces irreversibilities from mass transport limitations, since a pulsed potential or current relaxes the demand on the mass transfer of the reacting species, during the off-period of the pulse. Thus the net effect of pulsed electrolysis is an increase of the reacting species concentration in the diffusion layer, which in turn reduces the concentration overpotential. Even though the limiting overall reaction rate with pulsed current electrolysis has been shown to be lower than that for direct current (16), the pulsed current technique is sometimes preferable, since it can raise substantially the value of the instantaneous limiting current density, causing structural modifications of the electrodeposits. The instantaneous pulsed limiting current density, $(i_{p-c})_L$, has been defined by Cheh (16) as the instantaneous pulsed

current density which causes the lowest surface concentration of the reacting species to reach zero.

The effect of pulsed charging on the silver oxide electrode from a Ag-Zn battery has been investigated in a system consisting of sintered type plates (53 and 54). The discharge capacity of the Ag-electrode, following a pulsed current charge, was found to be greater than the normal capacity. This was attributed to the breakdown of the oxide film which had passivated part of the electrode surface. Moreover, the discharge capacity was found to be inversely proportional to pulse current, pulse length and pulse frequency, due to the formation of smaller and finer AgO crystals at high current density and pulse length. These fine AgO crystals form a tight coating on the electrode surface and since the pulse frequency is very high, a coating breakdown is not achieved. The electrolyte concentration was found to play an important role on the system performance, e.g. in a 50% KOH solution pulsed current charging resulted in a discharge capacity lower than that for direct current charging in the same solution.

Studies have also been conducted concerning the deposits on the Zn-electrode from a Ag-Zn battery (4). Best results were reported with current densities slightly greater than the critical value for moss-type deposition, short on-periods (10msec or less) and a small on/off ratio. These findings were attributed to dissolution of the

active mossy deposit during the open circuit period.

The reported pulsed current studies with Ni-Cd batteries are similar in nature to those with the Ag-Zn battery. In the former case, structural studies were performed under a greater variety of pulse modes. The test systems were usually commercially available batteries. Several different charging modes were applied and the best results showed a 10% - 15% increase of discharge capacity, reported with the Romanov-type reflex charge and the McCulloch-type reflex charge, both at 60Hz (52). These pulse modes are schematically represented in Fig. 1. Wagner and Williams (52), suggested that the magnitude of the discharge pulse was the predominent factor controlling the output. These authors found that the capacity was independent of the pulse frequencies tested (30-2000 Hz). Scanning electron micrographs of the Cd-electrode surface have shown a 20-fold decrease in the size of the hexagonal $Cd(OH)_2$ crystals after pulsed current charging as compared to an electrode from a faded cell.* A similar study was performed on faded batteries (52) which showed that the discharge capacity could be increased and the battery could be restored after charging with pulsed current under a particular set of conditions.

---

*Definitions of terms, from the battery field, used in this work are given in Appendix 6.

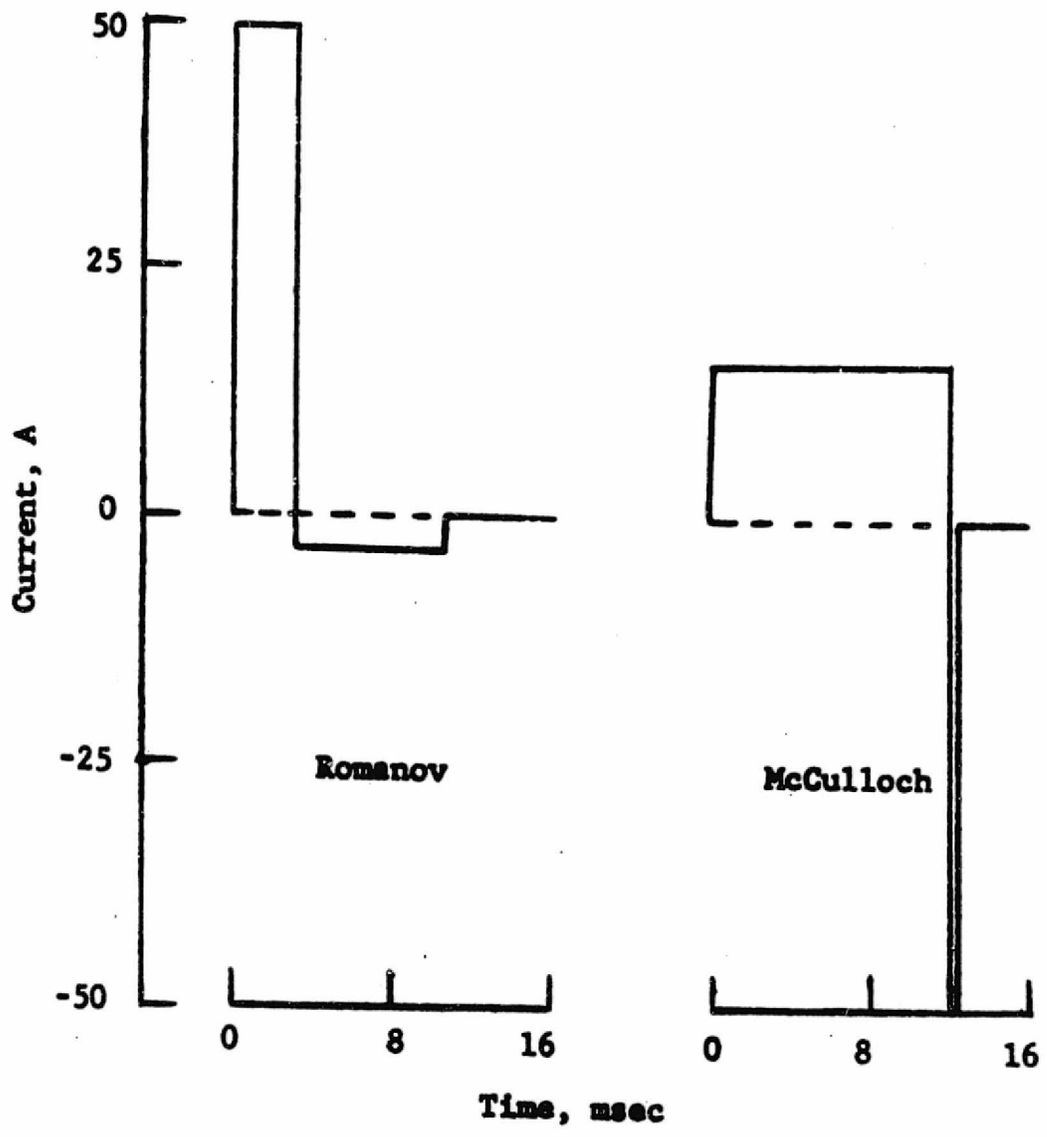

Figure 1. Schematic representation of Romanov and McCulloch type pulsed currents

Again, the capacity was found to decrease with an increase of pulsed current. The charging time was considerably shorter than that for constant potential charging.

Dunlop and Bounds (23) found that a pulsed current with a duty cycle of 25% and a frequency of 2Hz did not improve the charge efficiency* of the Ni-Cd cells. An increase of charge efficiency was observed with an increase in charging rate. This was attributed to the possible reduction of self-discharge losses with reduced charging time. The memory effect* and degradation* did not seem to be affected by the pulses used for charging the cells in their investigation.

In summary, pulsed current charging of Ni-Cd cells has been shown to be beneficial under some experimental conditions.

D. Experimental Techniques Used in This Investigation

Rotating Disk Electrode - is an important tool for studying the kinetics of heterogeneous reactions controlled by either mass transfer or combined mass transfer and activation. Since the hydrodynamic behavior of the system is well known, the solution of the convective diffusion equations has been obtained. Several solutions, of varying degrees of approximation, for this problem have been reported in the literature.

---

*Definitions of terms, from the battery field, used in this work are given in Appendix 6.

Levich (32) solved the differential equation for convective diffusion at large Sc (Schmidt number which is equal to ν/D), assuming negligible edge effects and a rate of the interfacial reaction much larger than that of the transport process. The maximum transport rate towards the disk was found to be

$$j_{max} = 0.62\ D^{2/3}\ \nu^{-1/6}\ \omega^{1/2}\ C_o \qquad (17)$$

where j_{max} is the maximum flux of the reacting species towards the electrode, D is the diffusion coefficient of the reacting species through the solution, ν is the kinematic viscosity of the solution, ω rotation speed and C_o concentration of the reacting species in the bulk of the solution.

The thickness of the diffusion boundary layer was found to be:

$$\delta = 1.61\ (D/\nu)^{1/3}(\nu/\omega)^{1/2} \qquad (18)$$

where δ is the diffusion layer thickness.

In terms of limiting current, eqn. (17) can be expressed as:

$$i_L = 0.62nF\ D^{2/3}\ \nu^{-1/6}\ \omega^{1/2}\ C_o \qquad (19)$$

where i_L is the limiting current, n is the number of electrons transferred and F is Faraday's constant. In the case of a reaction of high activation energy, both mass transfer and charge transfer may affect the reaction rate.

For a first-order irreversible reaction the measured current density was found by Levich (32) to be:

$$\frac{1}{i} = \frac{1}{i_a} + \frac{1}{0.62nF\,D\,\nu^{-1/6}\,\omega^{1/2}\,C_o} \qquad (20)$$

where i is the measured current density and i_a is the current density due to charge transfer.

In terms of limiting current eqn. (20) can be given as:

$$i_L = \frac{n\,F\,D\,C_o}{1.61\,D^{1/3}\,\nu^{1/6}\,\omega^{-1/2} + \frac{D}{k}} \qquad (21)$$

where k is the reaction rate constant.

Newman (40) presented a solution which incorporates a correction factor for finite values of Sc. For a reaction controlled by the rate of mass transport, the maximum flux was found to be:

$$j_{max} = -\frac{0.62048\,(\nu\omega)^{1/2}\,(\nu/D)^{-2/3}\,C_o}{1 + 0.2980\,(\nu/D)^{-1/3} + 0.14514\,(\nu/D)^{-2/3}} \qquad (22)$$

with a thickness of the diffusion boundary layer

$$\delta = \frac{[1 + 0.2980(\nu/D)^{-1/3} + 0.14514(\nu/D)^{-2/3}]D}{0.62048(\nu/D)^{-2/3}(\nu\omega)^{1/2}} \qquad (23)$$

The limiting current density then can be expressed as

$$i_L = \frac{0.62048\,nF\,(\nu/D)^{-2/3}\,(\nu\omega)^{1/2}\,C_o}{1 + 0.2980\,(\nu/D)^{-1/3} + 0.14514\,(\nu/D)^{-2/3}} \qquad (24)$$

From the equations given above it follows that direct measurements of limiting current as a function of rotation speed will reveal the rate controlling step in the reaction mechanism. In the case of mass transport control, it will allow the evaluation of the diffusion coefficient, whereas in the case of mixed control, with a first-order reaction,

the reaction rate constant k can be determined. Results for the rate constant could further be used for the evaluation of transfer coefficients and exchange current density.

Cylic Voltametry - is a technique used mainly for the identification of different steps involved in a complex reaction (1, 21, 22 and 26). Most of the information provided by these measurements is qualitative in nature. Quantitative information could be obtained only from the first couple of cycles. This limitation is due to the fact that continued cycling will gradually alter the concentration profiles near the electrode surface until steady state is reached. In the absence of coupled chemical reactions this results in a small shift of the peak potential E_p and a slight decrease in the values of the peak current i_p. For coupled chemical reactions large alterations in both E_p and i_p may occur. In addition, the expressions used for quantitative evaluation are valid for the first few cycles only, since the mathematical derivation was based on the assumption that no concentration gradients exist in the solution. Using the semi-infinite diffusion equation, for a reversible reaction controlled by diffusion and with soluble products, Delahay (21) derived:

$$i_p = 2.7 \times 10^5 \, n^{3/2} \, A \, D^{1/2} \, C_o \, v^{1/2} \qquad (25)$$

where i_p is the peak current and V is the sweep rate. When the rate of the reverse reaction is negligible throughout the potential region studied,

$$i_p = 3.01 \times 10^5 \, n \left(\frac{2.3 \, RT}{bF}\right)^{1/2} D^{1/2} \, C_o \, V^{1/2} \qquad (26)$$

where R is the universal gas constant, T is the temperature, b is the Tafel slope and F is Faraday's constant. For irreversible reactions the peak potential can also be expressed as a function of sweep rate.

$$E_p = E_{1/2} - b[0.52 - 1/2 \log \frac{b}{D} - \log k + 1/2 \log V] \qquad (27)$$

where E_p is the peak potential, $E_{1/2}$ is the half-wave potential and k is the reaction rate constant. From the above equations it follows that from the variation of E_p and i_p with sweep rate, the values of the diffusion coefficient, rate constant and Tafel slope could be calculated.

III

THEORETICAL CALCULATIONS ON THE REDUCTION OF CONCENTRATION OVERPOTENTIAL IN PULSED CURRENT ELECTROLYSIS

Consider a planar electrode in a well stirred solution. The experimental conditions are such that the counter electrode is far away from the working electrode, the concentration of the reacting species at the outer edge of the diffusion layer remains unchanged, the process is controlled by the mass transfer of the reacting species, current is the controlled variable and the nonfaradaic component of the applied current and electrical migration of the species are negligible. The surface concentration of the reacting species is a function of applied current. Cheh (16) had derived an expression for the surface concentration of the reacting ion as a function of pulsed current characteristics. Results are:

During periods when the current is on

$$\frac{nFD(C_i - C_o)}{i_p \delta} = 1 - \frac{8}{\pi^2} \sum_{j=1}^{\infty} \frac{\exp[-(2j-1)^2 a\tau]}{(2j-1)^2} \times \frac{\exp[(2j-1)^2 a\theta] - \exp[(2j-1)^2 a\theta_1]}{\exp[(2j-1)^2 a\theta] - 1} \qquad (28)$$

Where C_i and C_o are the concentration of the reacting species at the electrode-solution interface, and in the bulk solution respectively, i_p is the instantaneous pulse current density, δ is the thickness of the diffusion layer, $a = \frac{\pi^2 D}{4\delta^2}$, $\tau = t - N\theta$, t is time, N - number of cycles which have been completed at t, θ is the cycle time (cf. Fig. A1).

During periods when the current is off:

$$\frac{nFD\ (C_i - C_o)}{i_p \delta} = \frac{8}{\pi^2} \sum_{j=1}^{\infty} \frac{\exp[-(2j-1)^2 a\tau]}{(2j-1)^2} \times \frac{\exp[(2j-1)^2 a\theta] - \exp[(2j-1)^2 a\theta_2]}{\exp[(2j-1)^2 a\theta] - 1} \qquad (29)$$

where $\tau = t - N\theta - \theta_1$, θ_1 and θ_2 are the on- and off-time of the pulse. Details of the derivation are presented in Appendix 1A. The equations presented thus far are based on a previous investigation by Cheh (16), whereas the following development is a part of the present study.

Concentration overpotential is defined as,

$$\eta_c = \frac{RT}{nF} \ln \frac{C_i}{C_o} \tag{30}$$

where η_c is the concentration overpotential. Under d-c electrolysis from eqn. (A4) it follows that

$$\frac{D(C_o - C_i)}{(-\delta)} = \frac{i}{nF} \tag{31}$$

when $i = i_L$, eqn. (31) becomes

$$\frac{DC_o}{(-\delta)} = \frac{i_L}{nF} \tag{32}$$

taking the ratios of the two equations and rearranging

$$\frac{C_i}{C_o} = 1 - \frac{i}{i_L} \tag{33}$$

Substituting for $\frac{C_i}{C_o}$ in eqn. (30), the concentration overpotential under direct current electrolysis is described by:

$$(\eta_{d-c})_c = \frac{RT}{nF} \ln \left(1 - \frac{i}{(i_{d-c})_L}\right) \tag{34}$$

where $(i_{d-c})_L$ is the d-c limiting current.

Under pulsed current conditions, during periods when the current is on, the ratio of $\frac{C_i}{C_o}$ can be evaluated as a function of the pulsed current from eqns. (28) and (32)

$$\frac{C_i}{C_o} = 1 - \frac{i_p}{(i_{d-c})_L} \left[1 - \frac{8}{\pi^2} \sum_{j=1}^{\infty} \frac{\exp[-(2j-1)^2 a\tau]}{(2j-1)^2} \times \frac{\exp[(2j-1)^2 a\theta] - \exp[(2j-1)^2 a\theta_1]}{\exp[(2j-1)^2 a\theta] - 1} \right] \tag{35}$$

Thus,

$$(\eta_p)_c = \frac{RT}{nF} \ln \left[1- \frac{i_p}{(i_{d-c})_L} \left[1- \frac{8}{\pi^2} \sum_{j=1}^{\infty} \frac{\exp[-(2j-1)^2 a\tau]}{(2j-1)^2} \right. \right. \times$$

$$\left. \left. \frac{\exp[(2j-1)^2 a\theta] - \exp[(2j-1)^2 a\theta_1]}{\exp[(2j-1)^2 a\theta] - 1} \right] \right. \tag{36}$$

Similarly, during periods when the current is off

$$(\eta_p)_c = \frac{RT}{nF} \ln \left[1- \frac{i_p}{(i_{d-c})_L} \times \frac{8}{\pi^2} \sum_{j=1}^{\infty} \frac{\exp[-(2j-1)^2 a\tau]}{(2j-1)^2} \times \right.$$

$$\left. \frac{\exp[(2j-1)^2 a\theta] - \exp[(2j-1)^2 a\theta_2]}{\exp[(2j-1)^2 a\theta] - 1} \right] \tag{37}$$

In order to obtain an expression for the reduction of concentration overpotential in terms of a ratio between the pulse and d-c overpotentials, eqn. (36) is divided by eqn. (34) for periods when the current is on, while for those when the current is off the ratio of eqns. (37) and (34) is taken resulting in

$$\frac{(\eta_p)_c}{(\eta_{d-c})_c} = \ln \left[1- \frac{i_p}{(i_{d-c})_L} \left[1 - \frac{8}{\pi^2} \sum_{j=1}^{\infty} \frac{\exp[-(2j-1)^2 a\tau]}{(2j-1)^2} \times \right. \right. \tag{38}$$

$$\left. \left. \frac{\exp[(2j-1)^2 a\theta] - \exp[(2j-1)^2 a\theta_1]}{\exp[(2j-1)^2 a\theta] - 1} \right] - \ln\left(1 - \frac{i}{(i_{d-c})_L}\right) \right. \tag{38}$$

during periods when the current is on

and

$$\frac{(\eta_p)_c}{(\eta_{d-c})_c} = \ln \left[1- \frac{i_p}{(i_{d-c})_L} \times \frac{8}{\pi^2} \sum_{j=1}^{\infty} \frac{\exp[-(2j-1)^2 a\tau]}{(2j-1)^2} \times \right. \tag{39}$$

$$\left. \frac{\exp[(2j-1)^2 a\theta] - \exp[(2j-1)^2 a\theta_2]}{\exp[(2j-1)^2 a\theta] - 1} \right] - \ln\left(1 - \frac{i}{(i_{d-c})_L}\right)$$

during periods when the current is off.

Since the reduction is a function of time, the average reduction for one complete cycle is given by,

$$\left[\frac{(\eta_p)_c}{(\eta_{d-c})_c}\right]_{\text{Average}} = \frac{1}{\theta_1+\theta_2}\left[\int_0^{\theta_1}\left[\frac{(\eta_p)_c}{(\eta_{d-c})_c}\right]_{\text{eqn. (38)}} d\tau + \int_0^{\theta_2}\left[\frac{(\eta_p)_c}{(\eta_{d-c})_c}\right]_{\text{eqn. (39)}} d\tau\right] \tag{40}$$

A numerical evaluation of the reduction of concentration overpotential was carried out for the value of $a\theta$ equal to 0.5, and the values of $i_p/(i_{d-c})_L$ and θ_1/θ equal to 0.2, 0.4, 0.6 and 0.8. First, the instantaneous values of the reduction of concentration overpotential, $(\eta_p)_c/(\eta_{d-c})_c$, were determined from eqns. (38) and (39). All calculations were carried out for the periodic rather than the transient state of the system. An example for duty cycle of 0.2 and various $i_p/(i_{d-c})_L$ values is shown in Fig. 2. From Fig. 2, the region of $0 \leq a\tau \leq 0.1$ represents the period when the current is on. Since $(\eta_{d-c})_c$ is independent of $a\tau$, the variation of $(\eta_p)_c/(\eta_{d-c})_c$ is due to the variation of $(\eta_p)_c$. The latter gradually increases during the on period of the pulsed current, indicating a decrease in the reacting species concentration in the diffusion layer.

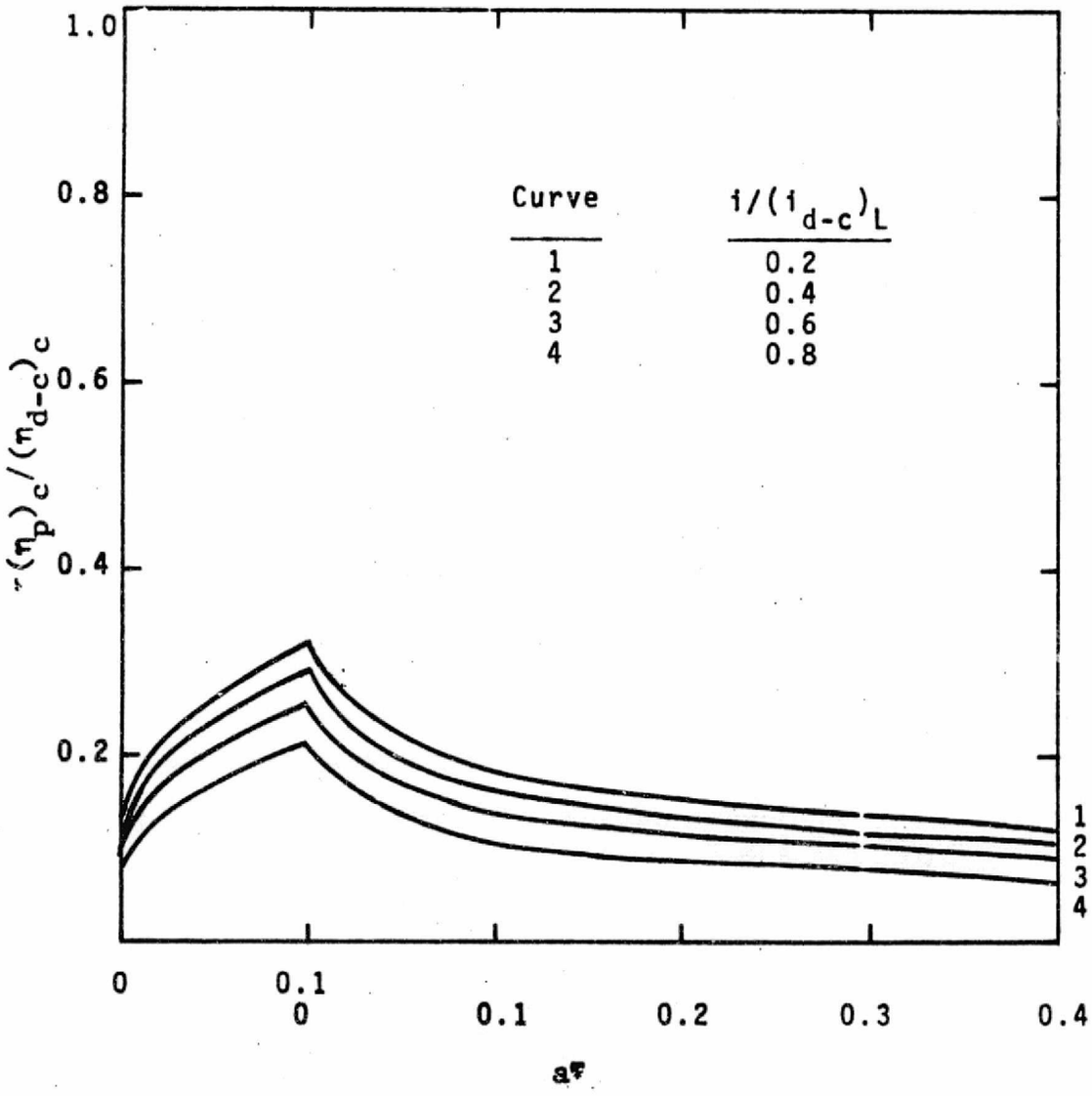

Figure 2. Instantaneous values of $(\eta_p)_c/(\eta_{d-c})_c$ during one complete cycle of the applied p-c, with a duty cycle of 0.2 and aθ of 0.5

This is due to the consumption of the reacting species by the electrode reaction. The region of $0 \leq a\tau \leq 0.4$ represents the period when the current is off. The decrease of $(\eta_p)_c$ in this region demonstrates an increase of the reacting species concentration in the diffusion layer, due to the absence of the electrode reaction. The average values of $(\eta_p)_c/(\eta_{d-c})_c$ were obtained by numerical integration of curves from Figs. 2 and A2-A4. Detailed calculations are given in Appendix 1B, results are summarized in Table A5 and Fig. 3. From Fig. 3 it follows that both duty cycle θ_1/θ and instantaneous pulsed current density have a strong effect on the average reduction of concentration overpotential. The reduction is greater at larger $i_p/(i_{d-c})_L$ values and shorter duty cycles. For example, at a duty cycle of 0.2 and $i_p/(i_{d-c})_L$ of 0.8, the concentration overpotential is reduced by 89.9%. Whereas at a duty cycle of 0.8 and $i_p/(i_{d-c})_L$ of 0.2, the concentration overpotential is reduced by 22.1%. It is important to note that under pulsed current conditions the duration of the electrolysis must be increased by a factor of $(\theta_1/\theta)^{-1}$ in order to carry out the same amount of electrolysis as under d-c conditions. The duration of the electrolysis under p-c with 0.2 duty cycle must be five times longer than that for d-c. The effect of duty cycle and instantaneous pulsed current density on the concentration overpotential can be explained in the following manner. As the d-c limiting current density is

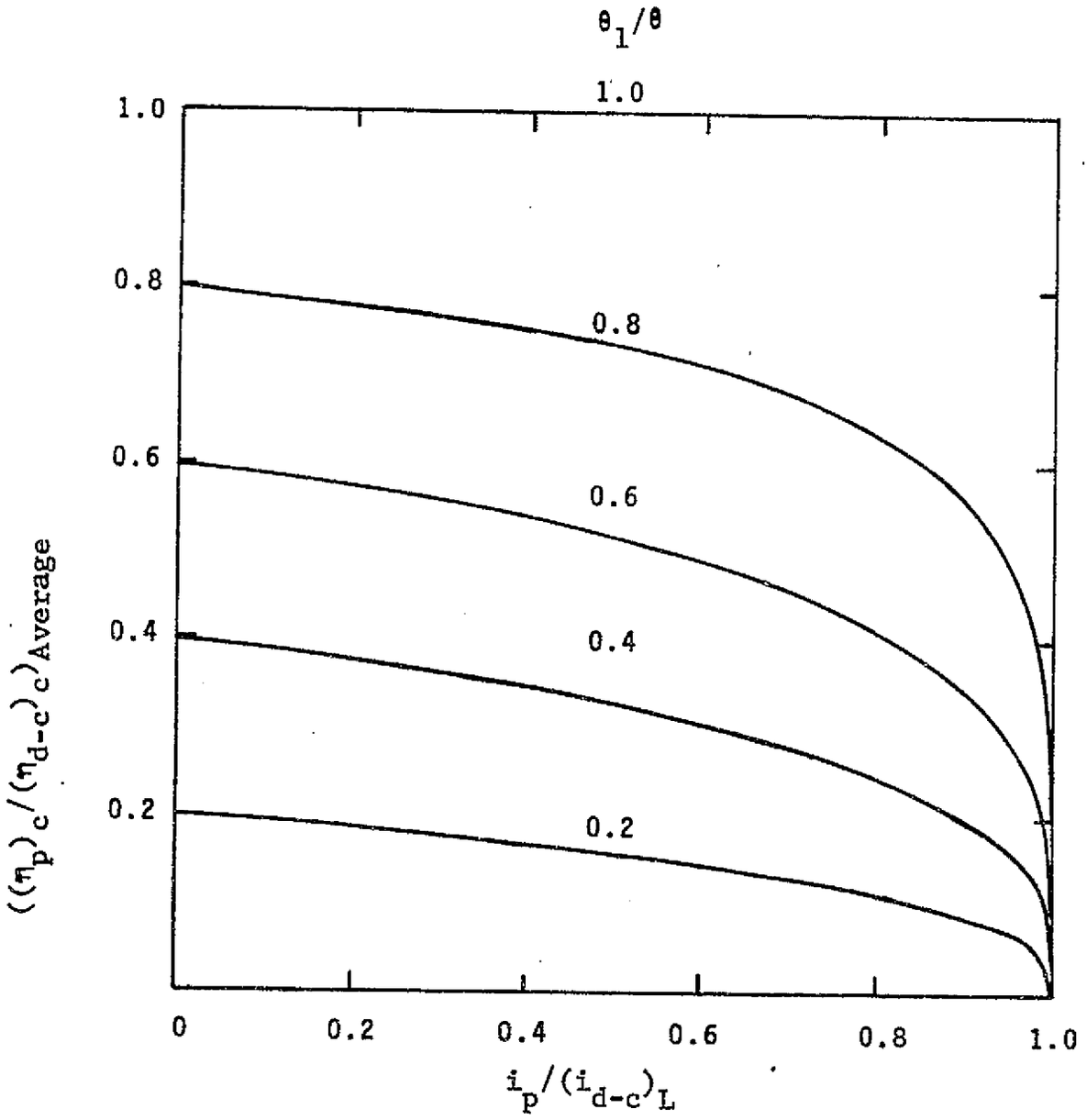

Figure 3. Average values of the reduction of concentration overpotential as a function of duty cycle and instantaneous p-c density, for aθ of 0.5

approached, i.e., larger $i_p/(i_{d-c})_L$ values, the magnitude of $(\eta_{d-c})_c$ can increase drastically. Also, for shorter duty cycles, the limiting current density for pulsed electrolysis can be signficantly higher than that under d-c conditions (16). This is of practical importance, since higher values of p-c could be utilized without the possible interference of gas evolution at the electrodes.

IV

EFFECT OF PULSED CURRENT CHARGING ON THE Ni-Cd CELL

From the literature review it becomes apparent that the effect of pulsed charging on the Ni-Cd cell behavior has not been well understood. However, by taking into consideration the information concerning the various aspects of the system, one can reasonably predict the effect of pulsed charging on the three major aspects of the Ni-Cd cell.

A. Mass Transfer

Pulsed current electrolysis reduces concentration overpotential. This should affect the charging of a Ni-Cd cell. However, its exact response can not be predicted due to the great complexity of the system. For instance, assuming a solid-state mechanism for both the Ni- and Cd-electrodes, the effect of pulsing on the concentration overpotential will not be as pronounced as predicted by the theoretical development presented in this work. The rate of charging is known to be one of the critical factors for determining the system performance. Hence

duty cycle and instantaneous current density should affect the charge acceptance. Consider a charging current of i_p equal to i_{d-c} and θ_1/θ of 0.1, the necessary charging time will be ten times larger than that for d-c. Consequently, the charging rate will be ten times slower. Since reduction of concentration overpotential causes a postponement of gas evolution, charging currents with instantaneous current density much larger than those used for d-c, could be applied. Thus a charging rate comparable to that under d-c conditions could be achieved. During periods when the current is off, self-discharge could take place, resulting in a decrease of charge acceptance at shorter duty cycles. Changes in the structure of the active material are also expected, since the crystalline structure of both the charged and discharged active materials depends on the concentration of the various species at the electrode-solution interface, which in turn is a function of the pulsed current.

B. Kinetics

Pulsed electrolysis can affect the kinetics of the charge reaction in the following manner. Under the condition of fast pulses, the nonfaradaic processes involving the electrical double layer could become important. Also, since the active materials at both electrodes are sensitive

to the applied potential (3, 8, 10, 12, 14, 30, 33 and 43), a given pulsed current could favor the formation of a particular type of active material, thus altering the composition of the electrode, which in turn causes a change in the reaction mechanism. The reaction kinetics could also be affected by the structural modifications of the electrode, due to pulsed charging.

C. Structure

Depending on the crystal growth mechanism, duty cycle and instantaneous current density could cause a change in the crystal size and structure, thereby affecting the discharge capacity of the system.

The effects of pulsed current charging on mass transfer, kinetics and electrode structure can not be treated in an isolated manner, due to the very complex dependence and interrelation between these three aspects of the system.

V

EXPERIMENTAL APPROACH

Experimentally, this investigation is aimed at a systematic study on the effect of pulsed current charging on the charge acceptance, mass transfer, kinetic and structural aspects of Ni-Cd cells. For this purpose, several different types of experiments were designed to analyze as well as to test the system behavior. Due to the complexity of the system, half cells and film electrodes were chosen for this work. To determine the effect of pulsed current characteristics which includes duty cycle, frequency and instantaneous pulsed current density, on charge acceptance, experiments under a variety of well-defined charge-discharge conditions were conducted with both Ni and Cd half cells. The ferro-ferricyanide system with a rotating disk electrode was used for the experimental verification of the theoretical formulation of the reduction of concentration overpotential under pulsed current electrolysis. This particular system was chosen due to its well-behaved charge transfer characteristics. To obtain an understanding of the mechanism of the reactions occurring at both the Ni- and Cd-electrodes, limiting current

measurements were performed as a function of rotation speed and potential scans at various sweep rates. The surface morphology of the electrodes was studied by means of SEM, while the active material composition was determined by X-ray diffraction.

A. Charge Acceptance Measurements

Apparatus - the experimental system consisted of a lucite cylindrical cell, 10 cm in diameter and 10 cm in depth, provided with a tightly fitted cover, a 1.4 x 1 cm^2 film $Ni(OH)_2$ or Cd sponge electrode, a Pt counter electrode and a 6.0M KOH electrolyte. Hg/HgO was used as the reference electrode which was connected to the cell via a salt bridge. A Kepco constant current source (Model CC 15-1.5M) was used as the power supply, while a Tacussel function generator (Model GSTP-3C) coupled to a Kepco power supply (Model BOP 36-1.5M) were used as the pulse source. The working electrode potential with respect to Hg/HgO was continuously recorded, for both the charge and discharge processes on an Esterline Angus recorder (Model E1101-S). The applied pulsed current characteristics were observed on a Tektronix oscilloscope (Model 5103N). The experimental procedure was automatically controlled by means of two electronic circuits, built specifically for this work and shown in Fig. A5, Appendix 2. A schematic representation of the experimental system is given in Fig. 4.

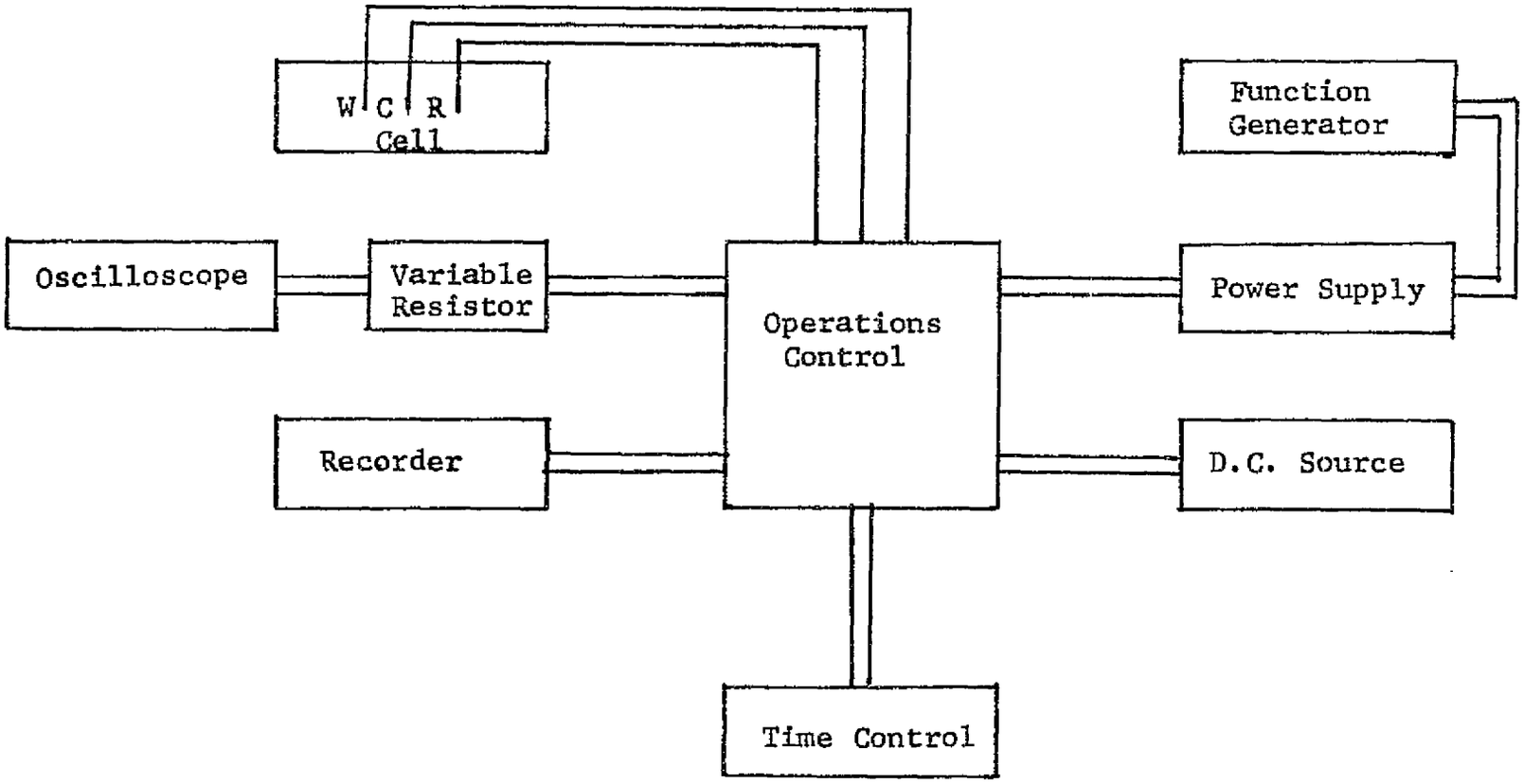

Figure 4. Apparatus for charge acceptance measurements

Procedure - for both the Ni- and Cd-electrodes the active material was prepared in the manner outlined below.

Electrodeposition of $Ni(OH)_2$ was carried out in a cell containing a 0.5 M $Ni(NO_3)_2$ solution, a cathode and an anode of high purity Ni (Inco 270). The electrodes were first polished with several grades of emery paper, the last one being 4/0, followed by washing in HNO_3 and distilled water. $Ni(OH)_2$ was formed by passing a cathodic current of 5 m A for periods of 20 or 30 minutes. After deposition the electrode was washed in distilled water and immediately immersed in the KOH solution, upon which experiments were initiated.

Cd sponge was prepared in a cell with 6.0 M KOH solution, a cathode and an anode of high purity Cd metal. The electrodes were first polished with several grades of emery paper, the last one being 4/0, followed by washing in HNO_3 and a solution of 1:1 mixture of H_3PO_4 and 30% H_2O_2. The active material was formed by passing a cathodic current of 5 m A for periods of 15 and 30 minutes. After deposition the Cd anode was replaced by a Pt electrode, upon which experiments were initiated.

Since the rate of discharge is known to affect the performance of Ni-Cd cells, while the major objective of this work is tc study the effect of pulsed charging current on the system behavior, all experiments were conducted under

identical discharge conditions at a constant current of 5 m A. In addition, all experiments were conducted at room temperature with mild stirring. First the effect of direct current charging on the performance of the Ni and Cd half cells was studied, in order to provide a basis for comparison with the results obtained under pulsed current conditions. The variables chosen were current density and charging time. Due to the aging effect, which diminished usually after the 3rd cycle, eight charge-discharge cycles were performed for all experiments.

Next, the effect of pulsed current on the charge acceptance of the half cells was investigated, under conditions comparable to the direct current ones. The electrodes were first subjected to three charge-discharge cycles under direct current conditions, followed by 5 cycles under pulsed current conditions. In this case the variables were chosen to be instantaneous current density, pulse frequency and duty cycle. Experiments were conducted at four different duty cycles; 0.1, 0.25, 0.5, 0.75, frequencies of 50 Hz and 200 Hz, and instantaneous current densities such that $i_p = i_{d-c}$ and $i_p = (\theta/\theta_1) i_{d-c}$.

B. Measurements on the Reduction of Concentration Overpotential

Apparatus - the system consisted of a Pt rotating disk electrode with an area of 0.46 cm^2, a Pt counter electrode, a saturated calomel reference electrode which was

connected to the cell by a salt bridge and a solution containing 3 m M $[Fe(CN)_6]^{-4}$, 3 m M $[Fe(CN)_6]^{-3}$ in 1 M KCl. A Tacussel function generator (Model GSTP-3C) coupled with a Kepco power supply (Model BOP36-1.5M) were used as the current source for both direct and pulsed current. The potential between the rotating disk electrode and the reference electrode was measured by a digital voltmeter under d-c conditions and recorded on a Tektronix oscilloscope (Model 5103N) under pulsed current conditions. Schematic representation is given in Fig. 5.

Procedure - in order to determine the concentration overpotential during d-c electrolysis and to evaluate parameters necessary for defining the operating conditions of p-c electrolysis, experiments were first conducted under d-c conditions and six rotation speeds. The procedure consisted of applying a constant d-c current and measuring the potential between the rotating disk electrode and the reference electrode.

From the results obtained under d-c conditions, the values of $(i_{d-c})_L$ were used to determine the values of the instantaneous peak current densities to be applied at the various rotation speeds. In addition, the thickness of the diffusion layer was calculated and used for evaluating θ, so that $a\theta = 0.5$. Detailed calculations are given in Appendix 3, the experimental conditions are summarized in

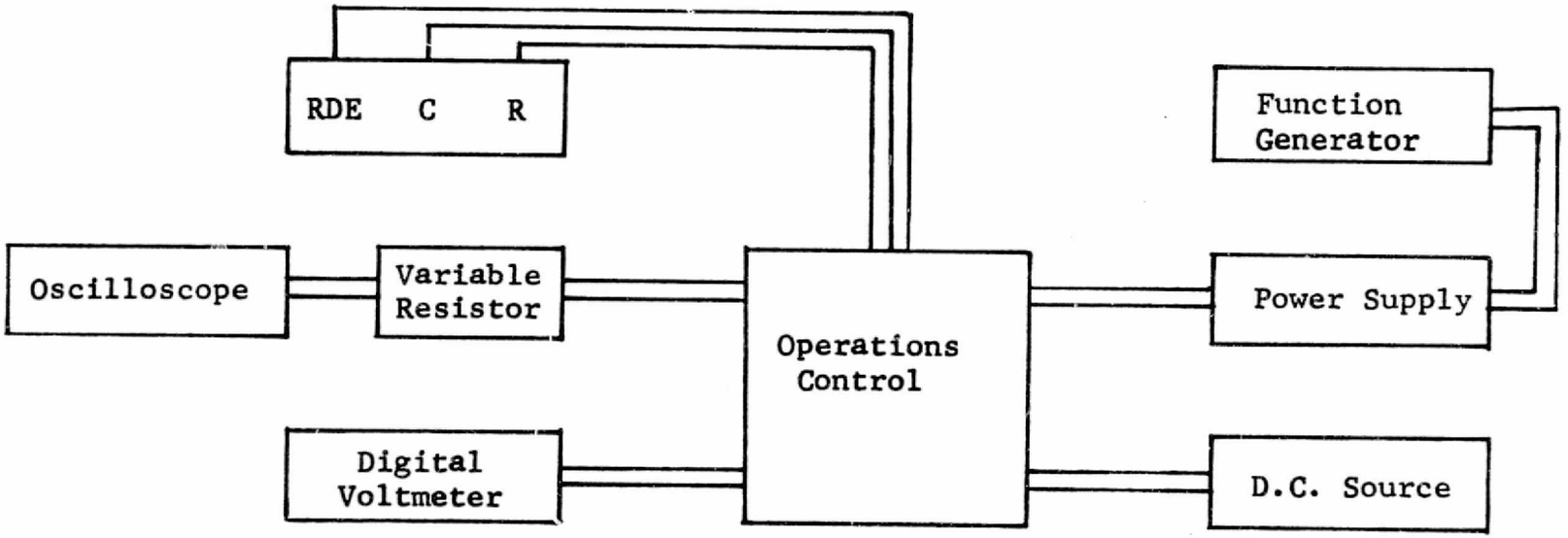

Figure 5. Apparatus for measurements of the reduction of concentration overpotential with the ferro-ferricyanide system

Table 1. The procedure consisted of applying a pulsed current and recording the potential between the rotating disk electrode and the reference electrode, on the oscilloscope.

C. Mechanistic Studies

1. Limiting Current Measurements

Apparatus - the experimental system was similar to that used for charge acceptance measurements. In this case the working electrode was a rotating disk film Ni- or Cd-electrode with a surface area of 1.4 cm^2. A Pine Instrument sweep generator (Model RDE3) and a Hewlett Packard x-y recorder (Model 7044A) were used to measure and record the current-potential behavior of the system. The system is schematically represented in Fig. 6.

Procedure - the active material of both Ni- and Cd-electrodes was prepared in the same manner as used for the charge acceptance measurements. The experiments were conducted under galvanostatic conditions and five rotation speeds, ranging from 400 to 3600 rpm. The procedure consisted of applying a linear sweep of 0.4 m A/min and recording the current-potential behavior of the system.

2. Cyclic Sweep Experiments

Apparatus - the half cells used in these experiments were identical to those used for charge acceptance measurements. A Pine Instrument sweep generator (Model RDE3) and

Table 1

Summary of experimental conditions for overpotential measurements of the ferro-ferricyanide system under p-c conditions

rpm	$\frac{\theta_l}{\theta}$	$\frac{i_p}{(i_{d-c})_L}$	i_{p_A} mA	θ_A msec	θ_{lA} msec	i_{p_C} mA	θ_C msec	θ_{lC} msec
1610	0.2	0.2	0.162	37.3	7.5	0.180	35.0	7.0
"	"	0.4	0.324	"	"	0.360	"	"
"	"	0.6	0.486	"	"	0.540	"	"
"	"	0.8	0.648	"	"	0.720	"	"
"	0.4	0.2	0.162	"	14.9	0.180	"	14.0
"	"	0.4	0.324	"	"	0.360	"	"
"	"	0.6	0.486	"	"	0.540	"	"
"	"	0.8	0.648	"	"	0.720	"	"
"	0.6	0.2	0.162	"	22.3	0.180	"	21.0
"	"	0.4	0.324	"	"	0.360	"	"
"	"	0.6	0.486	"	"	0.540	"	"
"	"	0.8	0.648	"	"	0.720	"	"
"	0.8	0.2	0.162	"	29.8	0.180	"	28.0
"	"	0.4	0.324	"	"	0.360	"	
"	"	0.6	0.486	"	"	0.540	"	
"	"	0.8	0.648	"	"	0.720	"	
915	0.2	0.2	0.122	65.6	13.1	0.134	61.6	12.3
"	0.2	0.6	0.366	"	"	0.402	"	"
"	0.4	0.6	0.366	"	26.2	0.402	"	27.6

Table 1 (continued)

rpm	$\frac{\theta_l}{\theta}$	$\frac{i_p}{(i_{d-c})_L}$	i_{p_A} mA	θ_A msec	θ_{lA} msec	i_{p_C} mA	θ_C msec	θ_{lC} msec
915	0.6	0.6	0.366	65.6	39.4	0.402	61.6	37.0
"	0.8	0.6	0.366	"	52.5	0.402	"	49.3
2500	0.2	0.2	0.204	24.0	4.8	0.232	22.6	4.5
	0.2	0.6	0.612	"	"	0.696	"	"
2500	0.4	0.6	0.612	24.0	9.6	0.696	22.6	9.0
"	0.6	0.6	0.612	"	14.4	0.696	"	15.6
"	0.8	0.6	0.612	"	19.2	0.696	"	17.1
3600	0.2	0.2	0.242	16.7	3.3	0.278	15.7	3.1
"	0.2	0.6	0.726	"	"	0.834	"	"
"	0.4	0.6	0.726	"	6.7	0.834	"	6.3
"	0.6	0.6	0.726	"	10.0	0.834	"	9.4
"	0.8	0.6	0.726	"	13.4	0.834	"	12.6

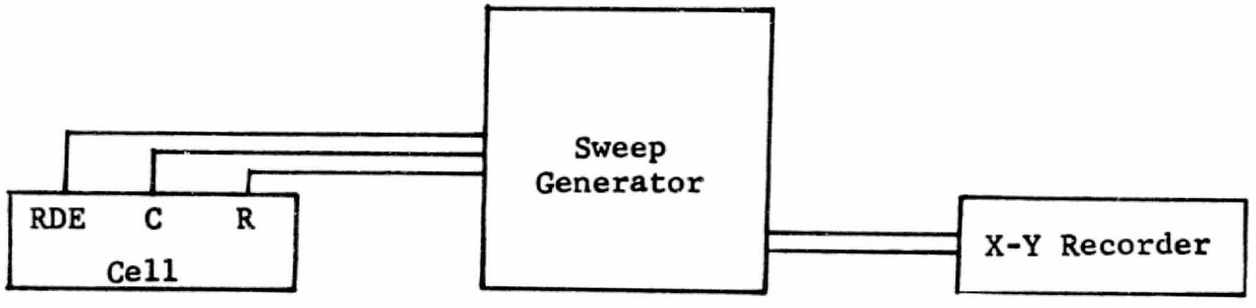

Figure 6. Apparatus for limiting current measurements

a Hewlett Packard x-y recorder (Model 7044A) were used to measure and record the current-potential behavior of the system. A schematic representation is given in Fig. 7.

Procedure - the active material for the Ni- and Cd-electrodes was prepared as previously described. Cyclic sweeps, under both potentiostatic and galvanostatic conditions, of several different sweep rates were applied to the system and the current-potential behavior recorded.

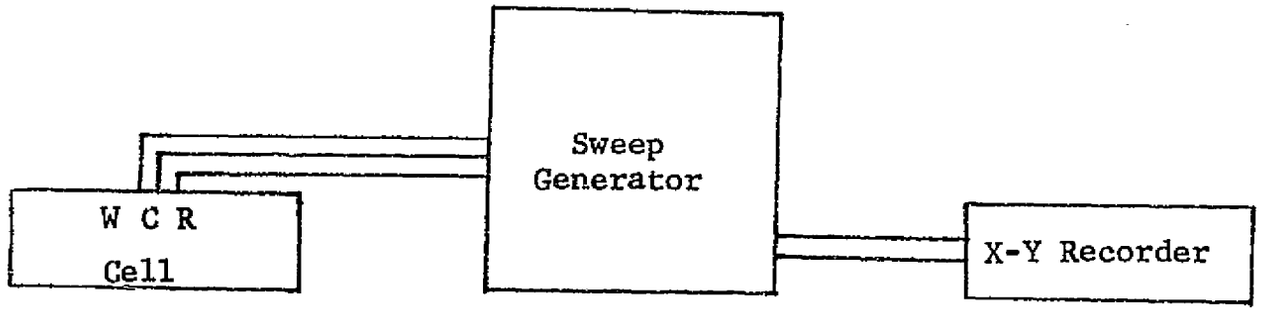

Figure 7. Apparatus for cyclic sweep experiments

VI

RESULTS

A. Charge Acceptance Measurements

A typical charge-discharge curve for the Ni-electrode under d-c charging conditions is represented in Fig. 8. In the literature the charge-discharge behavior of the system usually shows hysteresis effect when the electrode potential is given as a function of percent of capacity discharged. The curves from Fig 8 have been replotted to show hysteresis and are given in Fig. 9. Charge acceptance was calculated from the discharge curves by multiplying the discharge time by the discharge current. Results thus obtained for d-c charging are shown in Table 2, whereas those for p-c charging are presented in Tables 3 and 4. The cycle life of the electrode was also studied under both d-c and p-c charging conditions. Results are summarized in Table 5.

Typical charge-discharge curves for the Cd-electrode under d-c charging, as a function of time and percent of capacity discharged are shown in Figs. 10 and 11, respectively. The charge acceptance of the electrode under a variety of d-c and p-c conditions was calculated. Results are summarized in Tables 6-8. Under p-c charging conditions,

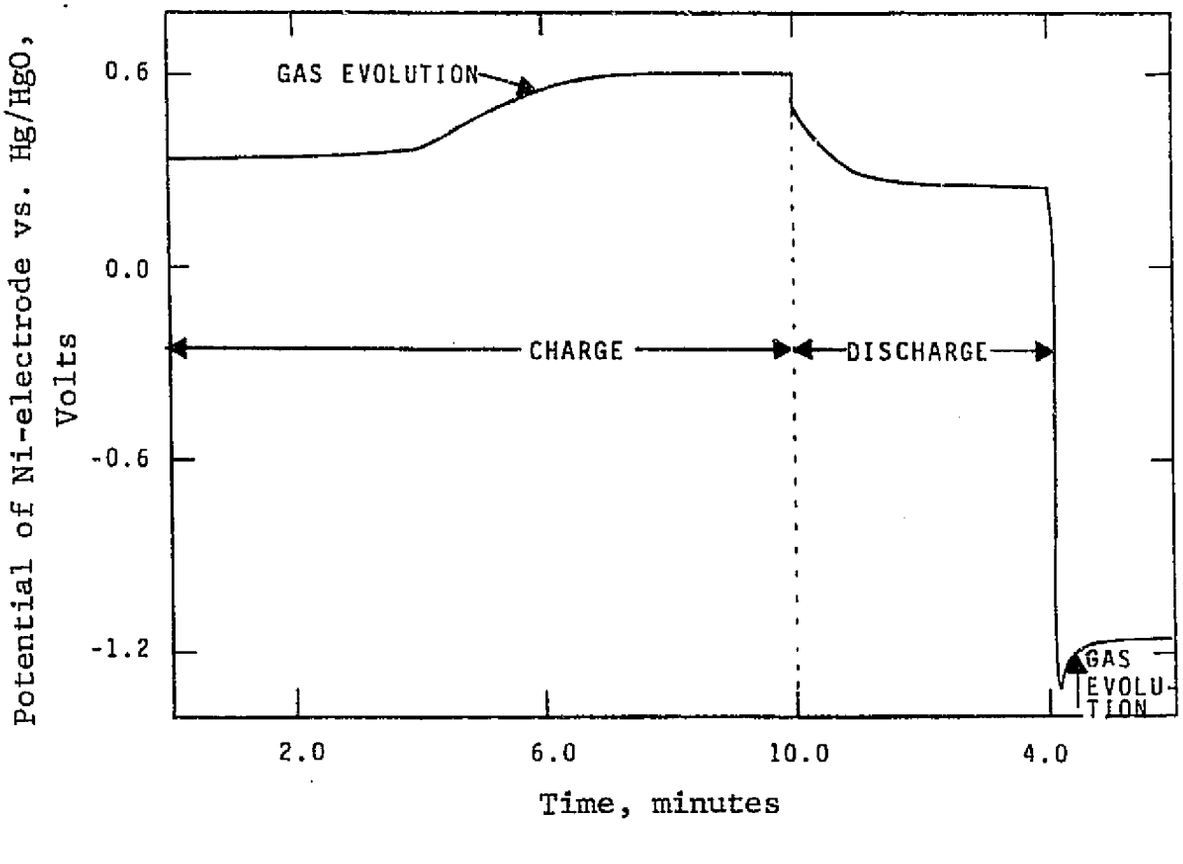

Figure 8. Typical charge-discharge behavior of the Ni-electrode

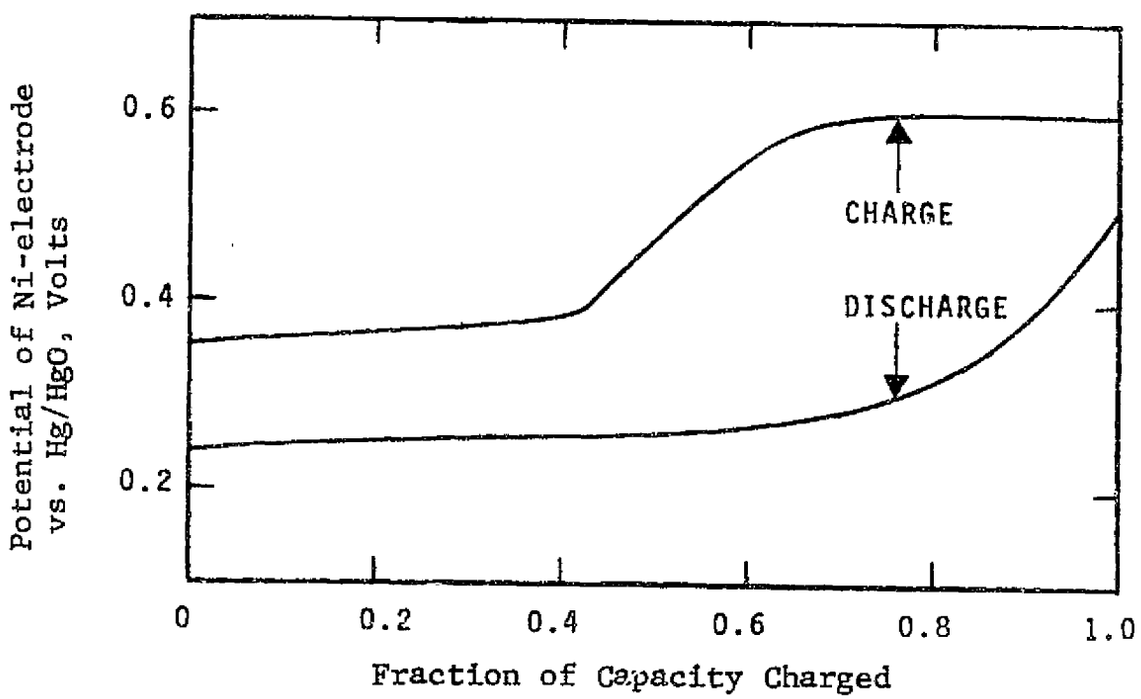

Figure 9. Typical charge-discharge behavior of the Ni-electrode as a function of fraction of capacity charged

Table 2

Charge acceptance of Ni-electrode under d-c charging conditions

Experiment #	No. of Runs	Active Material Preparation		Charging Current	Charging Time	Average Discharge Time	Average % Deviation	Average Charge Acceptance	Average % Deviation
		Current mA	Time Minutes	mA	Minutes	Minutes		mAhr	
N1	4	10	30	5	10	4.800	0.00	0.4	0.0
N2	4	5	30	5	10	4.570	2.18	0.381	2.10
N3	2	5	20	5	5	3.834	0.88	0.320	0.79
N4	3	5	20	5	10	3.935	2.00	0.328	2.04
N5	2	5	20	10	5	4.000	0.00	0.333	0.00
N6	3	5	20	10	10	4.200	1.52	0.350	1.51

Table 3

Charge acceptance of Ni-electrode under p-c charging conditions (active materials prepared at 5mA d-c for 20 min)

Experiment #	# of Runs	Charging Current mA	θ_1/θ	Frequency Cycles/ Sec	Charging Time Minutes	Average Discharge Time Minutes
N7	1	5	0.1	50	50	3.325
N8	2	50	0.1	50	5	3.697
N9	2	5	0.1	200	50	3.600
N10	2	50	0.1	200	5	3.834
N11	1	5	0.5	50	10	3.820
N12	4	10	0.5	50	5	4.076
N13	1	5	0.5	200	10	3.735
N14	2	10	0.5	200	5	3.867
N15	2	5	0.75	50	7	3.883
N16	1	7	0.75	50	5	3.925
N17	1	5	0.75	200	7	3.818
N18	2	7	0.75	200	5	3.916
N19	2	20	0.25	50	5	3.803
N20	2	5	0.25	50	20	3.646
N21	1	5	0.25	200	20	3.782
N22	1	20	0.25	200	5	3.800

Table 3 (continued)

Experiment #	Average % Deviation	Average Charge Acceptance mA hr	Average % Deviation	Average Charge Accept. p-c / Charge Accept. d-c
N7	-	0.277	-	0.867
N8	0.27	0.308	0.32	0.964
N9	0.90	0.300	2.67	0.939
N10	0.39	0.320	0.47	1.000
N11	-	0.318	-	0.995
N12	1.90	0.340	2.1	1.064
N13	-	0.311	-	0.973
N14	0.89	0.322	0.94	1.008
N15	0.88	0.324	0.93	1.014
N16	-	0.327	-	1.023
N17	-	0.318	-	0.995
N18	0.05	0.326	0.00	1.02
N19	0.45	0.317	0.32	0.992
N20	2.03	0.304	1.97	0.951
N21	-	0.315	-	0.986
N22	-	0.317	-	0.992

Table 4

Charge acceptance of Ni-electrode under p-c charging conditions (active materials prepared at 5mA d-c for 30 min)

Experiment #	d-c Preconditioning Current mA	d-c Preconditioning Time Minutes	Charging Current mA	θ_1/θ	Frequency Cycles/Sec	Charging Time Minutes
N23	5	10	10	0.1	50	50
N24	5	10	15	0.1	50	33
N25	10	5	20	0.1	50	25
			40	0.1	50	12.5
			30	0.1	50	16.6
			20	0.1	50	25
			30	0.1	50	16.6
			40	0.1	50	12.5
N26	10	5	40	0.1	50	12.5
			40	0.1	50	12.5

Table 4 (continued)

Experiment #	Discharge Time Minutes	Charge Acceptance mAhr	Charge Accept.p-c / Charge Accept.d-c	Cycle #
N23	1.67	0.140	0.367	8
N24	2.26	0.190	0.500	8
N25	2.330	0.194	0.510	8
	3.600	0.300	0.800	9
	3.600	0.300	0.800	10
	3.470	0.289	0.760	11
	3.500	0.289	0.760	12
	3.600	0.300	0.800	13
N26	3.600	0.300	0.800	8
	3.600	0.300	0.800	10

Table 5

Cycle life of Ni-electrode under d-c and p-c charging conditions

Exp. #	Charging Current mA	$\frac{\theta_1}{\theta}$	Frequency Cycles/ sec	Charging Time Min.	Discharge Time Min.	Charge Accept. mAhr	$\frac{\text{C.A. p-c}}{\text{C.A. d-c}}$	Cycle #
N27	5	-	-	5	3.835	0.3195		8
		-	-		3.000	0.250		20
		-	-		2.000	0.167		40
		-	-		0.500	0.042		80
N28	5	0.25	50	20	3.650	0.304	0.951	8
					3.400	0.283	1.13	20
					3.133	0.261	1.56	40
					1.000	0.083	1.98	80
N29	7	0.75	50	5	3.925	0.327	1.023	8
					3.200	0.267	1.070	20
					2.800	0.233	1.400	40
					1.400	0.117	2.800	80

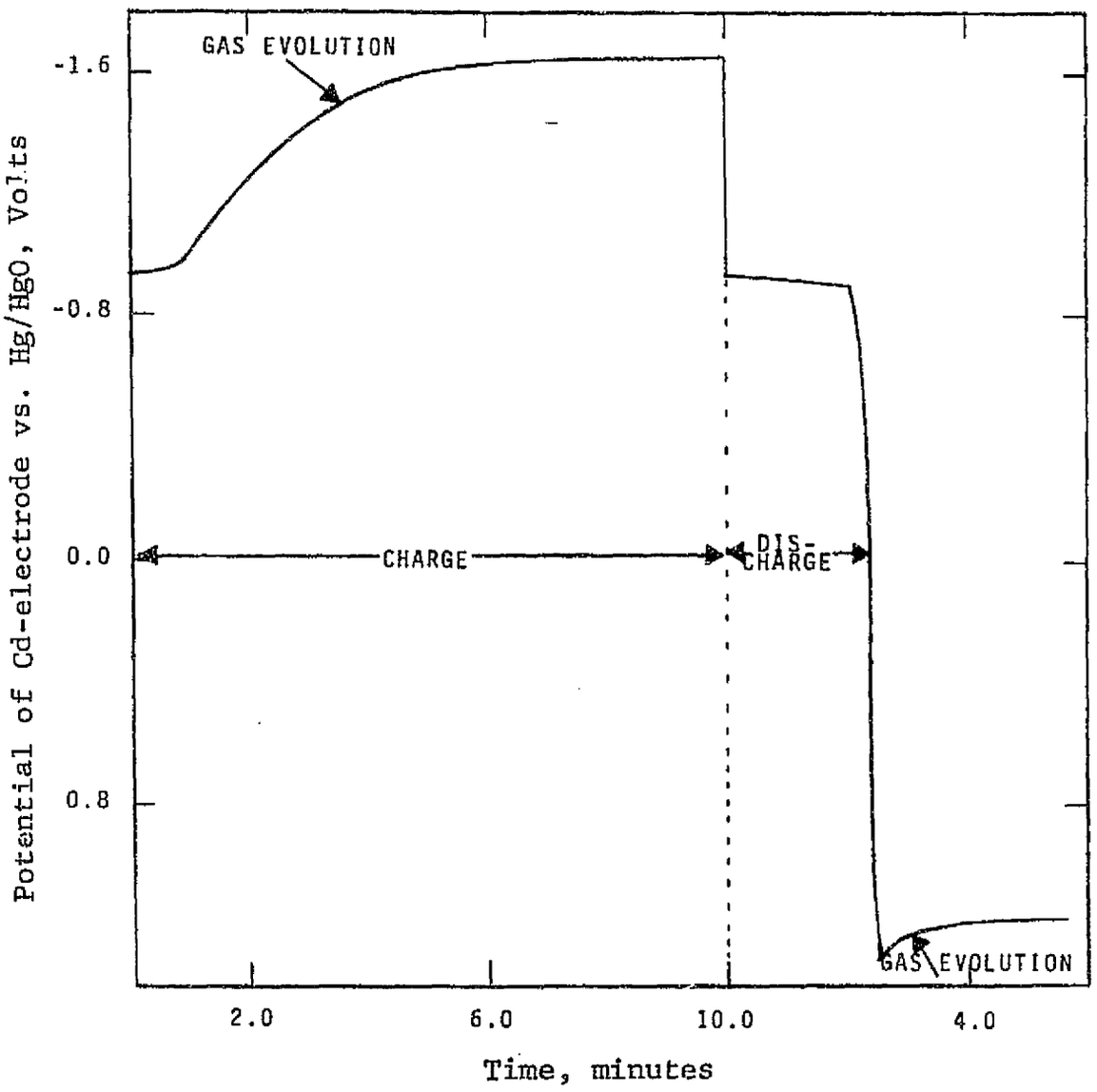

Figure 10. Typical charge-discharge behavior of the Cd-electrode

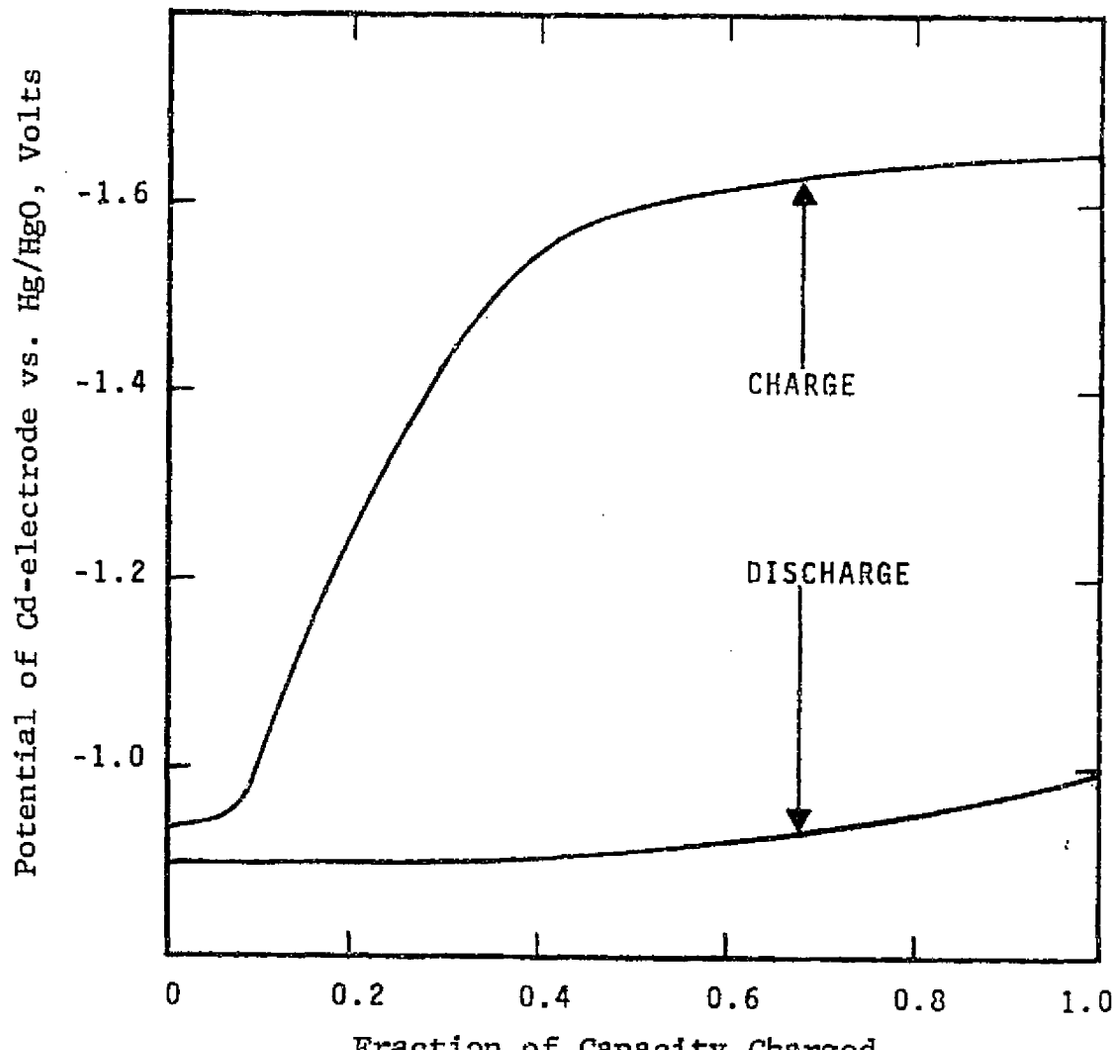

Figure 11. Typical charge-discharge behavior of the Cd-electrode as a function of fraction of capacity charged

Table 6

Charge acceptance of Cd-electrode under d-c charging conditions

Experiment #	No. of Runs	Charging Current mA	Charging Time Minutes	Average Discharge Time Minutes	Average % Deviation	Average Charge Acceptance mAhr	Average % Deviation
C1	10	5	5	1.865	1.060	0.156	0.632
C2	4	5	10	3.404	0.310	0.284	0.176
C3	3	5	15	4.000	0.540	0.333	0.150
C4	2	5	30	6.000	0.333	0.500	0.400
C5	4	10	5	4.800	0.230	0.400	0.250
C6	2	10	10	6.000	0.000	0.500	0.000

Table 7

Charge acceptance of Cd-electrode under p-c charging conditions

Experiment #	Number of Runs	Charging Current mA	$\frac{\theta}{\bar{\theta}}$	Frequency Cycles/ Sec	Charging Time Minutes
C7	2	5	0.1	50	50
C8	2	50	0.1	50	5
C9	1	5	0.1	200	50
C10	2	50	0.1	200	5
C11	2	5	0.5	50	10
C12	2	10	0.5	50	5
C13	1	5	0.5	200	10
C14	2	10	0.5	200	5
C15	2	5	0.75	50	7
C16	2	7	0.75	50	5
C17	1	5	0.75	200	7
C18	2	7	0.75	200	5
C19	2	5	0.25	50	20
C20	1	20	0.25	50	5
C21	2	5	0.25	200	20
C22	2	20	0.25	200	5

Table 7 (Continued)

Experiment #	Average Discharge Time Minutes	Average % Deviation	Average Charge Acceptance mAhr	Average % Deviation	Average Charge Accept.p-c / Charge Accept.d-c
C7	0.267	1.130	0.022	2.27	0.143
C8	1.856	0.600	0.156	0.640	0.997
C9	0.467	-	0.039	-	0.251
C10	1.951	0.333	0.162	0.307	1.045
C11	2.111	0.237	0.176	0.280	1.128
C12	2.267	1.014	0.189	0.529	1.215
C13	1.831	-	0.152	-	0.977
C14	1.905	0.260	0.158	0.316	1.020
C15	1.774	0.400	0.148	0.340	0.948
C16	1.838	1.000	0.153	0.653	0.984
C17	1.820	-	0.152	-	0.977
C18	1.937	0.230	0.162	0.600	1.039
C19	1.006	0.54	0.084	0.119	0.540
C20	1.944	-	0.162	-	1.042
C21	1.770	0.360	0.148	0.680	0.948
C22	2.020	0.330	0.168	0.591	1.083

Table 8

Charge acceptance of Cd-electrode under d-c and p-c charging conditions
(active material prepared at 5mA for 30 min.)

Exp. #	Charging Current mA	$\frac{\theta_1}{\theta}$	Frequency Cycles/ Sec	Charging Time Min.	Discharge Time Min.	Charge Acceptance mAhr	Charge Accept. p-c / Charge Accept. d-c
C23	5	-	-	5	1.98	0.165	-
C24	5	0.1	50	50	0.930	0.072	0.435
C25	5	0.5	50	10	2.040	0.170	1.003
C26	5	0.75	50	6.67	2.304	0.192	1.15
C27	10	0.10	50	25	1.176	0.098	0.600

self-discharge of the Cd-electrode was observed during the off period of the pulse. The dependence of self-discharge on duty cycle was studied and presented in Table 9.

B. Measurements on the Reduction of Concentration Overpotential

The anodic and cathodic limiting currents for the ferro-ferricyanide system were first measured under d-c conditions at six different rotation speeds. Results are summarized in Table 10 and shown in Fig. 12. Detailed calculations for all the results are presented in Appendix 3. From the experimental data, the overpotential at each applied current density was evaluated for all rotation speeds and summarized in Tables A7 to A11. Based on these tables a plot of current density versus overpotential was prepared and shown in Fig. 13. From Table 10 and eqns. (A16) and (A22) the values of the diffusion coefficients of the oxidized and reduced species were calculated at each rotation speed and tabulated in Table 11. In addition, the value of D was calculated from the slope of the line satisfying the relation that i_L is linear with respect to $\omega^{1/2}$ which is shown in Fig. 14. From this plot and eqn. (A25) the diffusion coefficients of the oxidized and reduced species were found to be 6.89×10^{-6} cm^2/sec and 8.42×10^{-6} cm^2/sec, respectively. The value of the exchange current density was calculated from eqn. (A30) at each rotation speed, results are

Table 9

Self-discharge of Cd-electrode during the off period of the pulse

Exp. #	Charging Current mA	$\frac{\theta_1}{\theta}$	Frequency Cycles/ sec	Charging Time Min.	Self-Discharge at off period of Pulse mA	Net Charge per Cycle of Pulse mAm sec
C28	5	0.1	50	50	0.2–0.5	6.4-1
C29	5	0.5	50	10	1.0–2.0	40–30
C30	5	0.75	50	6.67	1.5–3.5	67.5–57.5
C31	10	0.10	50	25	0.4–0.8	12.8–5.4

Table 10

Limiting current densities for the ferro-ferricyanide system at six rotation speeds

Rotation Speed Rad/Sec	$\omega^{1/2}$ $(Rad/Sec)^{1/2}$	Anodic Limiting Current Density mA/cm^2	Cathodic Limiting Current Density mA/cm^2
41.8879	6.4726	0.9115	0.9766
95.3186	9.7887	1.3238	1.4540
168.5988	12.9846	1.7578	1.9531
261.7994	16.1802	2.2135	2.5174
376.9911	19.4163	2.6259	3.0165
518.3628	22.7676	3.0816	3.5373

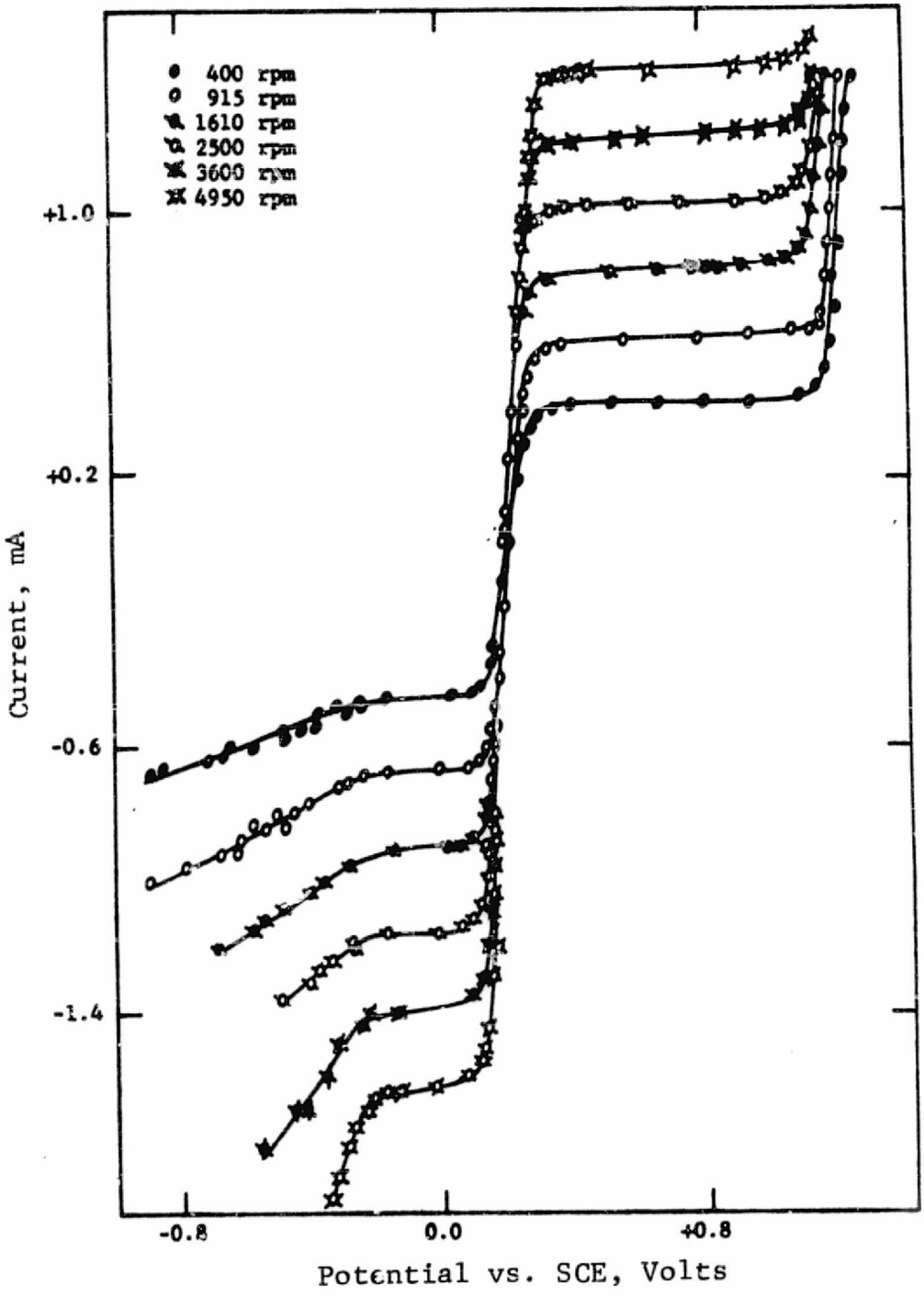

Figure 12. Current-potential plot at six rotation speeds for the ferro-ferricyanide system, under d-c conditions

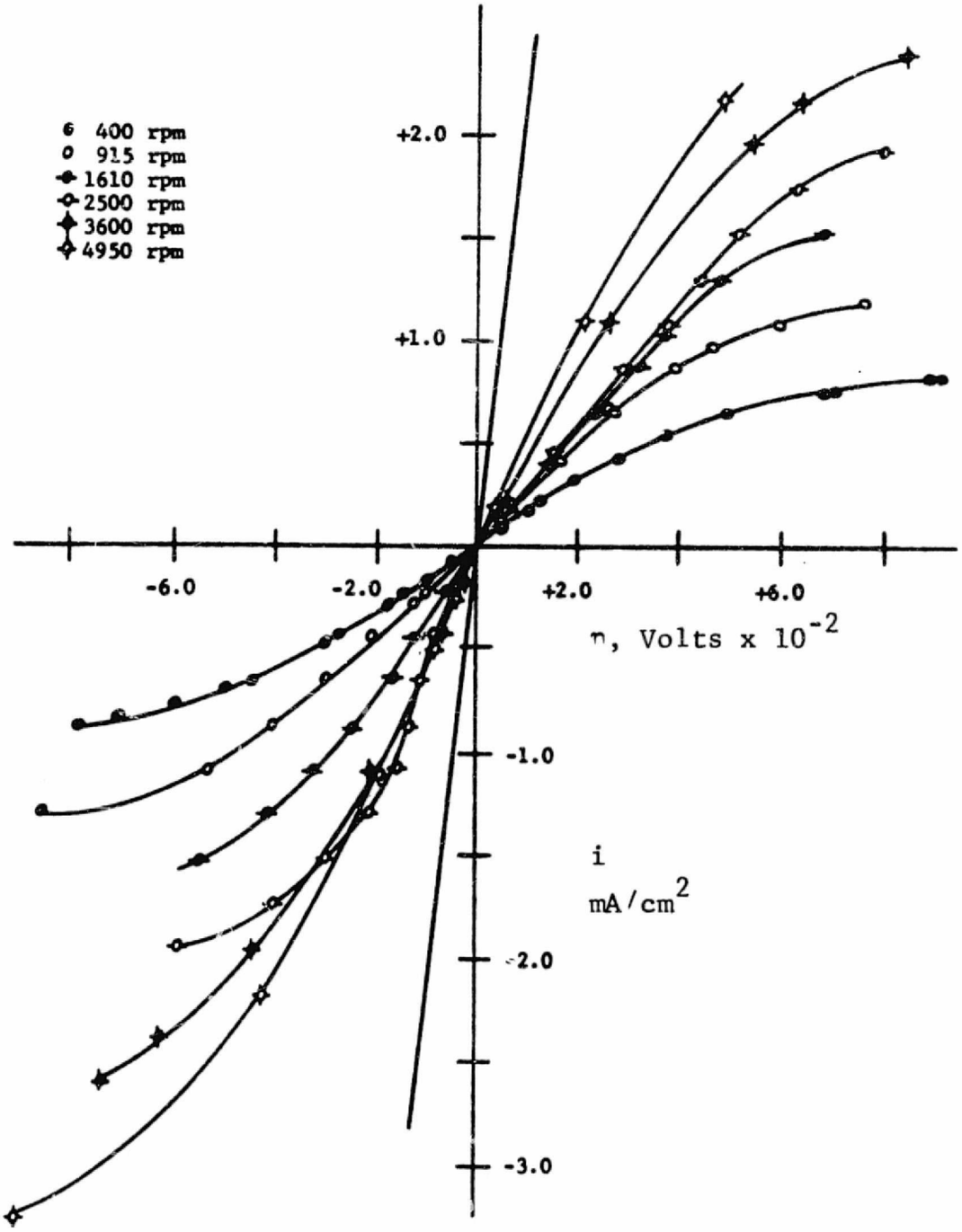

Figure 13. A plot of current density vs. overpotential at six rotation speeds for the ferro-ferricyanide system, under d-c conditions

Table 11

Diffusion coefficient calculations for the ferro-ferricyanide system, from eqns. (A16) and (A22)

	i_L mA	i_L mA/cm^2	$\omega^{1/2}$ (Rad/Sec)$^{1/2}$	A	A^{-1}	D cm^2/sec
Anodic	0.42	0.9115	6.4721	0.00784	127.5454	$7.235 * 10^{-6}$
	0.61	1.3238	9.7887	0.007529	132.8247	$6.8021 * 10^{-6}$
	0.81	1.7578	12.9846	0.007536	132.6892	$6.8127 * 10^{-6}$
	1.02	2.2135	16.1802	0.007616	131.2048	$6.9222 * 10^{-6}$
	1.21	2.6259	19.4163	0.007529	132.8204	$6.8025 * 10^{-6}$
	1.42	3.0816	22.7676	0.007535	132.7142	$6.8107 * 10^{-6}$
					$(D_A)_{Avg.}$ =	6.8975×10^{-6} cm^2/sec
Cathodic	0.45	0.9766	6.4721	0.0084	119.0433	$8.036 * 10^{-6}$
	0.67	1.4540	9.7887	0.008269	120.9308	$7.8458 * 10^{-6}$
	0.90	1.9531	12.9846	0.008374	119.4209	$7.8867 * 10^{-6}$
	1.16	2.5174	16.1802	0.008661	115.7537	$8.4194 * 10^{-6}$
	1.39	3.0165	19.4163	0.008649	115.6217	$8.4008 * 10^{-6}$
	1.63	3.5373	22.7676	0.008649	115.6170	$8.4013 * 10^{-6}$
					$(D_C)_{Avg.}$ =	8.165×10^{-6} cm^2/sec.

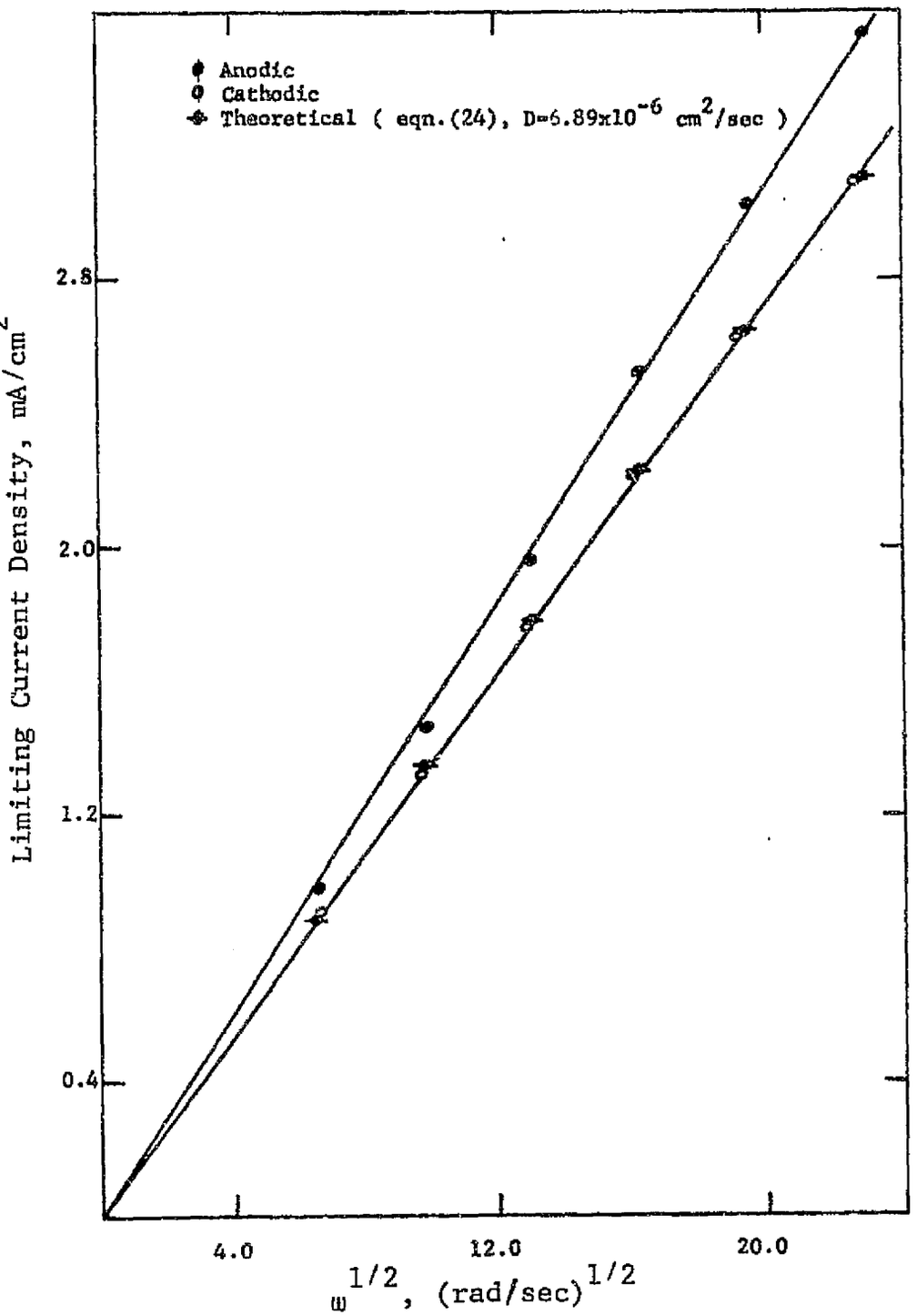

Figure 14. A plot used for evaluating the diffusion coefficients of the ferro-ferricyanide system

summarized in Table 12. The average value of the exchange current density was found to be 5.733 mA/cm^2. To determine the values of the transfer coefficients a plot of

$$\ln \frac{i}{1 - \exp\left(-\frac{nF}{RT}\eta\right)} \text{ vs } \eta$$

was prepared and shown in Fig. 15. From eqn. (A37) and the slopes of the lines, the transfer coefficients for the oxidation and reduction reactions were found to be 0.16 and 0.82, respectively.

Under pulsed current electrolysis, the average electrode potential was obtained by numerical integration of the curves taken from the oscilloscope, during one complete cycle of the applied pulsed current (cf. Appendix 3). The average value of the concentration overpotential was then obtained from a knowledge of the reversible electrode potential and the activation overpotential. The experimental data and the reduction of concentration overpotential for both anodic and cathodic reactions are summarized in Tables 13-16. The theoretically calculated and experimentally determined values of the reduction of concentration overpotential are given in Fig. 16.

C. Mechanistic Studies

1. Limiting Current Measurements

The anodic and cathodic limiting currents of the Ni-electrode were measured at five different rotation speeds, under galvanostatic conditions with a sweep rate of

Table 12

Exchange current density of the ferro-ferricyanide system at various rotation speeds obtained from eqn. (A30)

w rpm	i_{LA} mA/cm^2	i_{LC} mA/cm^2	$\frac{di}{d\eta}_{\eta \to o}$ $\frac{mA/cm^2}{V}$	i_o mA/cm^2
400	0.9115	-0.9766	17	5.8698
915	1.3238	-1.4540	24	5.5578
1610	1.7578	-1.9531	31	5.6920
2500	2.2135	-2.5175	38	5.6780
3600	2.6259	-3.0165	45	5.7807
4950	3.0816	-3.5373	50	5.8182

$(i_o)_{Avg.} = 5.733 mA/cm^2$

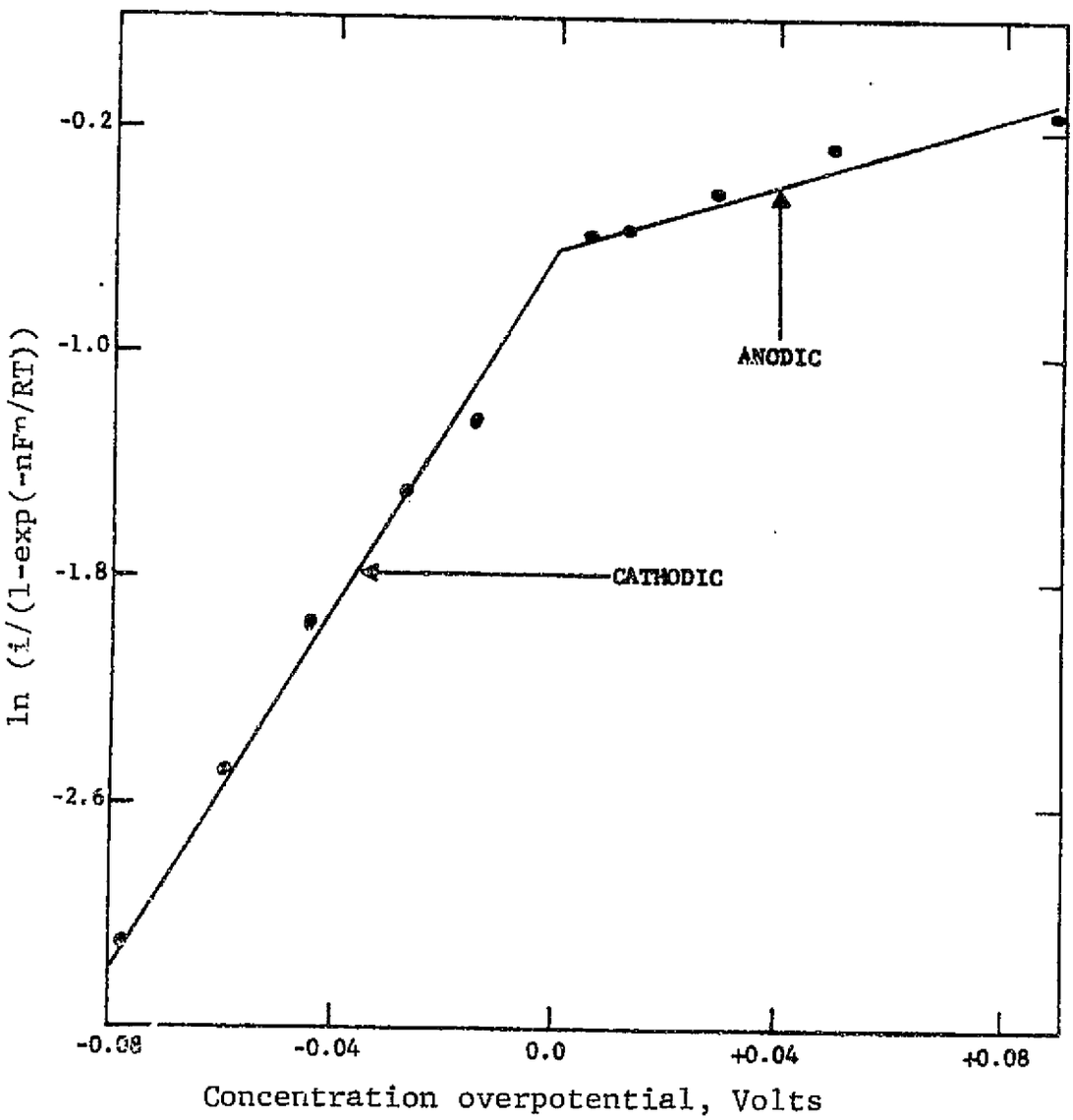

Figure 15. A plot used for evaluating the transfer coefficients of the ferro-ferricyanide system

Table 13

Ferro-ferricyanide system, experimental data and reduction of concentration overpotential during the anodic reaction, under p-c conditions and 1610 rpm

Exp. #	rpm	θ_1/θ	$\frac{i_p}{(i_{d-c})_L}$	i_p mA	i_p mA/cm^2	Potential Volts	V_o Volts
FA1			0.2	0.162	0.3515	0.21606	
FA2			0.4	0.324	0.7031	0.21861	
FA3	1610	0.2	0.6	0.486	1.0576	0.2213	0.212
FA4			0.8	0.648	1.4061	0.224	
FA5			0.2	0.162	0.3515	0.2182	
FA6			0.4	0.324	0.7031	0.2227	
FA7	1610	0.4	0.6	0.486	1.0546	0.2266	0.212
FA8			0.8	0.648	1.4061	0.2305	
FA9			0.2	0.162	0.3515	0.2204	
FA10			0.4	0.324	0.7031	0.2269	
FA11	1610	0.6	0.6	0.486	1.0546	0.2329	0.212
FA12			0.8	0.648	1.4061	0.2391	
FA13			0.2	0.162	0.3515	0.2227	
FA14			0.4	0.324	0.7031	0.2318	
FA15	1610	0.8	0.6	0.486	1.0547	0.2403	0.212
FA16			0.8	0.648	1.4061	0.2507	

Table 13 (Continued)

Exp. #	η_p Volts	η_a Volts	η_{d-c} Volts	$(\eta_p)_c$ Volts	$(\eta_{d-c})_c$ Volts	$\frac{(\eta_p)_c}{(\eta_{dc})_c}$
FA1	0.00406	0.002	0.013	0.00206	0.011	0.1873
FA2	0.00661	0.0032	0.025	0.00341	0.0218	0.1565
FA3	0.0093	0.0045	0.038	0.0048	0.0335	0.1433
FA4	0.012	0.0065	0.056	0.0055	0.0495	0.1111
FA5	0.0062	0.002	0.013	0.0042	0.011	0.381
FA6	0.0107	0.0032	0.025	0.0075	0.0218	0.344
FA7	0.0146	0.0045	0.038	0.0101	0.0335	0.3018
FA8	0.0185	0.0065	0.056	0.012	0.0495	0.2424
FA9	0.0084	0.002	0.013	0.0064	0.011	0.5818
FA10	0.0149	0.0032	0.025	0.0117	0.0218	0.5385
FA11	0.0209	0.0045	0.038	0.0164	0.0335	0.4896
FA12	0.0271	0.0065	0.056	0.0206	0.0495	0.416
FA13	0.0107	0.002	0.013	0.0087	0.011	0.7909
FA14	0.0198	0.0032	0.025	0.0166	0.218	0.7615
FA15	0.0283	0.0045	0.038	0.0238	0.0335	0.7104
FA16	0.0387	0.0065	0.056	0.0322	0.0495	0.6505

Table 14

Ferro-ferricyanide system, experimental data and reduction of concentration overpotential during the anodic reaction, under p-c conditions and three rotation speeds

Exp. #	rpm	θ_l/θ	$\frac{i_p}{(i_{d-c})_L}$	mA	i_p mA/cm^2	Potential Volts	V_o Volts
FA21		0.2	0.2	0.122	0.2647		
FA22	915	0.2	0.6	0.366	0.7942		0.212
FA27		0.2	0.2	0.204	0.4427	0.2167	
FA28	2500	0.2	0.6	0.612	1.328	0.2236	
FA33		0.2	0.2	0.242	0.5251	0.2165	
FA34		0.2	0.6	0.726	1.5754	0.2230	
FA36	3600	0.4	0.6	0.726	1.5754	0.2285	0.212
FA37		0.6	0.6	0.726	1.5754	0.2348	
FA38		0.8	0.6	0.726	1.5754	0.2427	

Table 14 (continued)

Exp. #	η_p Volts	η_a volts	η_{d-c} volts	$(\eta_p)_c$ volts	$(\eta_{d-c})_c$ volts	$\frac{(\eta_p)_c}{(\eta_{dc})_c}$	$1-\frac{\theta}{\theta_1}\frac{(\eta_p)_c}{(\eta_{dc})_c}$
FA21		0.0014	0.01		0.0086		
FA22		0.0038	0.034		0.0302		
FA27	0.0047	0.0021	0.016	0.0026	0.0139	0.187	0.065
FA28	0.0112	0.0060	0.0452	0.0056	0.0392	0.143	0.285
FA33	0.0045	0.0025	0.0129	0.002	0.0104	0.1923	0.0385
FA34	0.011	0.0061	0.0405	0.0049	0.0344	0.1424	0.288
FA36	0.0165	0.0061	0.0405	0.0104	0.0344	0.302	0.245
FA37	0.0228	0.0061	0.0405	0.0167	0.0344	0.4855	0.1908
FA38	0.0307	0.0061	0.0405	0.0276	0.0344	0.7151	0.1061

Table 15

Ferro-ferricyanide system, experimental data and reduction of concentration overpotential during the cathodic reaction, under p-c conditions and 1610 rpm

Exp. #	rpm	$\frac{\theta_1}{\theta}$	$\frac{i_p}{(i_{d-c})_L}$	i_p mA	i_p mA/cm^2	Potential Volts	V_o Volts
FC1			0.2	0.18	0.3906	0.2085	
FC2			0.4	0.36	0.7812	0.2053	
FC3	1610	0.2	0.6	0.54	1.1718	0.2024	0.212
FC4			0.8	0.72	1.5624	0.19906	
FC5			0.2	0.18	0.3906	0.2067	
FC6			0.4	0.36	0.7812	0.20239	
FC7	1610	0.4	0.6	0.54	1.1718	0.1975	0.212
FC8			0.8	0.72	1.5624		
FC9			0.2	0.18	0.3906	0.20483	
FC10			0.4	0.36	0.7812	0.1989	
FC11	1610	0.6	0.6	0.54	1.1718	0.1918	0.212
FC12			0.8	0.72	1.5624	0.1832	
FC13			0.2	0.18	0.3906	0.2029	
FC14			0.4	0.36	0.7812	0.1953	
FC15	1610	0.8	0.6	0.54	1.1718	0.1849	0.212
FC16			0.8	0.72	1.5624	0.171	

Table 15 (Continued)

Exp. #	η_p Volts	η_a Volts	η_{d-c} Volts	$(\eta_p)_c$ Volts	$(\eta_{d-c})_c$ Volts	$\frac{(\eta_p)_c}{(\eta_{d-c})_c}$
FC1	0.0035	0.0018	0.011	0.0017	0.0092	0.1848
FC2	0.0067	0.0038	0.021	0.0029	0.0172	0.1686
FC3	0.0096	0.0051	0.036	0.0045	0.0309	0.1456
FC4	0.01294	0.0071	0.060	0.00584	0.0529	0.1104
FC5	0.0053	0.0018	0.011	0.0035	0.0092	0.3804
FC6	0.00961	0.0038	0.021	0.00581	0.0172	0.338
FC7	0.0145	0.0051	0.036	0.0094	0.0309	0.3042
FC8	0.0198	0.0071	0.060	0.0127	0.0529	0.240
FC9	0.00717	0.0018	0.011	0.00537	0.0092	0.584
FC10	0.0131	0.0038	0.021	0.0093	0.0172	0.5407
FC11	0.0202	0.0051	0.036	0.0151	0.0309	0.489
FC12	0.0288	0.0071	0.060	0.0217	0.0529	0.4102
FC13	0.0091	0.0018	0.011	0.0073	0.0092	0.7935
FC14	0.0167	0.0038	0.021	0. 0129	0.0172	0.75
FC15	0.0271	0.0051	0.036	0.022	0.0309	0.712
FC16	0.041	0.0071	0.060	0.0339	0.0529	0.6408

Table 16

Ferro-ferricyanide system, experimental data and reduction of concentration overpotential during the cathodic reaction, under p-c conditions and three rotation speeds

Exp. #	rpm	$\frac{\theta l}{\theta}$	$\frac{i_p}{(i_{d-c})_L}$	i_p mA	i_p mA/cm^2	Potential Volts	V_o Volts
FC17		0.2	0.2	0.134	0.2908	0.2085	
FC18		0.2	0.6	0.402	0.8723	0.2036	
FC19	915	0.4	0.6	0.402	0.8723	0.1963	0.212
FC20		0.6	0.6	0.402	0.8723	0.1900	
FC21		0.8	0.6	0.402	0.8723	0.1817	
FC22		0.2	0.2	0.232	0.5034	0.2084	
FC23		0.2	0.6	0.696	1.5103	0.2178	
FC24	2500	0.4	0.6	0.696	1.5103	0.1983	0.212
FC25		0.6	0.6	0.696	1.5103	0.1943	
FC26		0.8	0.6	0.696	1.5103	0.1893	
FC27		0.2	0.2	0.278	0.6033	0.2077	
FC28		0.2	0.6	0.834	1.8097	0.1994	
FC29	3600	0.4	0.6	0.834	1.8097	0.1947	0.212
FC30		0.6	0.6	0.834	1.8097	0.1888	
FC31		0.8	0.6	0.834	1.8097	0.1822	

Table 16 (continued)

Exp. #	η_p Volts	η_a Volts	η_{d-c} Volts	$(\eta_p)_c$ Volts	$(\eta_{d-c})_c$ Volts	$\frac{(\eta_p)_c}{(\overline{\eta_{dc}})_c}$
FC17	0.0035	0.0012	0.0134	0.0023	0.0122	0.1885
FC18	0.0094	0.004	0.041	0.0054	0.037	0.146
FC19	0.0157	0.004	0.041	0.0117	0.037	0.3162
FC20	0.022	0.004	0.041	0.018	0.037	0.4865
FC21	0.0303	0.004	0.041	0.0263	0.037	0.7108
FC22	0.0036	0.0022	0.0097	0.0014	0.0075	0.1867
FC23	0.01022	0.0070	0.029	0.00322	0.022	0.1464
FC24	0.0137	0.007	0.029	0.0067	0.022	0.3045
FC25	0.0177	0.007	0.029	0.0107	0.022	0.4864
FC26	0.0227	0.007	0.029	0.0157	0.022	0.7136
FC27	0.0043	0.0029	0.011	0.0014	0.0081	0.173
FC28	0.0126	0.0082	0.039	0.0044	0.0308	0.143
FC29	0.0173	0.0082	0.039	0.0091	0.0308	0.2955
FC30	0.02317	0.0082	0.039	0.01497	0.0308	0.486
FC31	0.0298	0.0082	0.039	0.0216	0.0308	0.7013

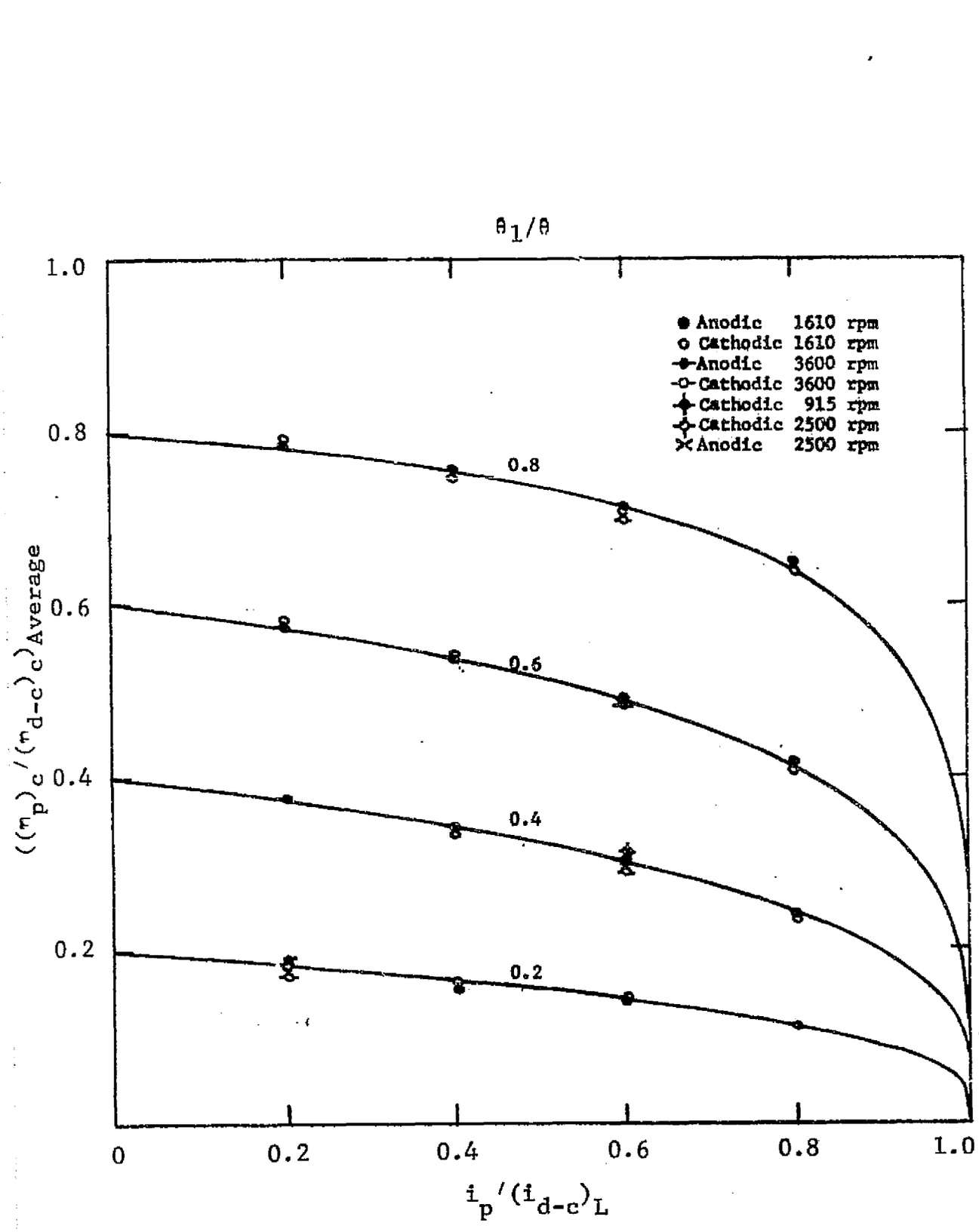

Figure 16. Theoretical and experimental values of the average reduction of concentration overpotential as a function of duty cycle and instantaneous p-c density, for aθ of 0.5

0.4 mA/min . Results are shown in Fig. 17. In addition, experiments were conducted with various sweep rates and a rotation speed of 400 rpm as shown in Fig. 18. Cyclic sweeps at two different sweep rates were performed and are represented in Fig. 19.

The anodic and cathodic limiting currents for the Cd-electrode were measured at five different rotation speeds with a sweep rate of 0.5 mA/min. Results are summarized in Fig. 20. All the results for Ni- and Cd-electrodes were based on an average obtained from duplicate runs.

2. Cyclic Sweep Experiments

Cyclic potential sweeps were performed for the stationary film Ni-electrode under mild stirring conditions and several sweep rates. Results are given in Figs. 21-23. In order to compare the system behavior with that reported by MacArthur (33), experiments were conducted under conditions similar to those used in his work. Results are shown in Fig. 24. In addition, cyclic sweeps under controlled current were carried out at several sweep rates as shown in Fig. 25.

Cyclic potential sweeps for the stationary film Cd-electrode were conducted at a sweep rate of 0.1 V/min Results are shown in Fig. 26. In addition, cyclic sweeps under controlled current and several different sweep rates were performed and shown in Fig. 27. All the results for Ni- and Cd-electrodes were based on an average from

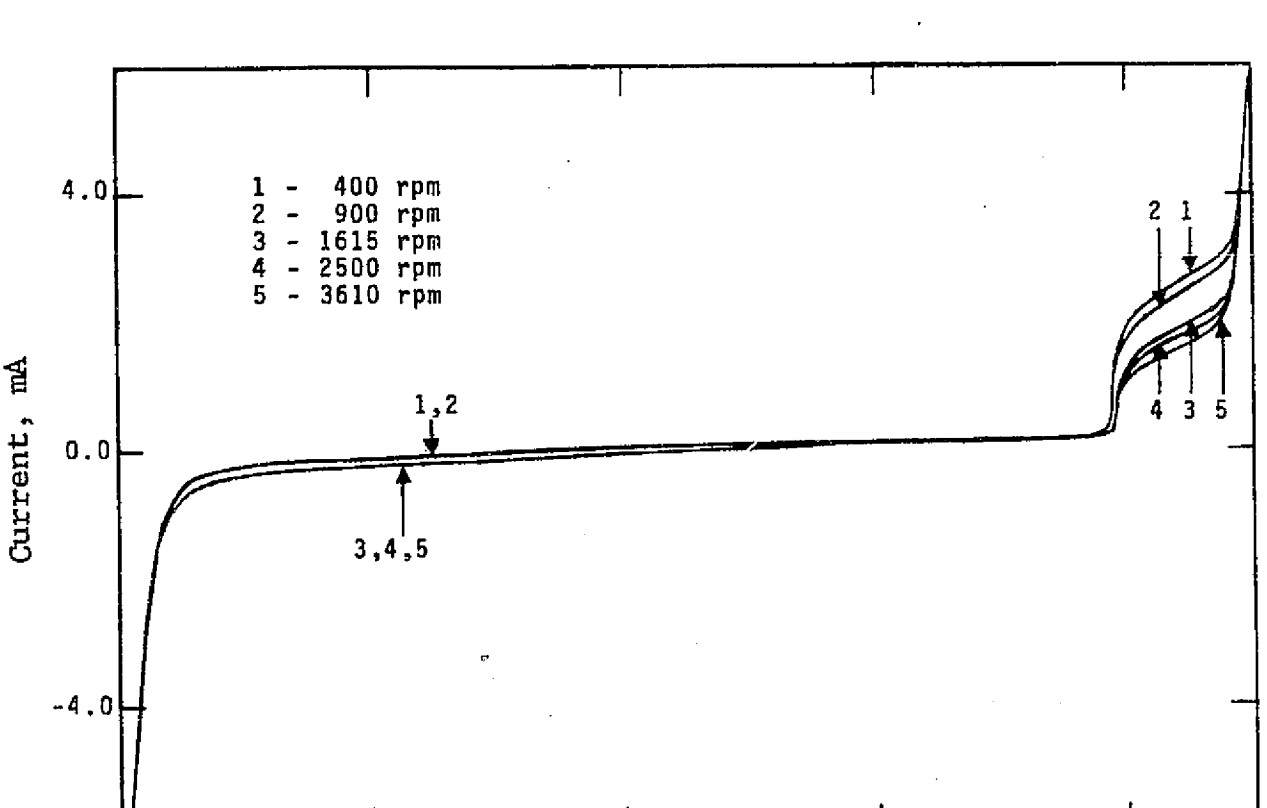

Figure 17. Current-potential behavior of the Ni-electrode at five rotation speeds and a sweep rate of 0.4mA/min

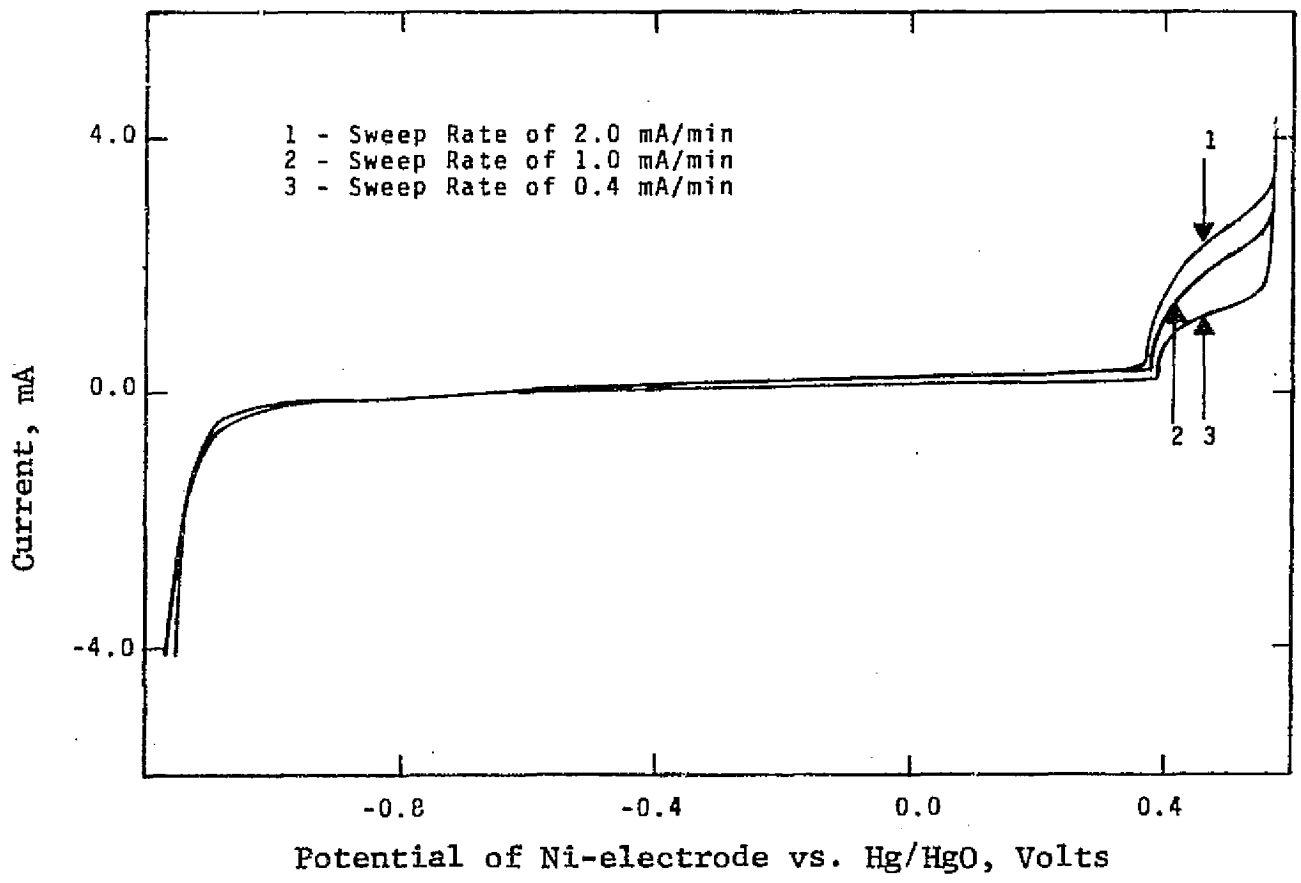

Figure 18. Current-potential behavior of the Ni-electrode at several sweep rates and 400 rpm

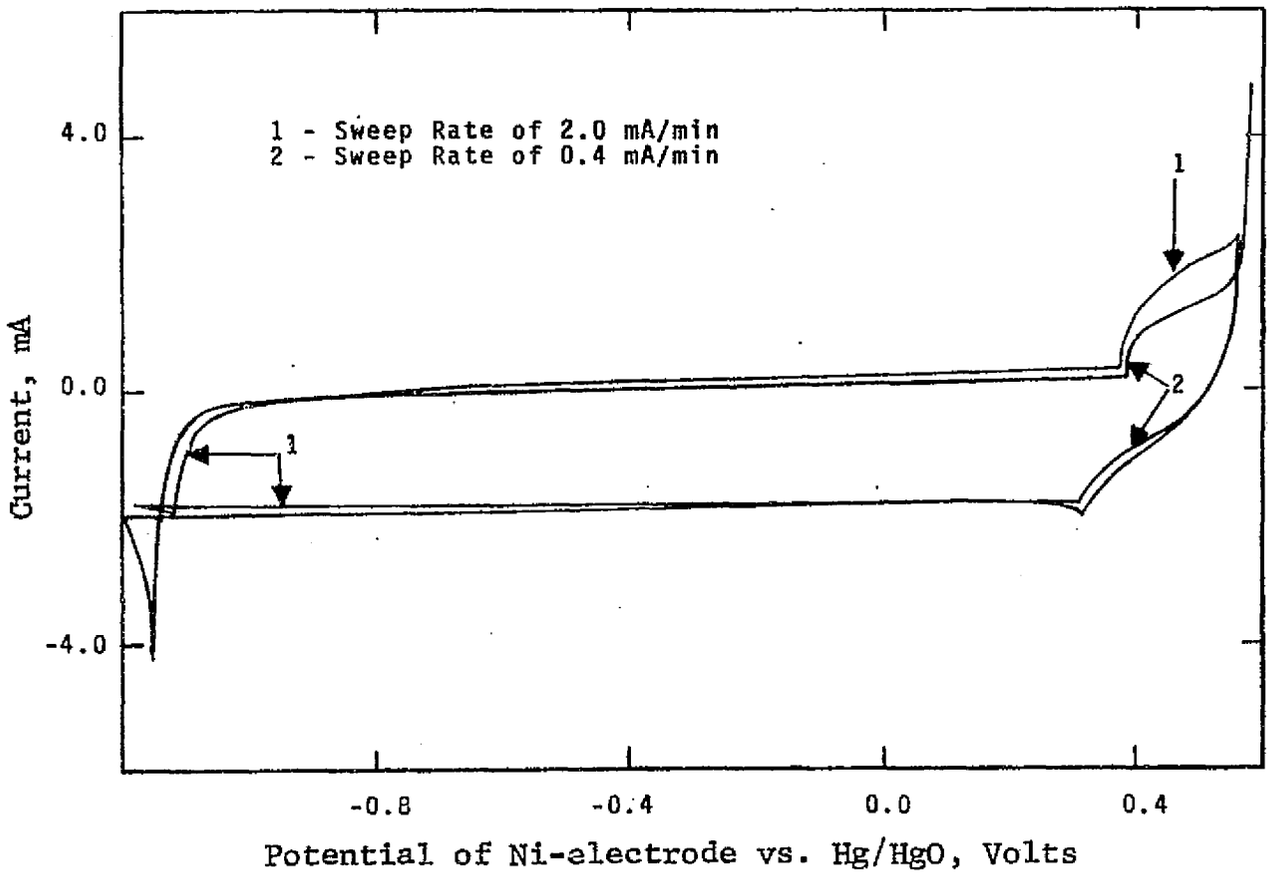

Figure 19. Ni-electrode, full sweeps at 400 rpm

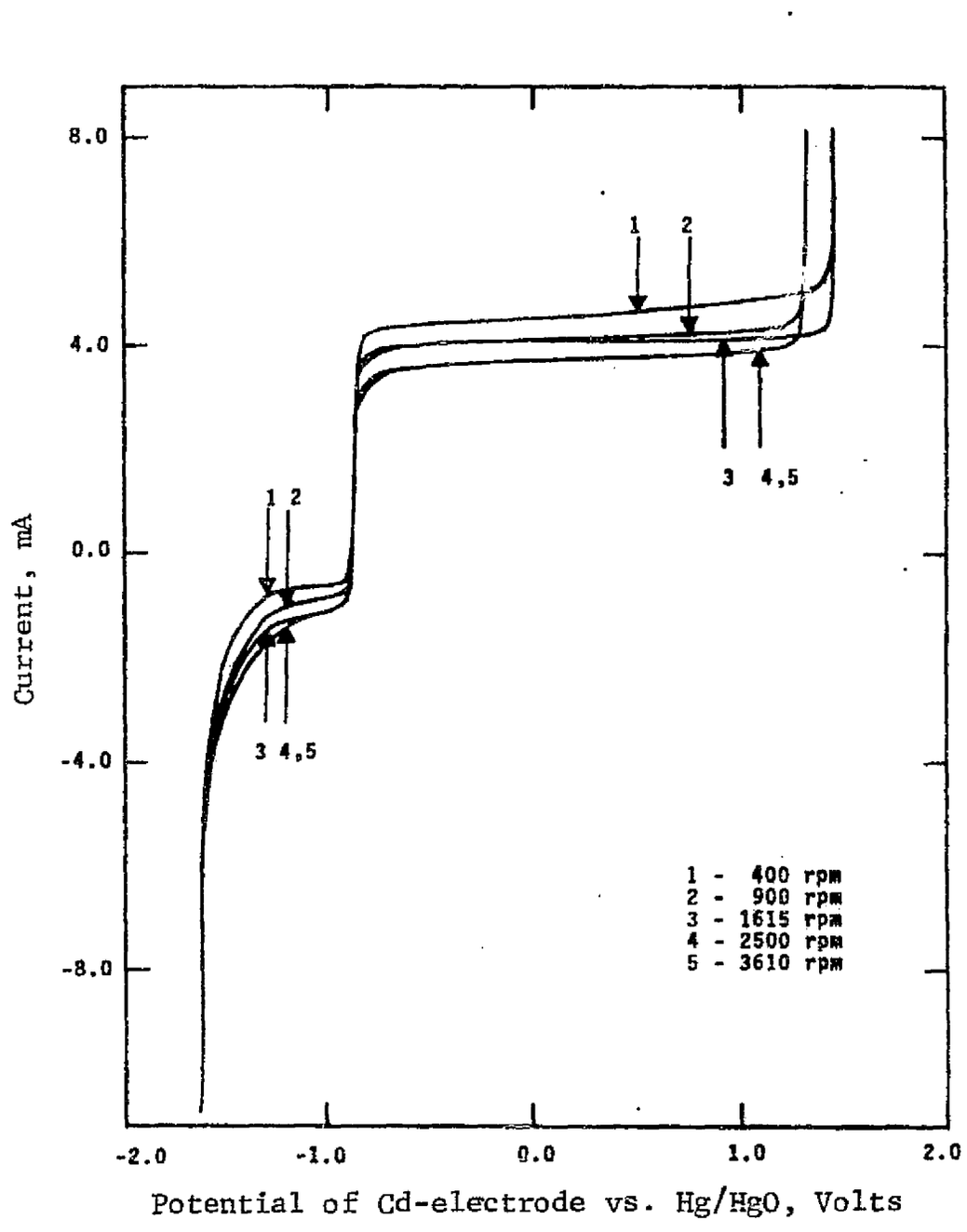

Figure 20. Current-potential behavior of the Cd-electrode at five rotation speeds and a sweep rate of 0.5mA/min

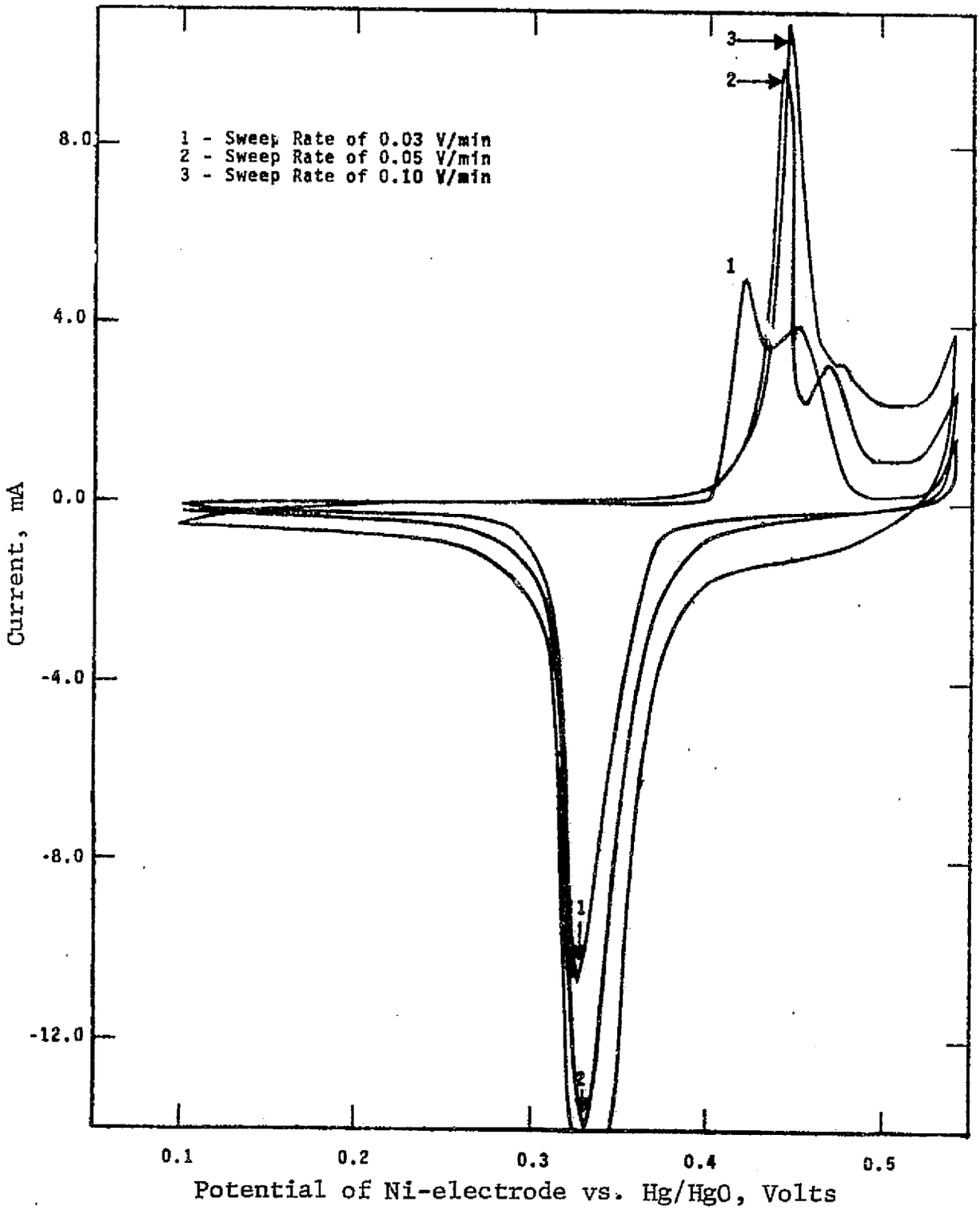

Figure 21. Cyclic potential sweep for the Ni-electrode at three sweep rates

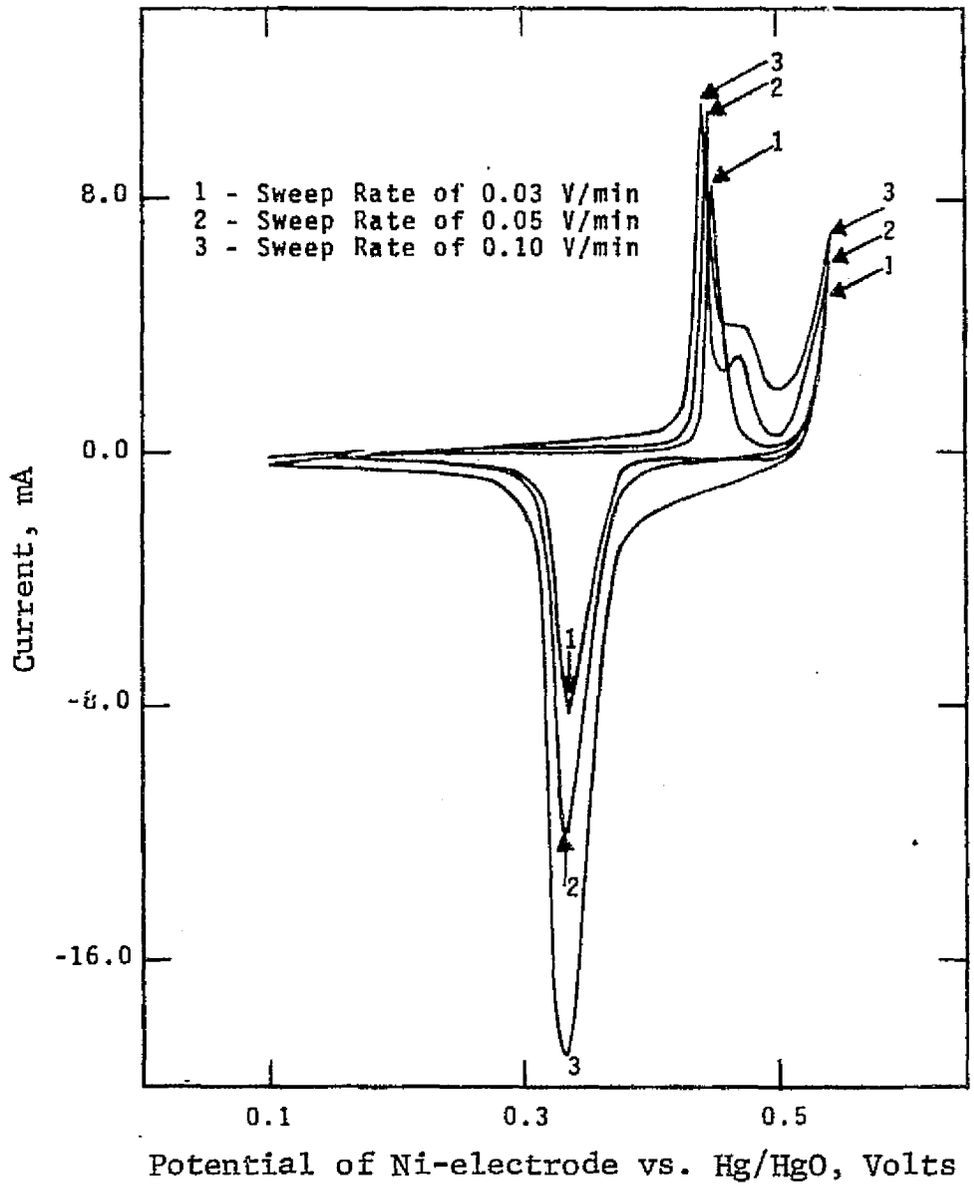

Figure 22. Cyclic potential sweep for the Ni-electrode at three sweep rates

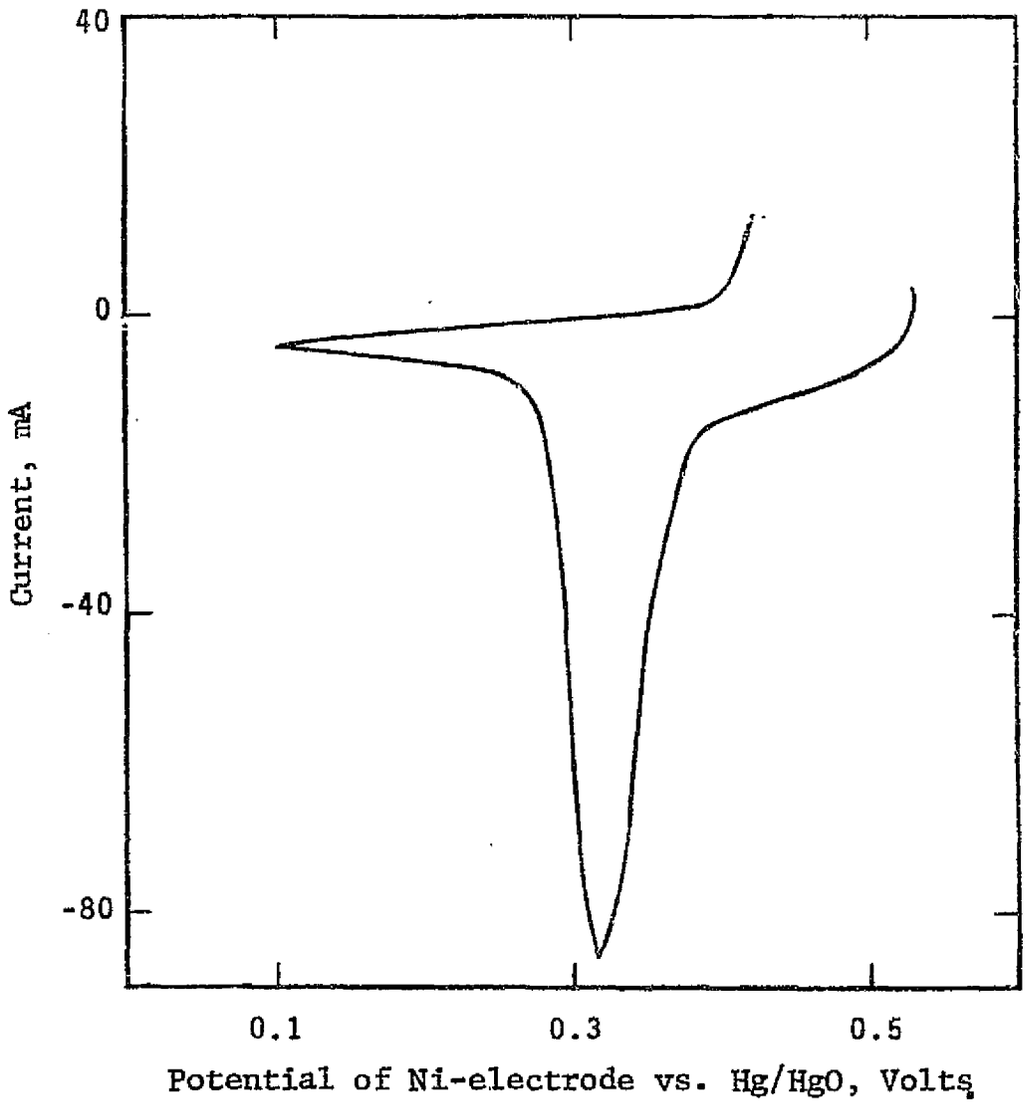

Figure 23. Cyclic potential sweep for the Ni-electrode at a sweep rate of 1V/min

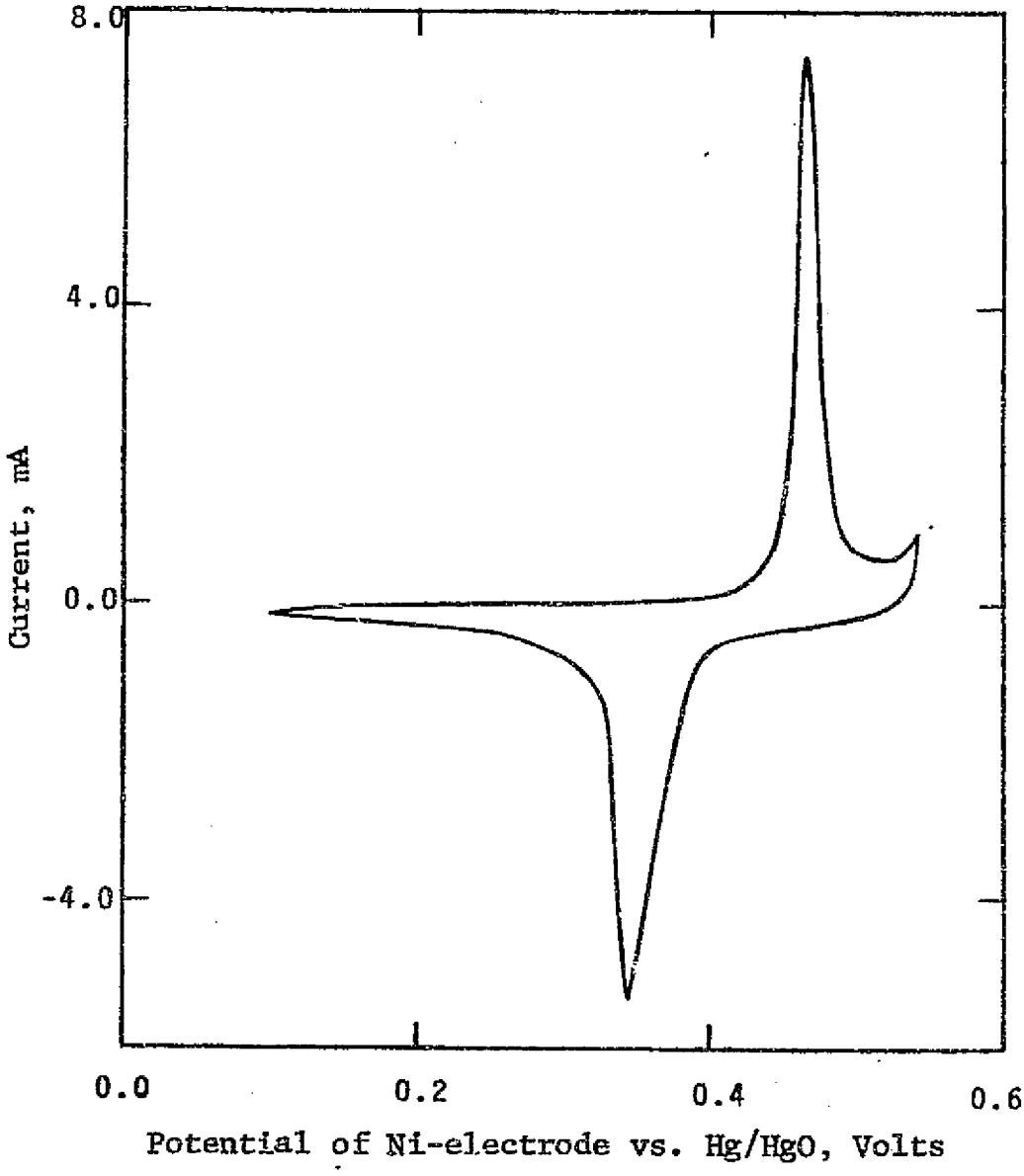

Figure 24. Cyclic potential sweep for the Ni-electrode at a sweep rate of 1.8 V/h and conditions similar to those used by MacArthur (33)

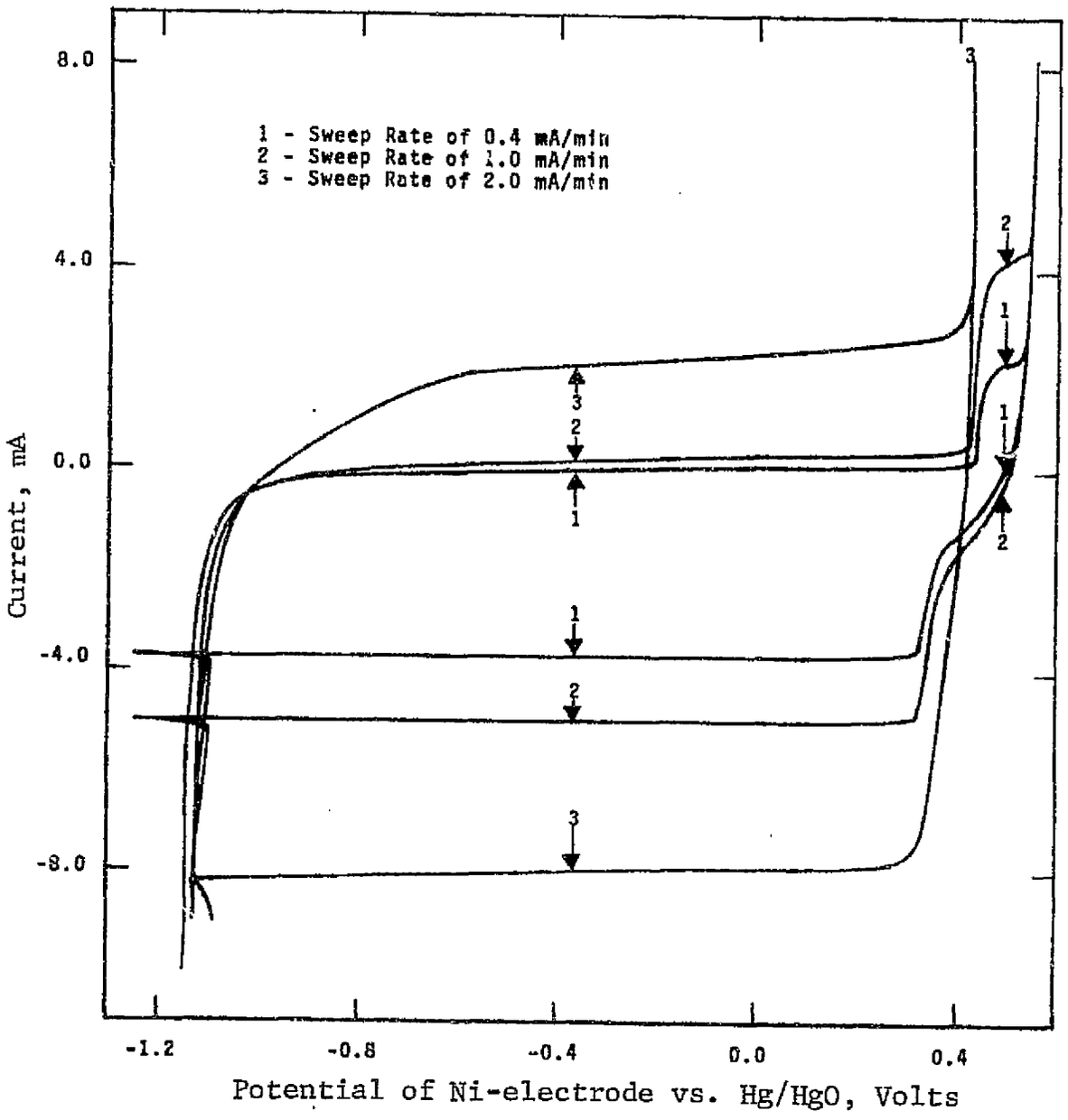

Figure 25. Cyclic sweep for the Ni-electrode under controlled current conditions and three sweep rates

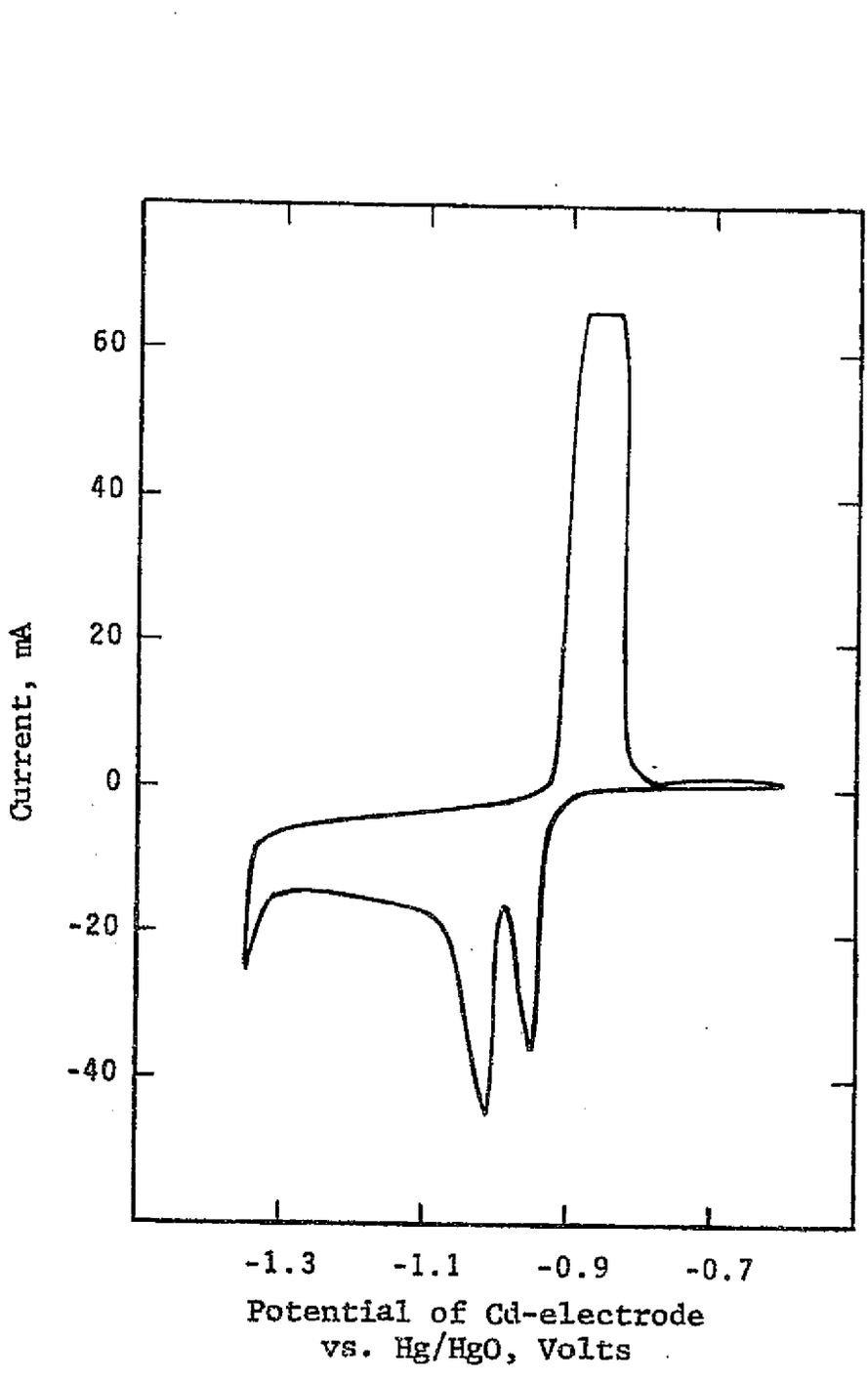

Figure 26. Cyclic potential sweep for the Cd-electrode at a sweep rate of 0.1V/min

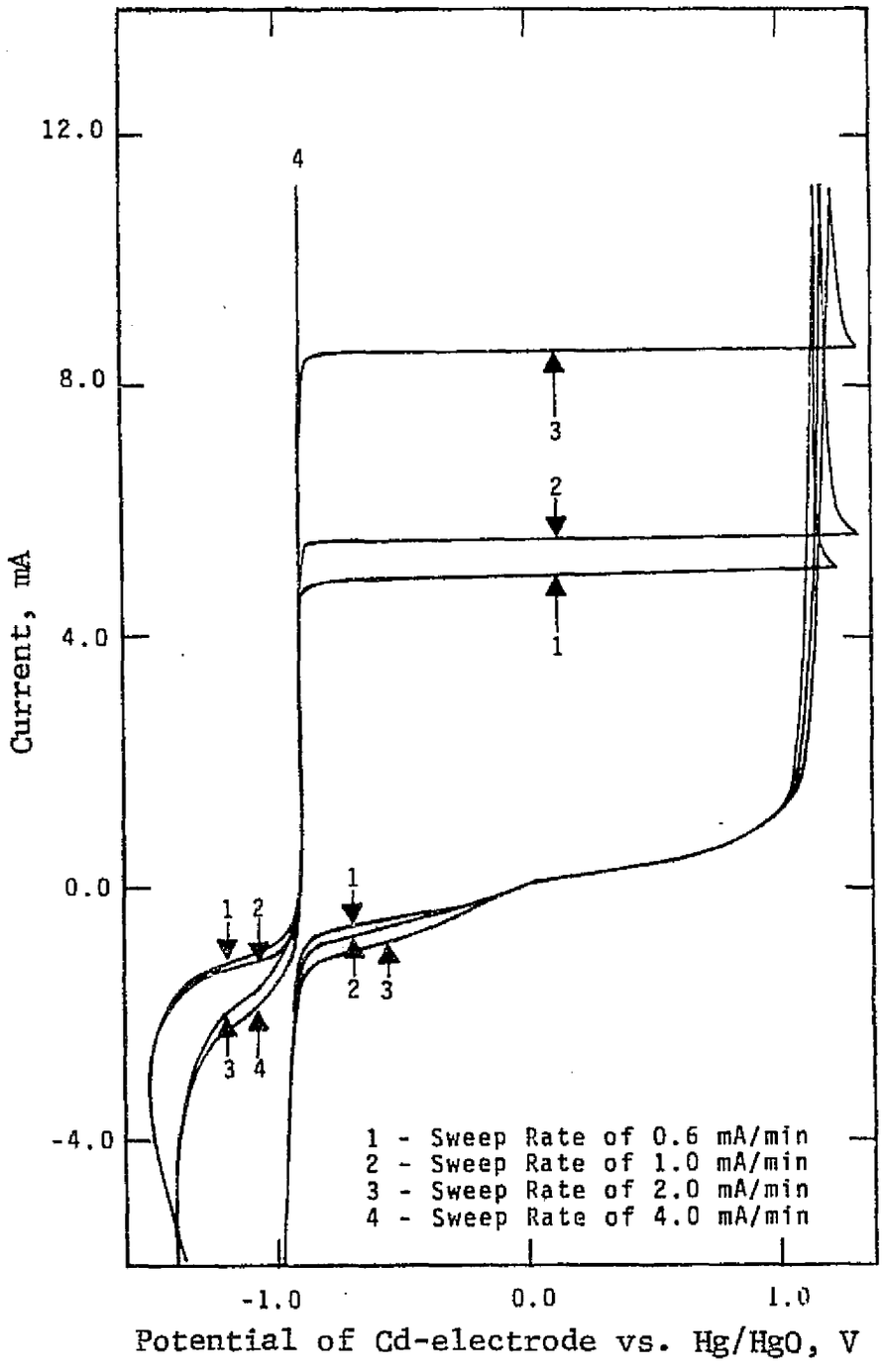

Figure 27. Cyclic sweep for the Cd-electrode under controlled current conditions and four sweep rates

duplicate experiments.

D. Structural Studies

1. SEM

The surface morphology of a charged Ni-electrode was studied with electrodes charged under d-c and various p-c conditions. Two drying methods, one in air and one in vacuum were employed for the preparation of the samples. Magnifications of 3000x and 10000x were found to provide useful information. Typical pictures of the electrode surface at magnifications of 3000x and 10000x are shown in Figs. 28 and 29, respectively.

Similarly, for a charged Cd-electrode, studies were performed on electrodes charged under d-c and several different p-c conditions. In order to observe the extent of uniformity of the surface, montages of magnification of 3000x were prepared and shown in Figs. 30-35. In addition, particular sections from the montages which were typical of the surface were magnified at 10000x and 30000x and shown in Figs. 36 and 37 and Figs. 38 and 39, respectively.

2. TEM

In order to observe the different phases existing in the charged active material of the Cd-electrode, TEM was performed on two samples charged under d-c and p-c conditions. Results are shown in Fig. 40.

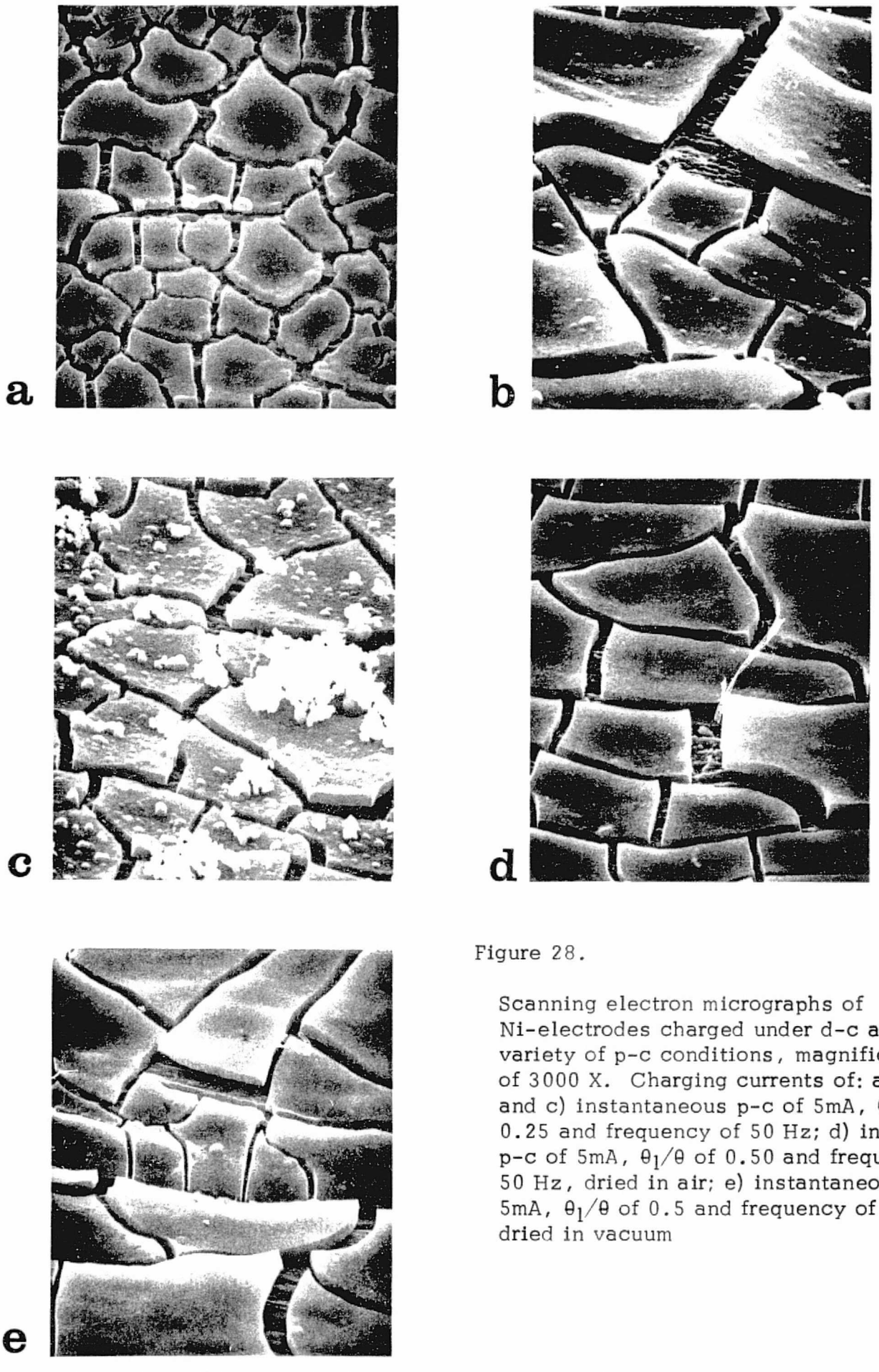

Figure 28.

Scanning electron micrographs of Ni-electrodes charged under d-c and variety of p-c conditions, magnification of 3000 X. Charging currents of: a) d-c; b) and c) instantaneous p-c of 5mA, θ_1/θ of 0.25 and frequency of 50 Hz; d) instantaneous p-c of 5mA, θ_1/θ of 0.50 and frequency of 50 Hz, dried in air; e) instantaneous p-c of 5mA, θ_1/θ of 0.5 and frequency of 50 Hz, dried in vacuum

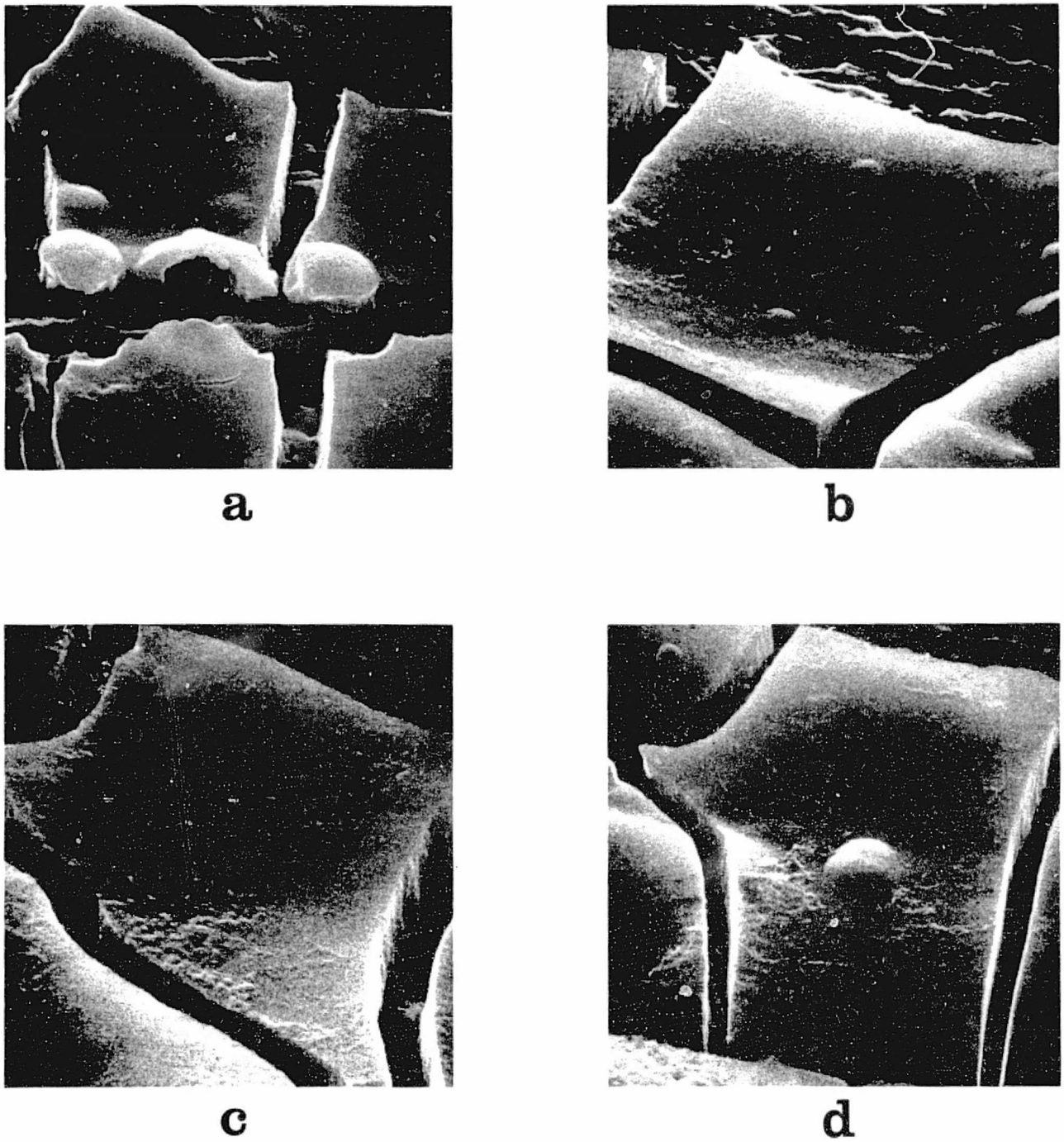

Figure 29. Scanning electron micrographs of Ni-electrodes charged under d-c and variety of p-c conditions, magnification of 10000 X. Charging currents of: a) 5mA d-c; b) instantaneous p-c of 5mA, θ_1/θ of 0.25 and frequency of 50 Hz; c) instantaneous p-c of 5mA; θ_1/θ of 0.5 and frequency of 50 Hz, dried in air; d) instantaneous p-c of 5mA, θ_1/θ of 0.5 and frequency of 50 Hz, dried in vacuum

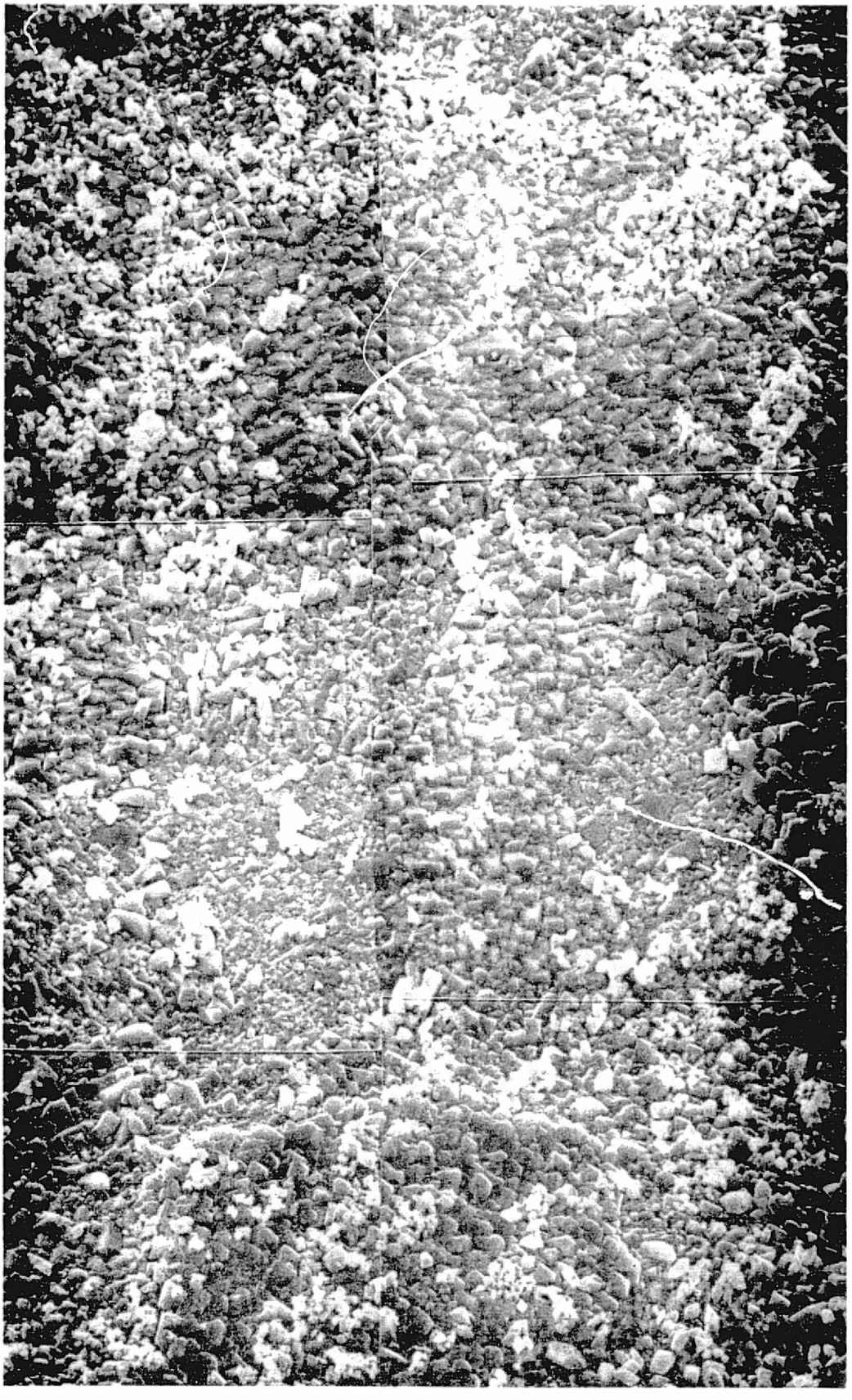

Figure 30. Scanning electron micrograph of a Cd- electrode charged with 5mA d-c, montage at magnification of 3000 x

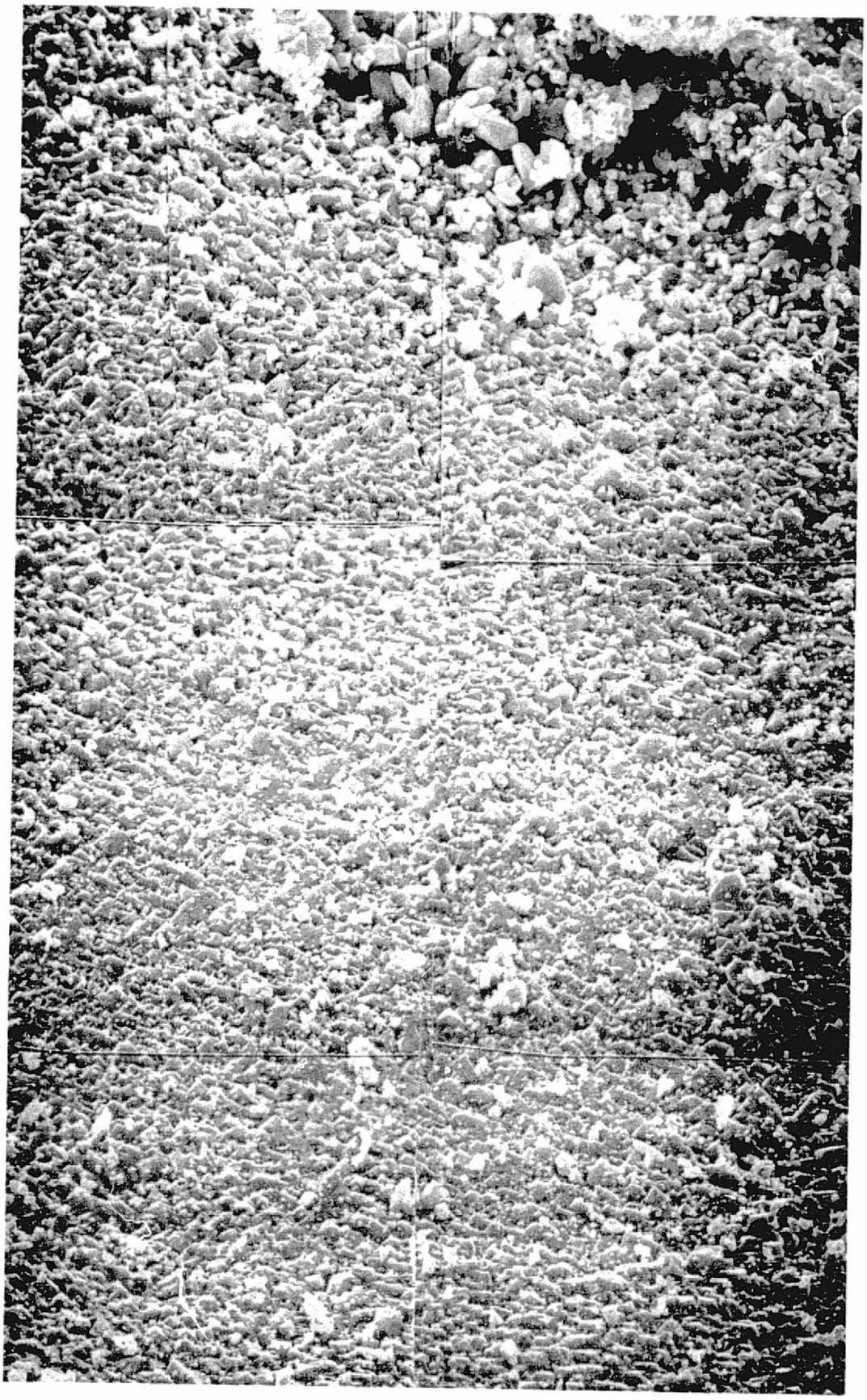

Figure 31. Scanning electron micrograph of a Cd-electrode charged with 5mA instantaneous p-c, 0.1 duty cycle and 50 Hz frequency, montage at magnification of 3000 X

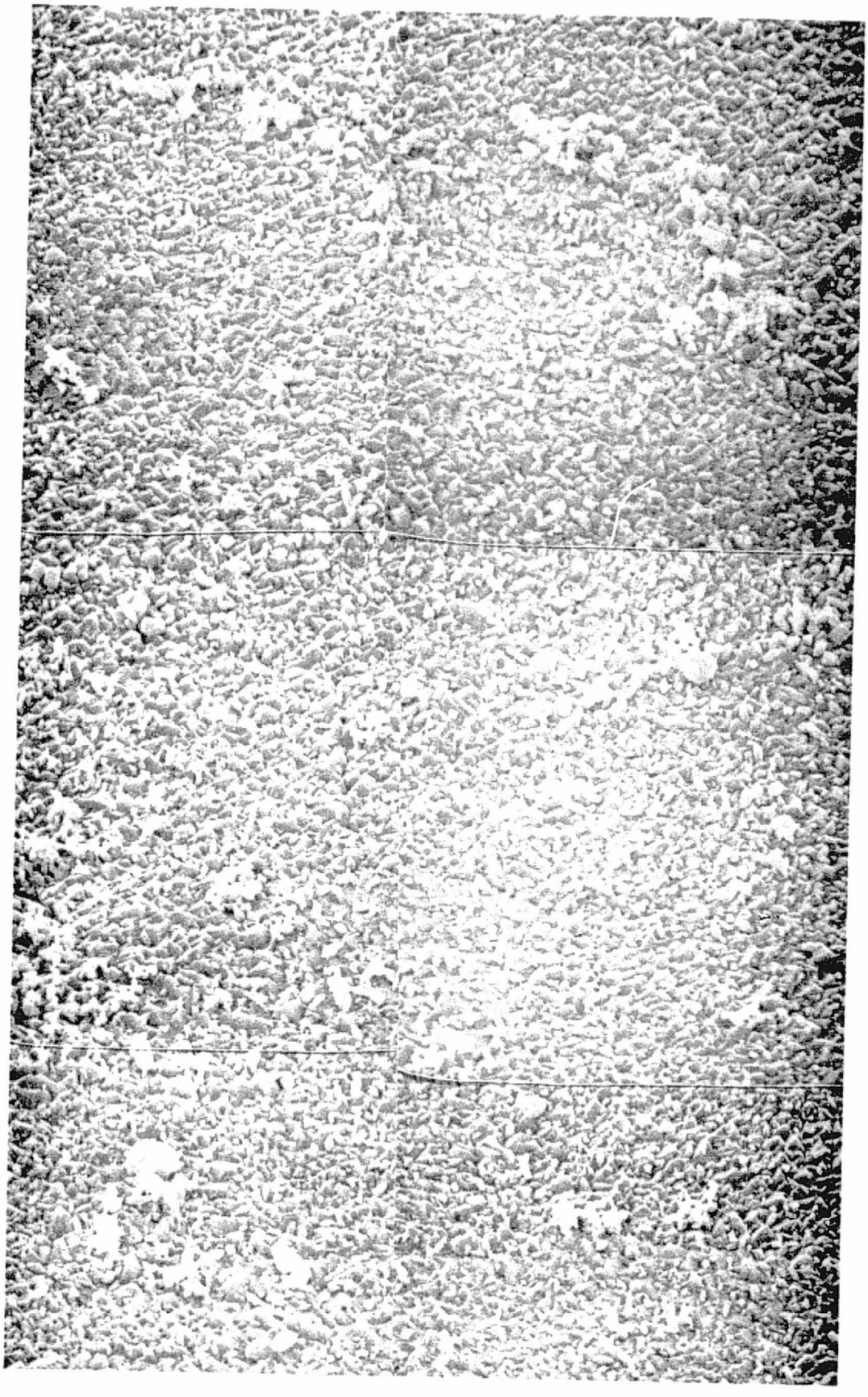

Figure 32. Scanning electron micrograph of a Cd-electrode with 5mA instantaneous p-c, 0.25 duty cycle and 50 Hz frequency, montage at magnification of 3000 X

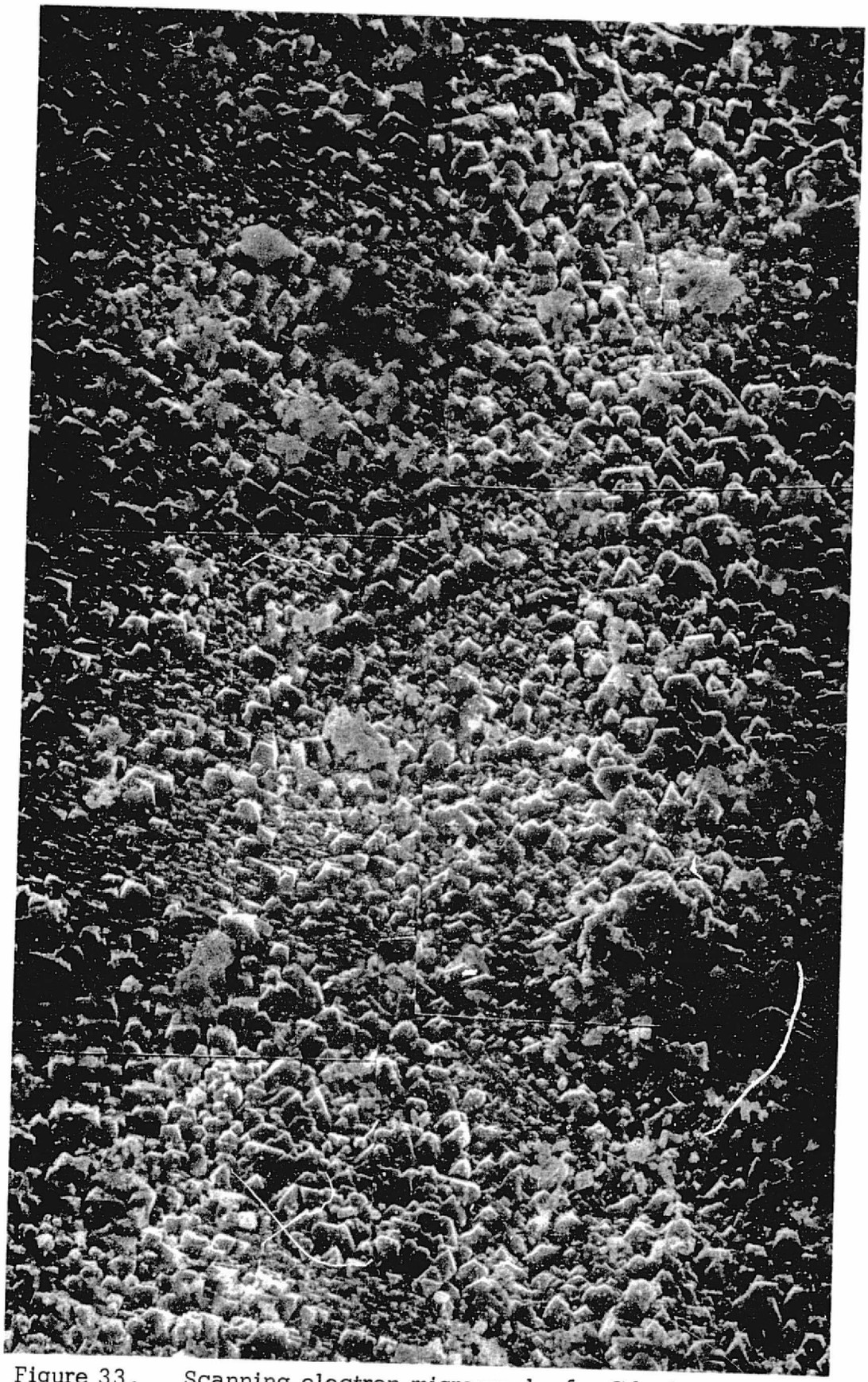

Figure 33. Scanning electron micrograph of a Cd-electrode charged with 5mA instantaneous p-c, 0.5 duty cycle and 50 Hz frequency, montage at magnification of 3000 X

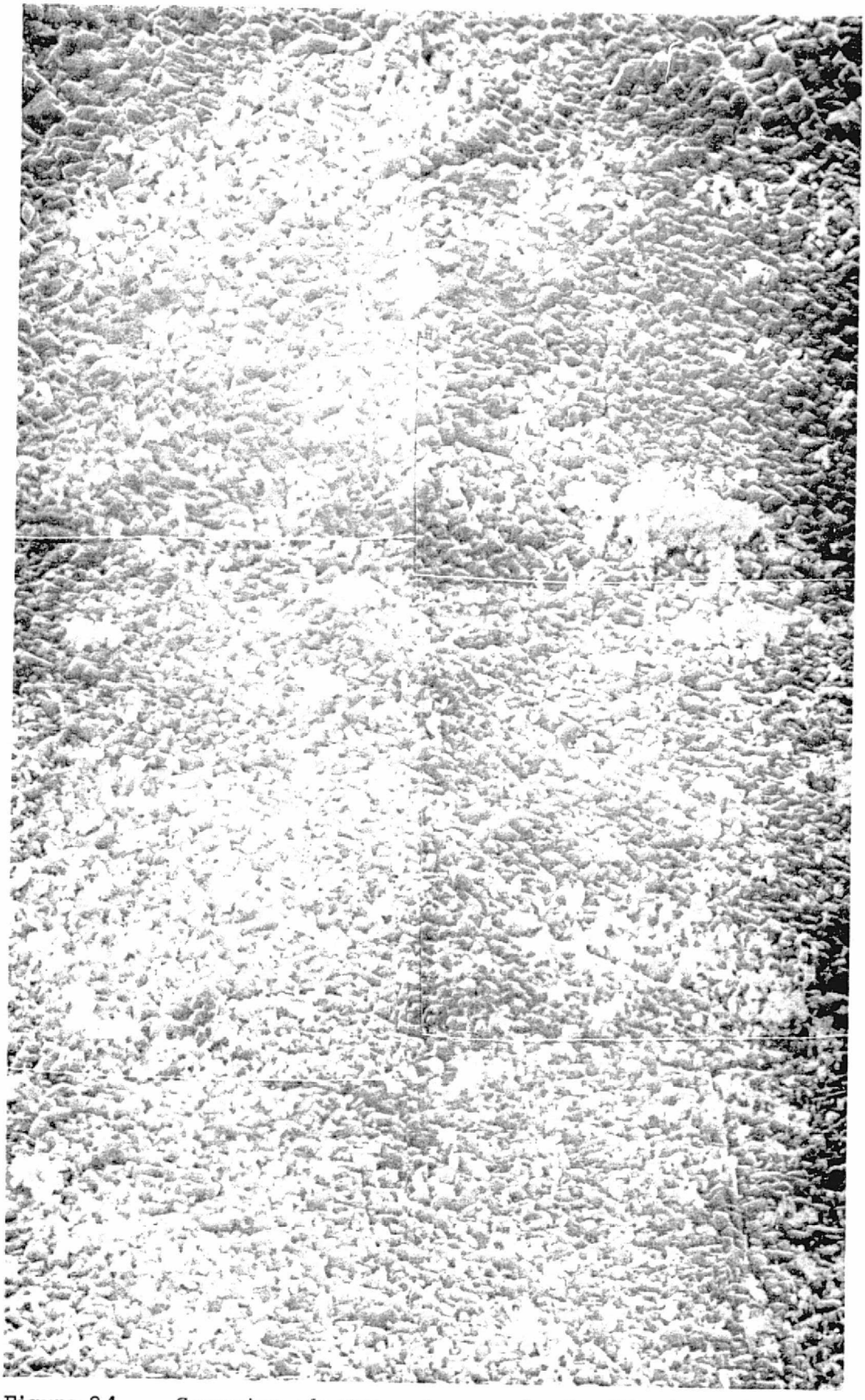

Figure 34. Scanning electron micrograph of a Cd-electrode charged with 10mA instantaneous p-c, 0.5 duty cycle and 50 Hz frequency, montage at magnification of 3000 X

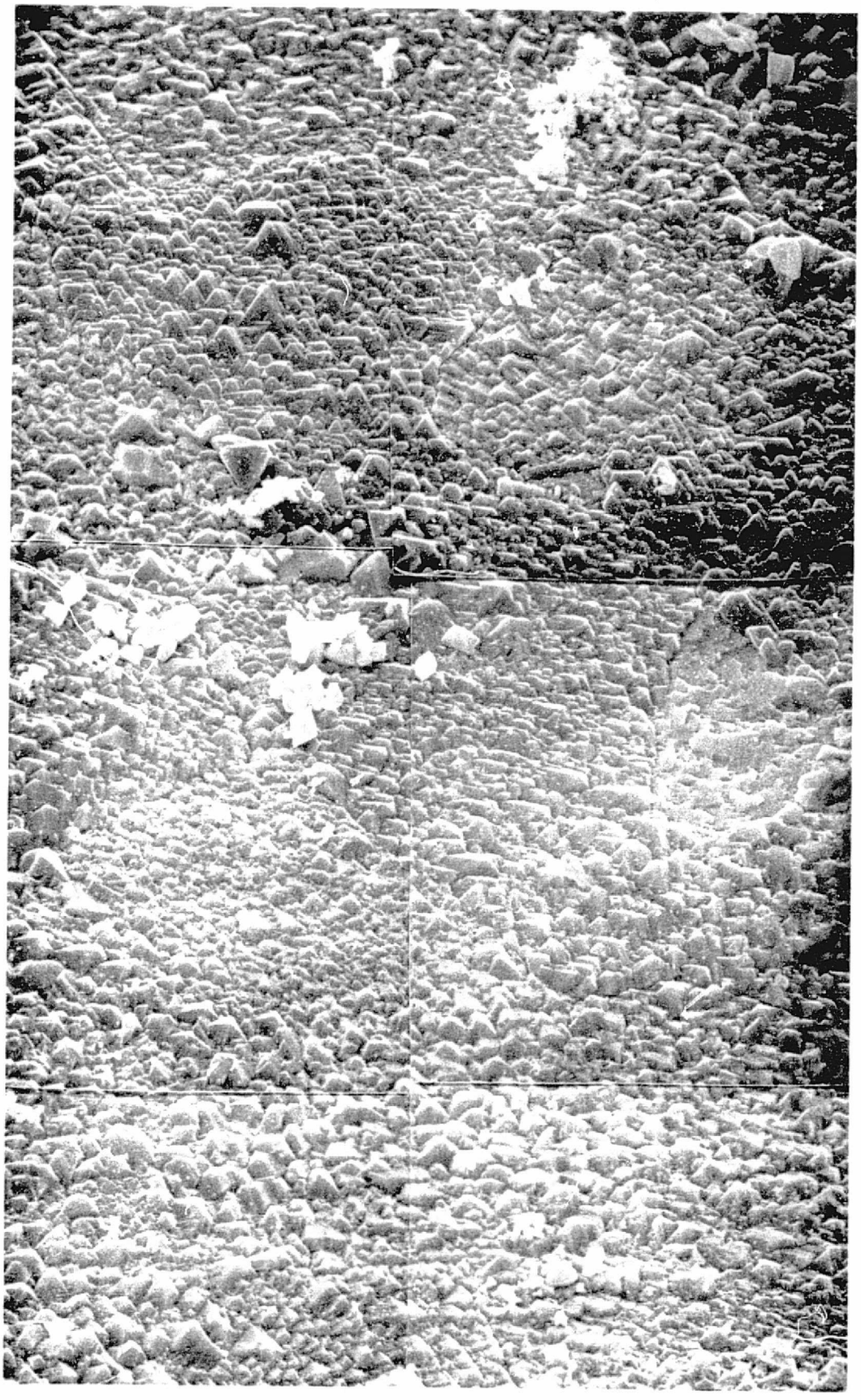

Figure 35. Scanning electron micrograph of a Cd-electrode charged with 5mA instantaneous p-c, 0.75 duty cycle and 50 Hz frequency, montage at magnification of 3000 X

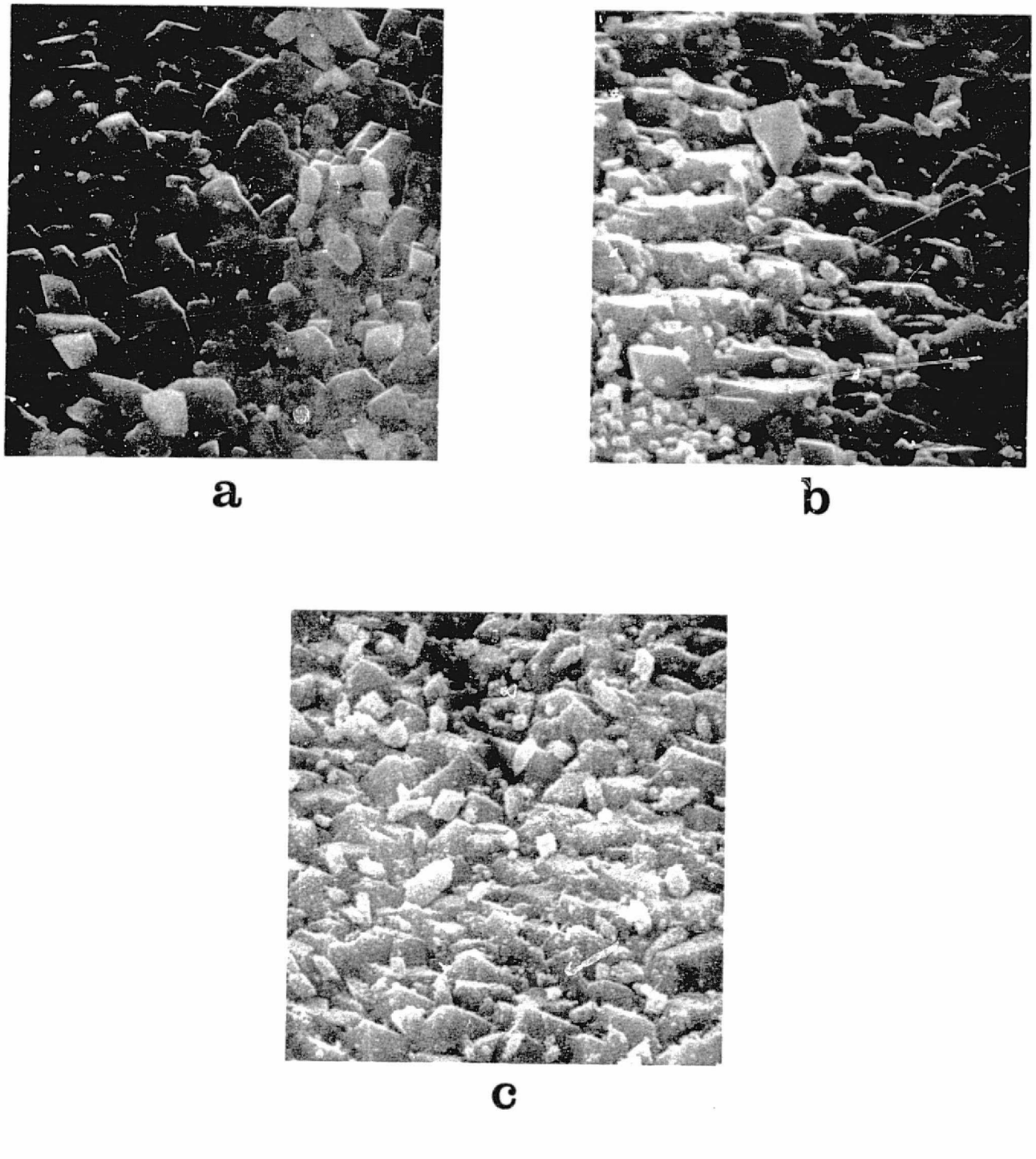

Figure 36. Scanning electron micrographs of Cd-electrodes charged under d-c and variety of p-c conditions, magnification of 10000 X. Charging currents of: a) 5mA d-c; b) 5mA c) 5mA instantaneous p-c, 0.25 duty cycle and 50 Hz frequency.

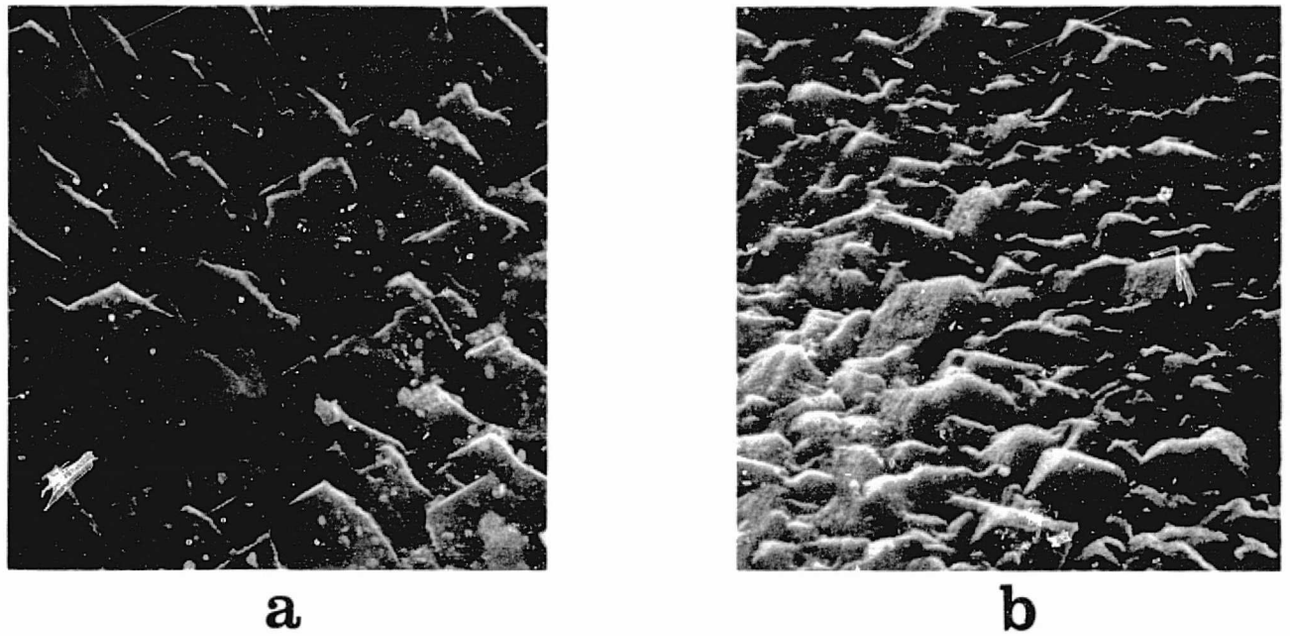

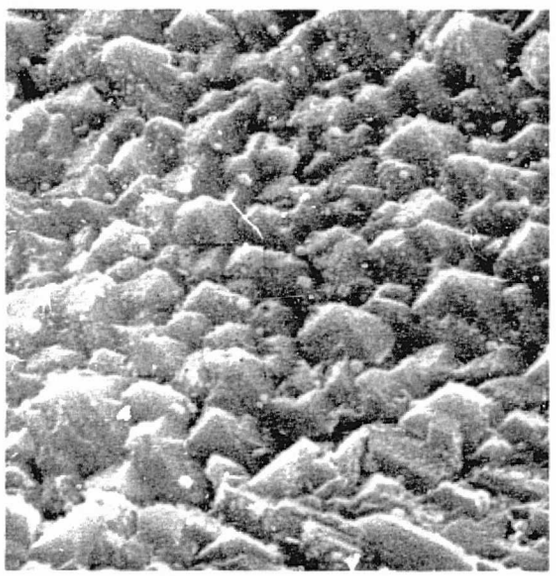

Figure 37. Scanning electron micrographs of Cd-electrodes charged under variety of p-c conditions, magnification of 10000 X. Charging currents of: a) 5mA instantaneous p-c, 0.5 duty cycle and 50 Hz frequency; b) 10mA instantaneous p-c, 0.5 duty cycle, and 50 Hz frequency; c) 5mA instantaneous p-c, 0.75 duty cycle and 50 Hz frequency.

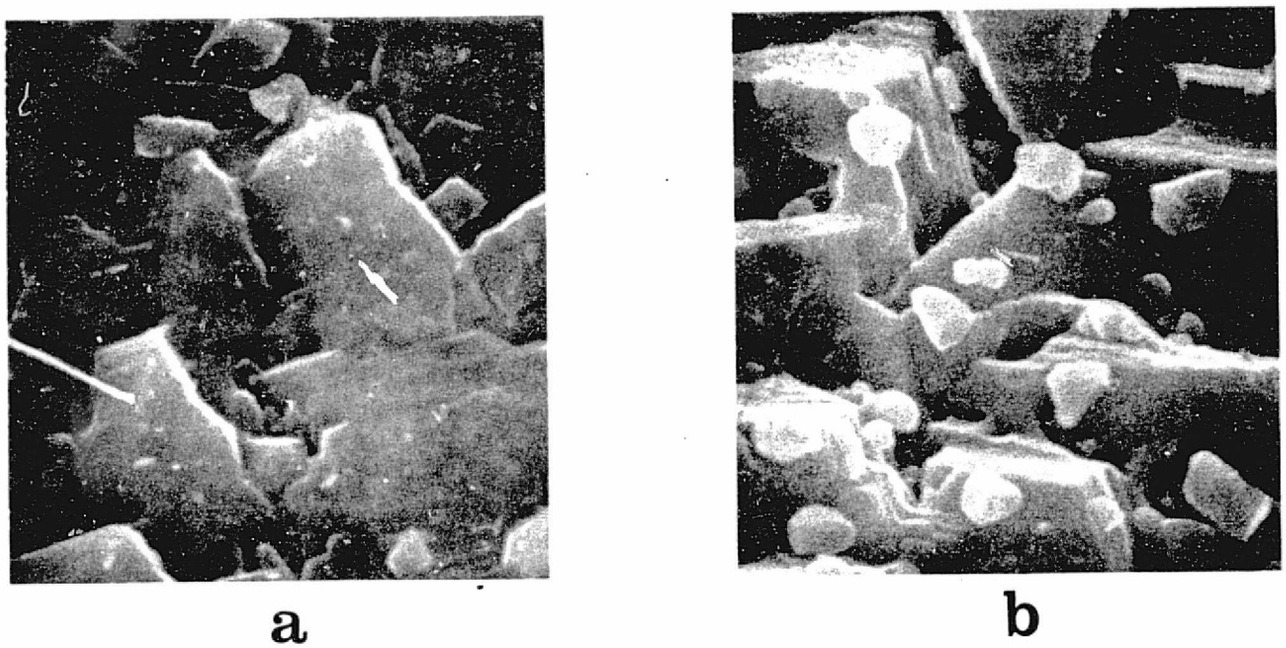

Figure 38. Scanning electron micrographs of Cd-electrodes charged under d-c and variety of p-c conditions, magnification of 30000 X. Charging currents of: a) 5mA d-c; b) 5mA instantaneous p-c, 0.1 duty cycle and 50 Hz frequency; c) 5mA instantaneous p-c, 0.25 duty cycle and 50 Hz frequency

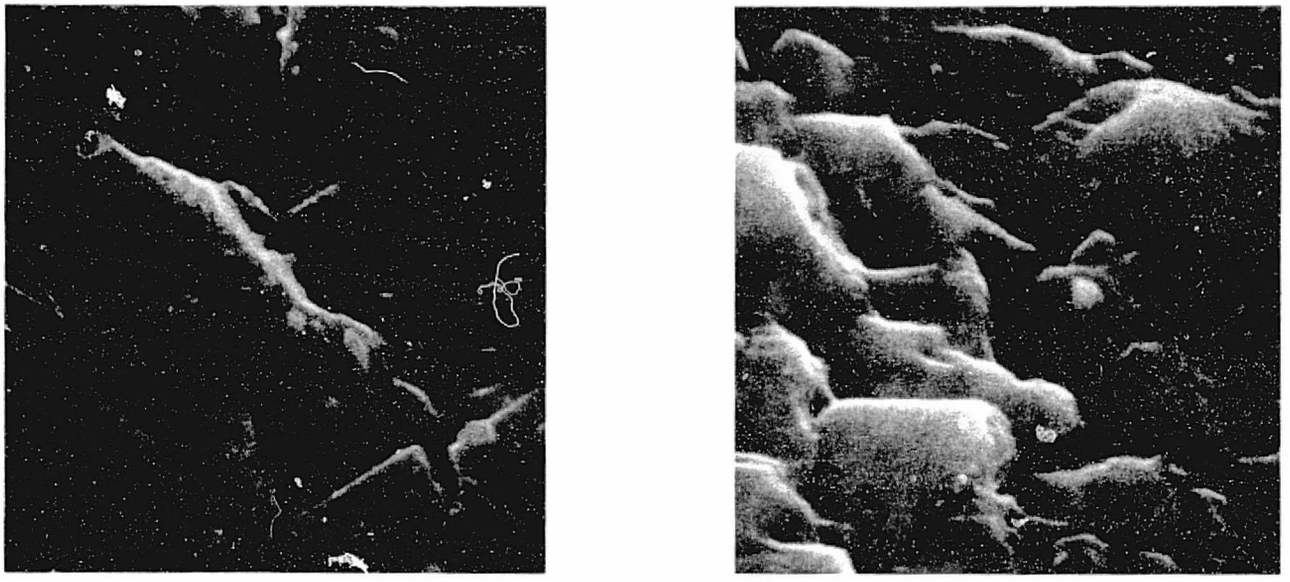

a

b

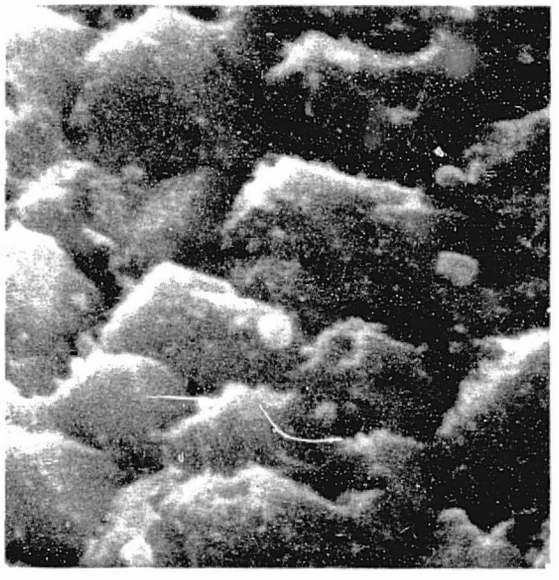

c

Figure 39. Scanning electron micrographs of Cd-electrodes charged under variety of p-c conditions, magnification of 30000 X. Charging currents of: a) 5mA instantaneous p-c, 0.5 duty cycle and 50 Hz frequency; b) 10mA instantaneous p-c, 0.5 duty cycle and 50 Hz frequency; c) 5mA instantaneous p-c, 0.75 duty cycle and 50 Hz frequency

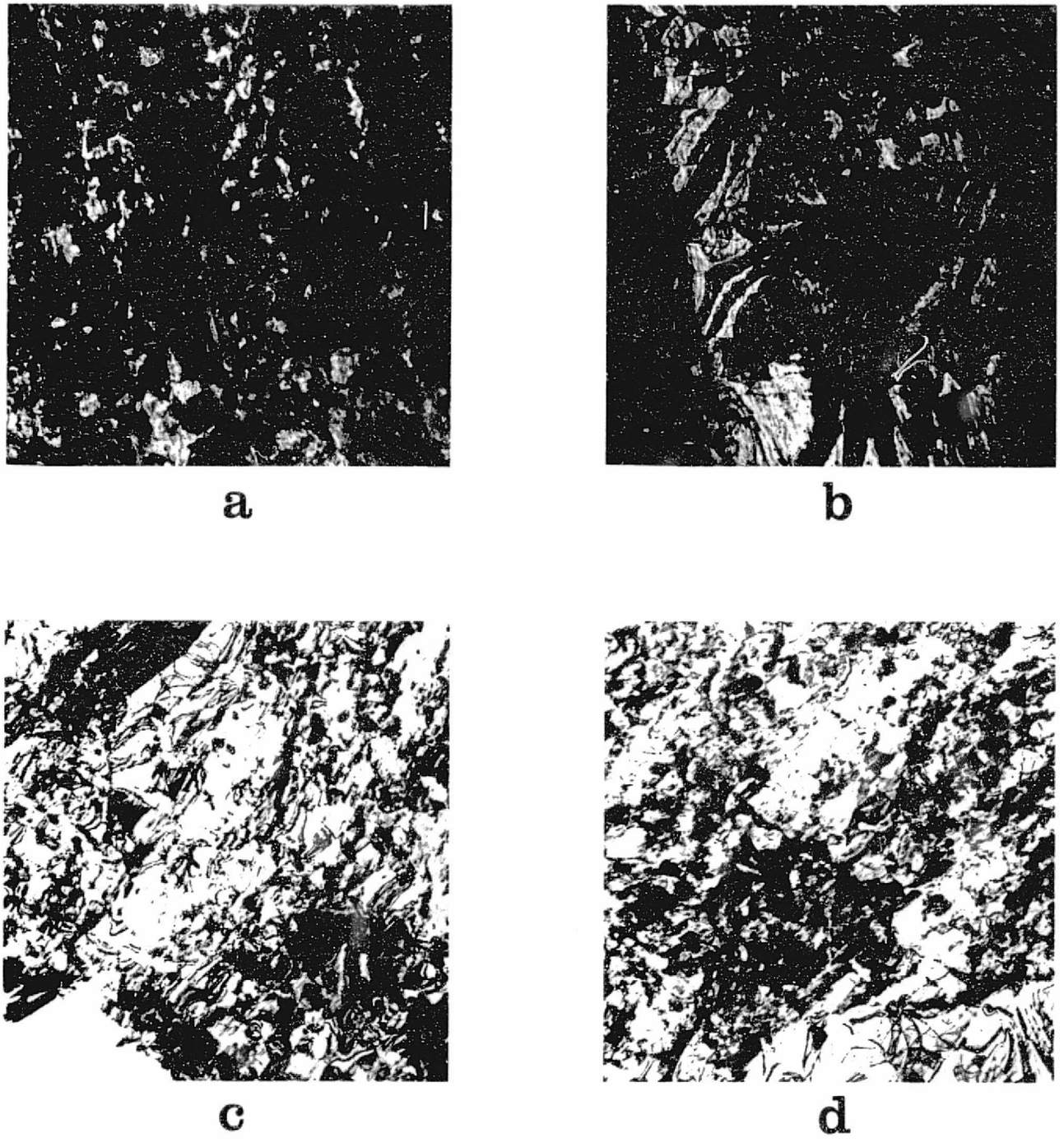

Figure 40. Transmission electron micrographs of Cd-electrodes charged under d-c and p-c conditions, magnification of 26400 X. Charging currents of: a) and b) 5mA d-c, near and away from the surface, respectively; c) and d) 5mA instantaneous p-c, 0.5 duty cycle and 50 Hz frequency, near and away from the surface, respectively

3. X-ray Diffraction

Surface scans were performed on Cd-electrodes charged with d-c and a variety of pulsed currents. The diffraction patterns thus obtained are shown in Figs. 41-45.

In order to avoid the influence on the samples diffraction pattern by substrate orientation, the powder method was used for some of the above mentioned samples. Due to the high level of background noise, little information was obtained from these diffraction patterns. A typical result is shown in Fig. 46.

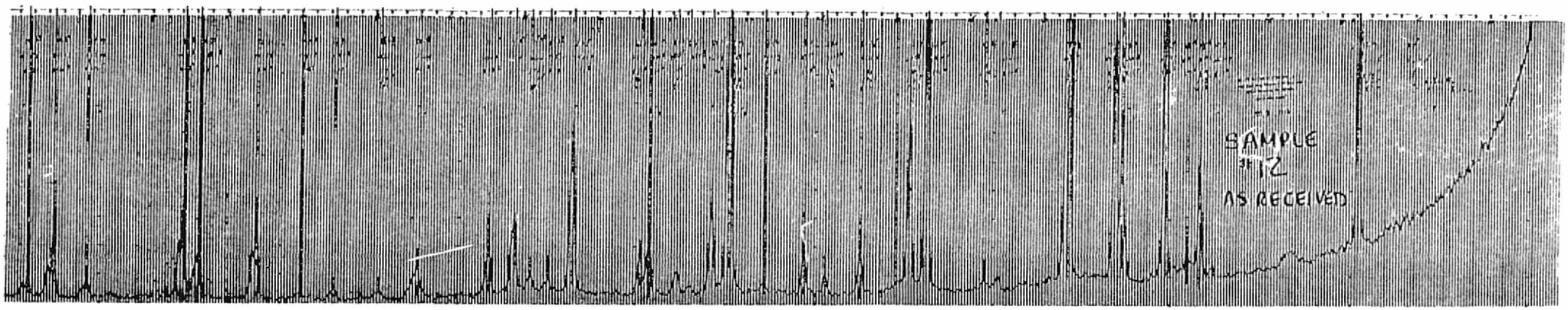

Figure 41. X-ray diffraction pattern of a Cd-electrode charged with 5mA d-c

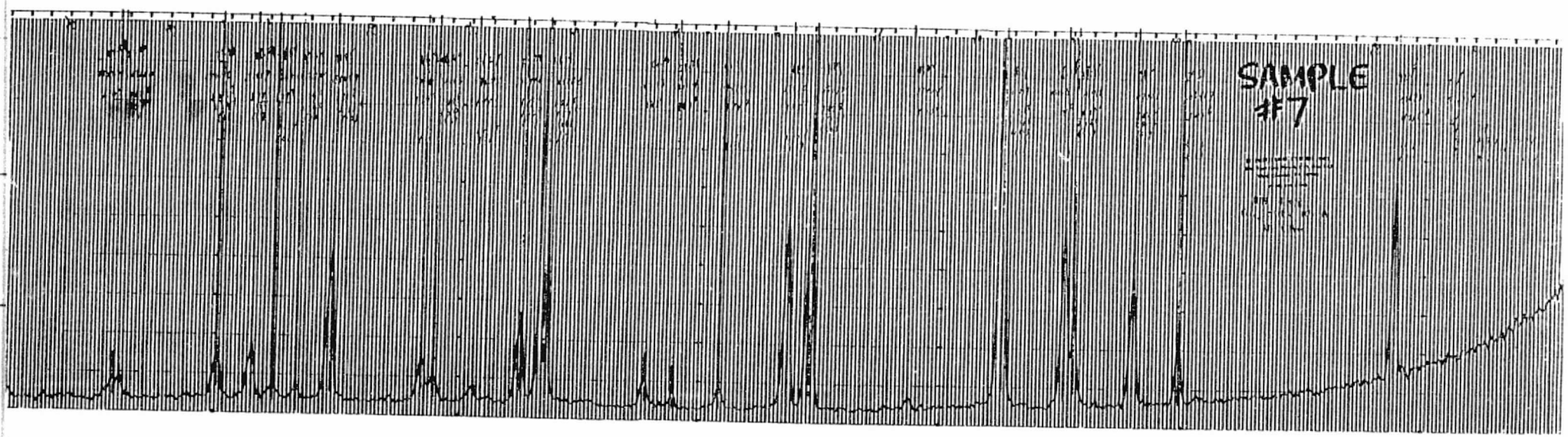

Figure 42. X-ray diffraction pattern of a Cd-electrode charged with 5mA instantaneous p-c, 0.1 duty cycle and 50 Hz frequency

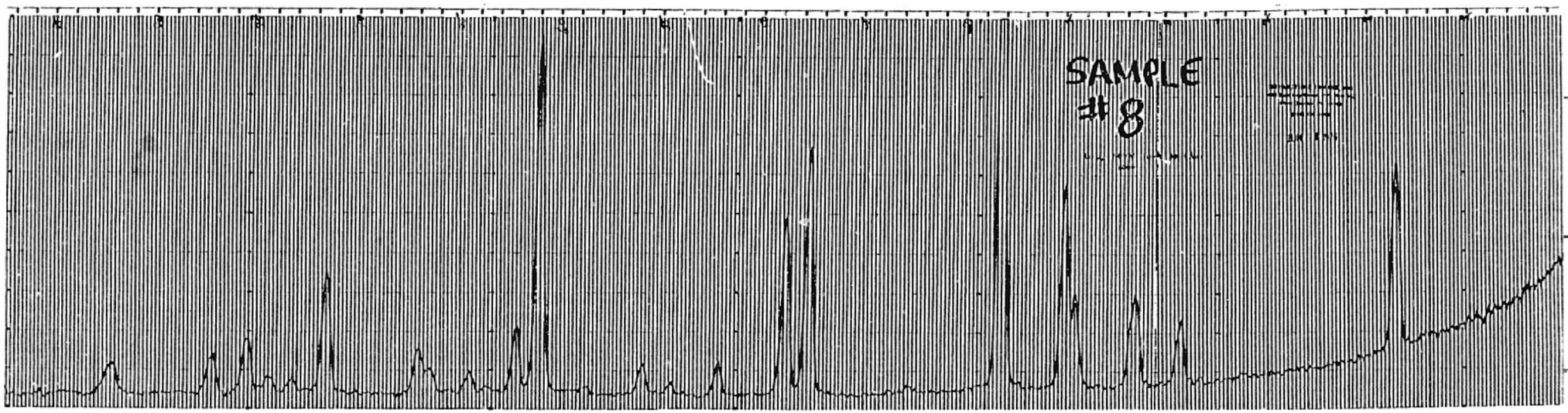

Figure 43. X-ray diffraction pattern of a Cd-electrode charged with 5mA instantaneous p-c, 0.25 duty cycle and 50 Hz frequency

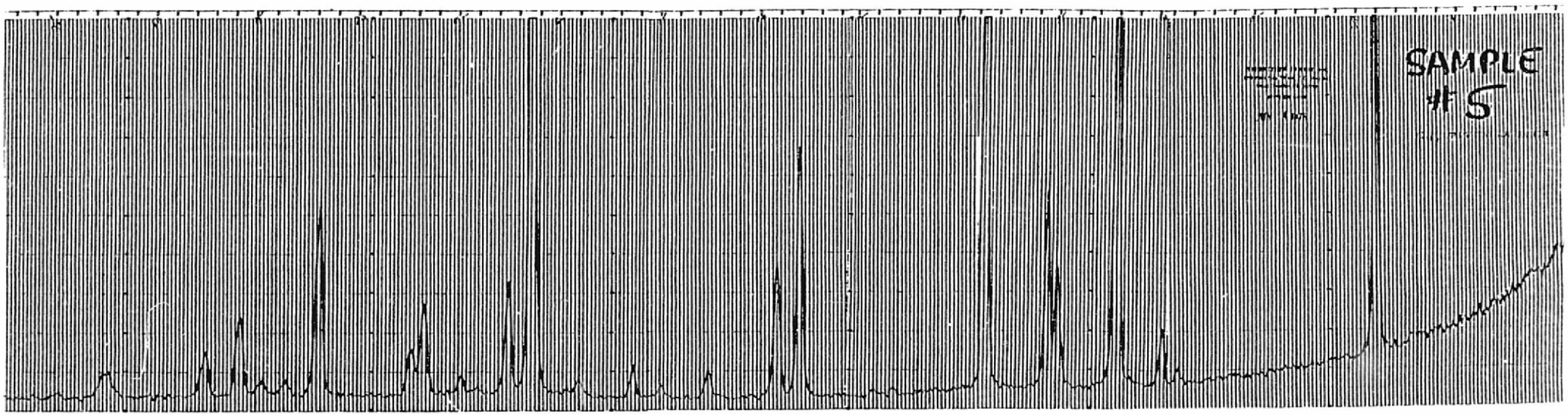

Figure 44. X-ray diffraction pattern of a Cd-electrode, charged with 10mA instantaneous p-c, 0.5 duty cycle and 50 Hz frequency

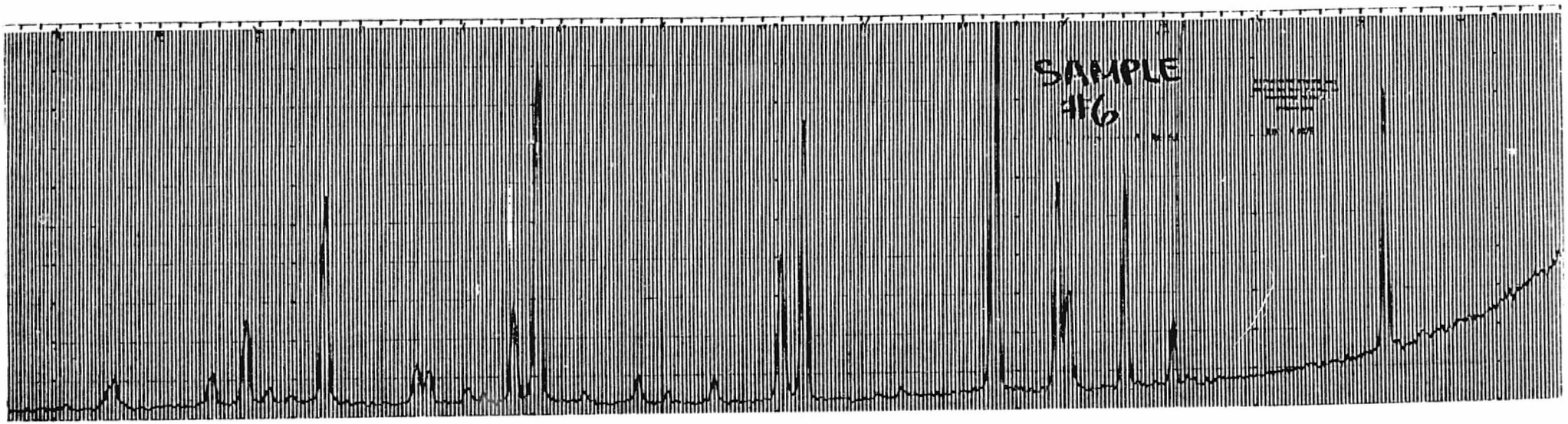

Figure 45. X-ray diffraction pattern of a Cd-electrode charged with 5mA instantaneous p-c, 0.75 duty cycle and 50 Hz frequency

Figure 46. X-ray diffraction pattern of a Cd-electrode charged with 5mA d-c, obtained by the powder method

VII

DISCUSSION

In order to explain the system behavior under both d-c and p-c charging conditions in terms of kinetic, mass transfer and structural considerations, thermodynamic and mechanistic models, which describe the system in a satisfactory manner, must first be established. The effects of pulsed current charging on charge acceptance can then be explained in terms of these models.

A. Ni-electrode

Thermodynamics - to evaluate the reversible electrode potential, the following equation, suggested by MacArthur (33) is assumed to describe the electrode reaction:

$$2[\text{Red}] + m\text{KOH} \longrightarrow 2[\text{Ox}] + nH_2O + 2e^- \qquad (41)$$

Assuming $a_{red} = a_{ox} = 1$, the reversible electrode potential can be evaluated from eqn. (6)

$$E_r = 0.411 - \frac{0.0591}{2} \log \frac{(a_{KOH})^{0.494}}{(a_{H_2O})^{0.0012}}$$

where

$$a_{KOH} = \gamma_{\pm}^2 \, m^2 \qquad (42)$$

and a_{H_2O} can be evaluated by graphical integration of the Gibbs-Duhem equation

$$d \ln a_{H_2O} = \frac{m}{55.50825} d \ln a_{KOH} \quad (43)$$

where m is the molality of the electrolyte solution. Detailed calculations are shown in Appendix 4A. The reversible electrode potential for the electrode under the experimental conditions of the present work was found to be 0.3874V. The result is in good agreement with the values reported by MacArthur (33).

Mechanistic Considerations - from mechanistic studies and charge acceptance measurements made in this work together with literature information the solid-state mechanism, rather than the dissolution-precipitation mechanism, is most appropriate in describing the reactions at the Ni-electrode, under the conditions used in this work. The proposed reaction mechanism consists of the following two steps: a fast charge transfer and a slow diffusion of proton through a solid phase, the latter one being the rate determining step.

During discharge (reduction)

$$NiOOH + e^- \longrightarrow HO\text{-}Ni\text{-}O^- \quad (44a)$$

and $$HO\text{-}Ni\text{-}O^- + H^+ \longrightarrow Ni(OH)_2 \quad (44b)$$

thus creating a proton vacancy at the $HO\text{-}Ni\text{-}O^-$ site this vacancy is then filled by a proton, formed by the dissociation of water molecules from the electrolyte. The proton diffuses from the electrode-solution interface into the solid phase lattice forming $Ni(OH)_2$. Another product

formed on discharge is Ni_3O_4, which forms a passivating film, thus reducing the electrode capacity by preventing the rest of the active material from discharging. A graphical representation of the discharge reaction is given in Fig. 47b. During charge

$$Ni(OH)_2 \xrightarrow{\text{fast}} NiOOH + H^+ + e^- \qquad (45)$$

thus liberating a proton, H^+, which diffuses through the solid phase, mostly $Ni(OH)_2$ with a small amount of NiOOH, to the electrode-solution interface, where it reacts with hydroxide ions from the electrolyte to form water. In addition Ni_3O_4 is also oxidized to NiOOH. A schematic representation of the charge reaction is shown in Fig. 47a. Assuming the composition of both the charged and discharged active materials are those proposed by MacArthur (33), the overall electrode reaction can be written as:

$$6[NiOOH \times \tfrac{7}{6} H_2O \times \tfrac{3}{8} KOH] + 3H_2O^* + 6e^- \underset{\text{charge}}{\overset{\text{discharge}}{\rightleftharpoons}}$$
$$3[Ni(OH)_2 \times \tfrac{2}{3} H_2O] + Ni_3O_4 + \tfrac{9}{8} KOH + 6H_2O + 4OH^- \qquad (46)$$

The experimental evidence, from the present work, which is in support of the above proposed mechanism can be described as follows.

From the potential sweep experiments Figs. 21-23, a plot of i_{pa} and i_{pc} vs. $V^{1/2}$ was prepared in Fig. A.7 and from the slopes of these lines, the values of the diffusion coefficient of the proton for the oxidation and

*These water molecules provide H^+ for the reduction of NiOOH.

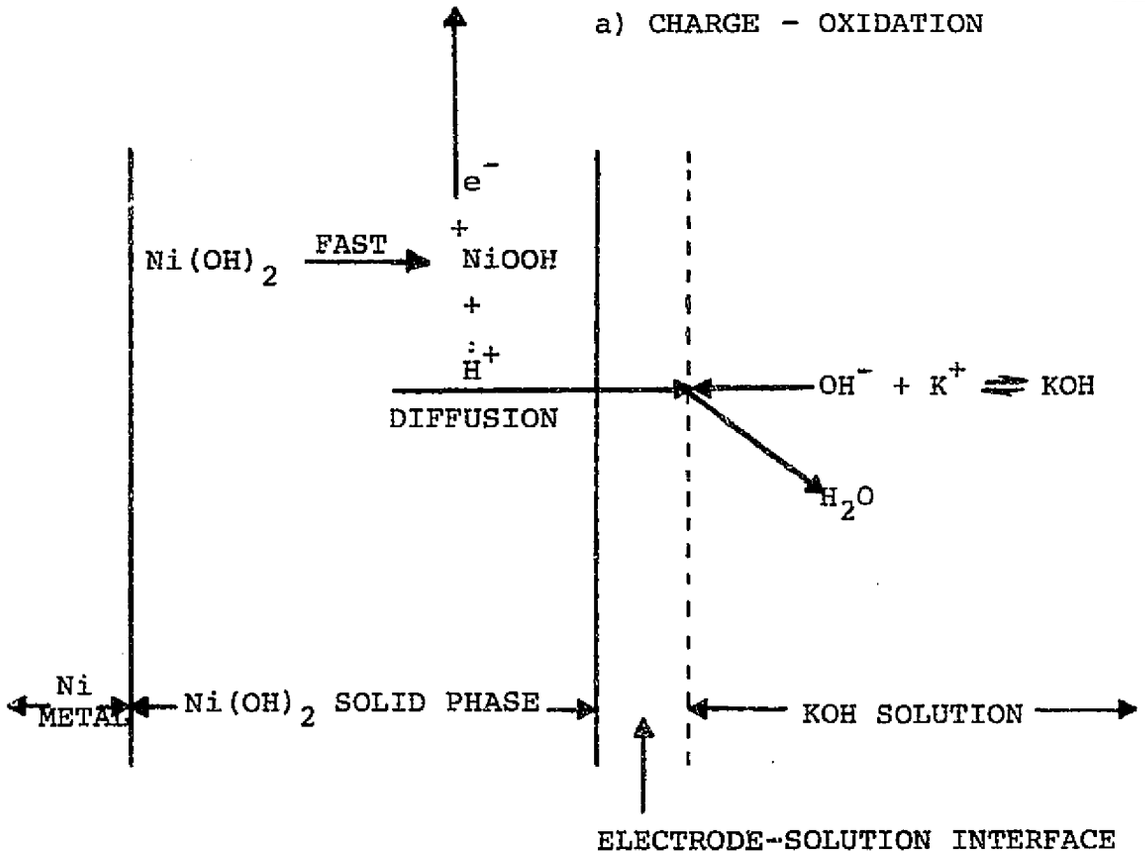

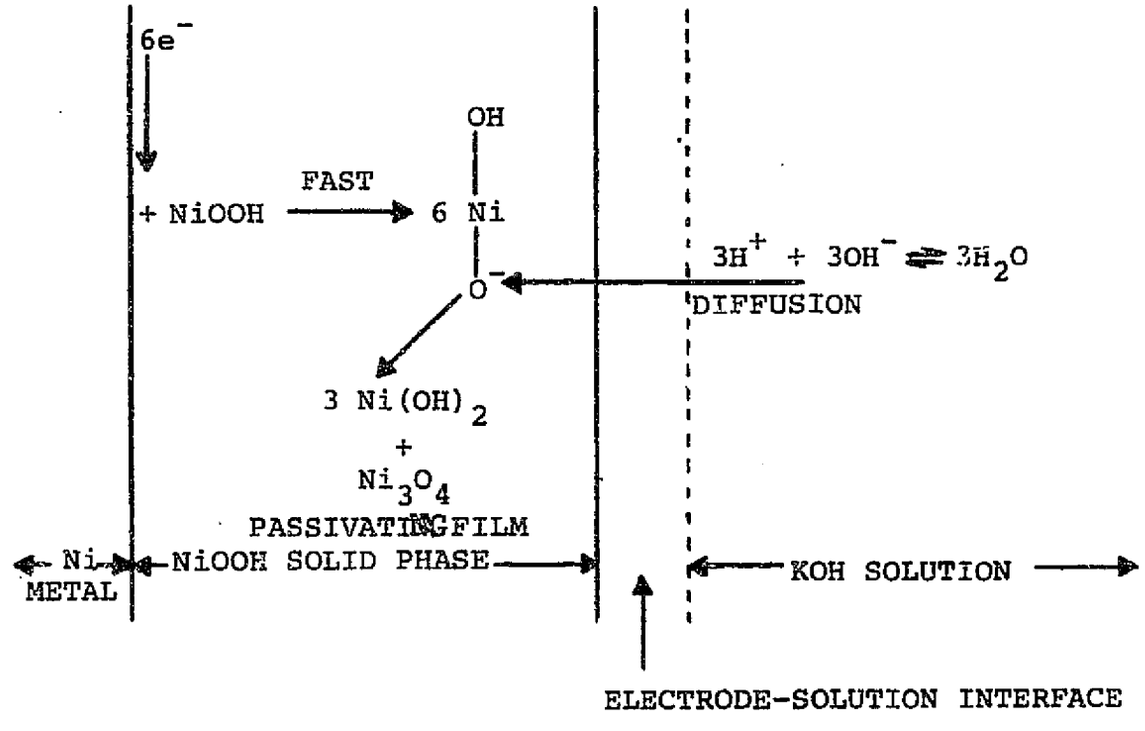

Figure 47 a) and b). Mechanism of the reactions occurring at the Ni-electrode

reduction reactions were calculated, as shown in Appendix 4B. The diffusion coefficients of the proton during the oxidation and reduction reactions were found to be 5.28×10^{-10} cm^2/sec and 2.16×10^{-9} cm^2/sec, respectively. These values are consistent with diffusion through a solid phase. The two diffusion coefficients vary by approximately an order of magnitude, which probably indicates that H^+ diffuses through two different materials, hence supporting the proposed mechanism. Comparing these values with the ones reported by MacArthur (34), good agreements were found, although his calculations were more rigorous. From a plot of E_{pa} and E_{pc} vs log V (Fig. A8), and eqn. (27) the values of the transfer coefficients were calculated (Appendix 4B) and found to be $\alpha_{ox} = 0.49$ and $\alpha_{red} = 1.70$. It is known that for a multi step reaction (6,7):

$$\alpha_{ox} + \alpha_{red} = \frac{n}{\nu} \qquad (47)$$

where n is the number of electrons involved in the reaction and ν is the number of times the rate controlling step occurs in order n electrons to be transferred. From eqn. (46) and according to the proposed mechanism, the rate controlling step, namely H^+ transfer through the solid phase, must occur 3 times in order for 6 electrons to be transferred. Therefore $\alpha_{ox} + \alpha_{red}$ for this

reaction should be equal to 2. Comparing this with the experimental value of 2.17, the agreement is considered to be satisfactory. In addition, from cyclic potential sweeps two oxidation peaks were observed at slow sweep rates, whereas at faster ones, they were found to merge into one. This is in agreement with previous findings (33) that both α and β forms of $Ni(OH)_2$ are present. The oxidation of α-$Ni(OH)_2$, occurs first which is then followed by the oxidation of β-$Ni(OH)_2$, at potentials 30mV more anodic. In addition, the amount of β-$Ni(OH)_2$ is considerably smaller than that of the α form. Supporting the findings of the cyclic potential sweeps, are the results obtained from cyclic sweeps under controlled current as shown in Fig. 25, where again a change of behavior is observed with a variation of sweep rate. The potential at which oxidation is initiated was found to increase with a decrease of sweep rate, the same was obtained for the potential at which reduction is initiated. These are consistent with the behavior exhibited during the cyclic potential sweeps.

From the limiting current measurements, Fig. 17, the effect of diffusion, through a liquid phase, on both the anodic and cathodic processes was found to be insignificant, since the limiting current either did not vary or varied very slightly with a change of rotation speed. According to reactions controlled by mass transport through a liquid, the value of the limiting current

should increase with an increase of rotation speed (cf. eqns. (19) and (24)). This was found to be true for the cathodic reaction, thus supporting the proposed mechanism of H^+ transfer first through a liquid (electrode-solution interface), then through a solid phase, whereupon it enters into reaction to form the final product. However, for the oxidation reaction a decrease in i_L was observed with increase of rotation speed. According to the oxidation mechanism of Fig. 47a, rotation speed should have no effect on the limiting current, since the transport of H^+ occurs first through the solid phase and the formation of products does not have such a pronounced dependence on the presence of H^+ as compared to the cathodic reaction. A possible explanation for this observation could be the existence of another reaction which is competing with the proposed one. Such reaction could promote the formation of a different active material thereby causing a shift in the limiting current. A second possibility is the oxidation of Ni_3O_4. The amount of Ni_3O_4 could increase under a particular set of conditions, thus increasing its contribution to the overall reaction, which in turn will affect the limiting current.

In summary, our findings from several different types of experiments are consistent with the proposed electrode reaction mechanism. However, it is important to note, that the values of the diffusion coefficients and

the transfer coefficients are not of great accuracy, since the calculations were approximate in nature.

Charge Acceptance Measurements - from the results of d-c charging experiments, shown in Table 2, a decrease of charging efficiency was observed with an increase of charging current and charging time. These losses could be mostly due to gas evolution, which in turn is a function of the amount of Ni_3O_4 formed during reduction. When the electrode is discharged, according to the proposed mechanism, a Ni_3O_4 passivity film is formed, thus preventing some of the NiOOH from reacting. Consequently, the reoxidation during the subsequent charge cycle requires less A-hr as compared to the previous cycle. Hence, if the amount of A-hr supplied to the system is kept constant, gas will evolve. An increase in charge acceptance was observed with increase of charging current and time, suggesting that even after gas evolution has started, some charge is being accumulated at the electrode. In other words, during gas evolution the current efficiency for the oxidation of $Ni(OH)_2$ is greater than zero. Also, an increase of charging rate was found to cause an increase in both charge acceptance and charging efficiency, which is in agreement with results reported by Dunlop et al. (23).

The amount of charge accumulated during the 8th cycle was compared to that during the first cycle and represented in terms of a percentage of the initial charge.

This was accomplished by noting the time of gas evolution during charge for the first and the eighth cycles. Results are summarized in Table 17. Percent of charge accumulated during the 8th cycle was found to decrease with an increase of charging time, charging current and rate of charge. This observation suggests that the improvement of charge acceptance with increase of charging rate is not caused by an increase of the amount of charge accumulated but possibly by the formation of a different form of the active material, which exhibits a better performance on discharge. This material is probably β-NiOOH.

From the experiments under p-c charging conditions, the charge acceptance was compared to that under d-c charging conditions and presented in terms of a ratio which is given in Tables 3 and 4. Generally, an increase in charge acceptance with increase in duty cycle was observed. Also, an increase in the instantaneous pulsed current density was found to cause an increase in charge acceptance for all duty cycles and frequencies, whereas a variation in frequency itself was found to have almost no effect on the system performance. It is important to note that the effects mentioned above are not of a significant magnitude. Calculations for the percent of charge accumulated during the eight cycle were performed and summarized in Table 18. Comparing these with the values obtained under d-c charging conditions, an increase in

Table 17

Ni-electrode, per cent of initial charge accumulated during the eight cycle under d-c charging conditions

1. Assuming the current efficiency for oxidation of Ni to be 0% after gas evolution begins.

2. Assuming the current efficiency for oxidation of Ni to be 50% after gas evolution begins.

Experiment #	Q_1%	Q_2%
N1	66.65	84.22
N2	55.56	78.97
N3	81.99	91.00
N4	61.50	82.72
N5	59.37	80.56
N6	66.65	89.64

Table 18

Ni-electrode, per cent of initial charge accumulated during the eight cycle under p-c charging conditions

Experiment #	Q_1%	Q_2%
N7	100.00	100.00
N8	81.38	90.70
N11	97.23	98.58
N12	81.35	90.67
N13	85.27	92.60
N14	75.95	87.97
N16	60.00	80.00
N17	74.98	89.97
N18	75.95	87.97
N19	89.39	94.66
N20	100.00	100.00
N21	100.00	100.00
N22	86.56	93.25

the percent of charge accumulated is generally noticed.

These results show that the losses due to gas evolution have decreased with p-c charging. This is in agreement with the interpretation involving the reduction of concentration overpotential as well as with the expected effects of p-c charging. In addition, a decrease in the percent of charge accumulated during the 8th cycle is noticed with an increase of duty cycle, once again confirming the effect of pulsing on mass transfer of the proton, i.e. at longer duty cycles postponement of gas evolution will not be as pronounced as at shorter duty cycles. However, from the mechanistic model and the fact that at duty cycles of 0.1 and 0.25, the charge accumulated during the 8th cycle is 100% of that during the first cycle, one may conclude that the postponement of gas evolution could not be entirely attributed to a reduction of concentration overpotential. Another cause for such behavior could be structural modifications or the presence of a different active material, which prevents the formation of Ni_3O_4 during reduction. In addition, at shorter duty cycles (e.g. 0.1 and 0.25) the charge acceptance is smaller than that under d-c conditions. This could be attributed to the self-discharge which takes place during the off period of the current. However this could not explain the observed maximum in charge acceptance, which occurred at a peak

current of 10mA, duty cycle of 0.5 and frequency of 50Hz. Once again it becomes apparent that the response of the system under consideration is extremely complex. The overpotential during discharge was calculated from $\Delta E = E - E_r$, and a plot of ΔE vs. fraction of capacity discharged was prepared in Fig. 48 a-d. In general a decrease of overpotential during discharge was observed with an increase of duty cycle during charge, suggesting the formation of a different active material. As previously mentioned, the system was found to exhibit a maximum at a 10mA instantaneous current, 0.5 duty cycle and 50Hz frequency, the value of the overpotential ΔE in this case was the smallest, and the charge accumulated during the 8th cycle was 81% of the initial charge. Minimum charge acceptance was observed at 5mA instantaneous current, duty cycle of 0.1 and frequency of 50Hz, the value of ΔE during discharge was the largest and the charge accumulated during the 8th cycle was 100% of the initial charge.

Structural Studies - SEM pictures of Ni-electrodes charged under variable conditions, showed that the active material is amorphous, and the surface morphology is affected by the degree of dehydration of the active material as shown in Figs. 28 and 29. In addition, it was observed that under p-c charging conditions the active material layer was thinner as compared to that under d-c conditions. Blister formation was observed

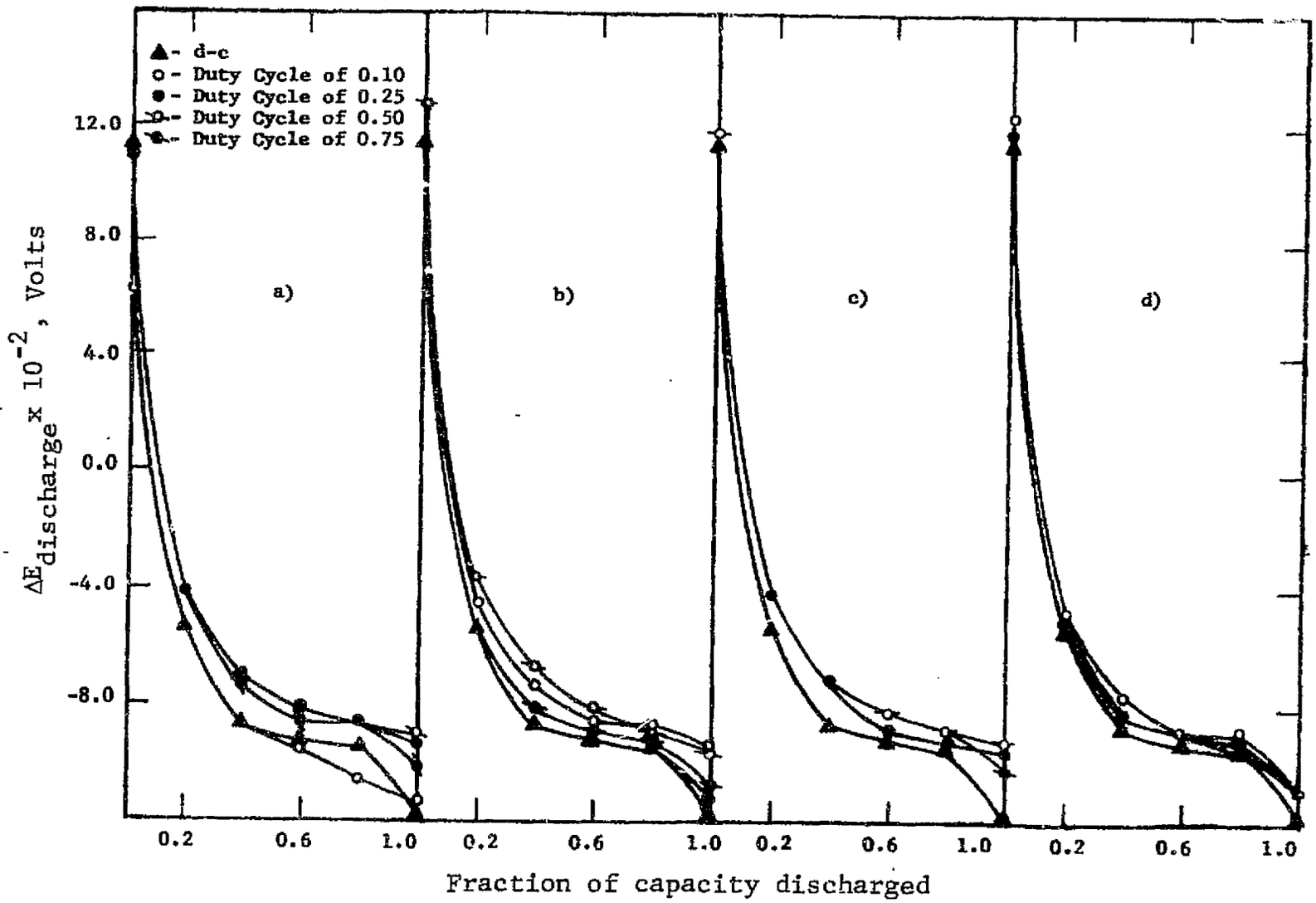

Figure 48. A plot of $\Delta E_{discharge}$ vs. fraction of capacity discharged for the Ni-electrode

under p-c charging conditions, which increased with a decrease in duty cycle (v. Fig. 29). The presence of a different material, crystalline in nature, was observed on the surface of samples charged with 5mA instantaneous current, 0.25 duty cycle and 50Hz frequency.

In summary, under the experimental conditions used in this work, the solid-state mechanism describes the electrode reaction most satisfactorily, with the rate controlling step being the proton transfer through a solid phase and the cause of passivation during discharge - formation of Ni_3O_4 film. The effect of pulsed current charging on the charge acceptance of the electrode is not very significant. This is due to the fact that the rate controlling step is mass transfer of a proton through a solid phase. Thus the effect of pulsing on concentration overpotential is relatively small. Pulsed-current charging can affect the reaction kinetics which in turn can modify the structure and composition of the electrode. In general, charge acceptance was found to increase with increase in duty cycle, instantaneous current and charging rate. This emphasizes the importance of self-discharge (during charge) on the charge acceptance of the electrode. Poor charge acceptance seems to be connected with blister formation on the electrode surface. This is in agreement with previous investigations reported in the literature (19). A decrease in duty cycle seems to promote blister

formation on the electrode surface which is consistent with a decrease in charge acceptance.

B. Cd-electrode

Thermodynamics - the reversible electrode potential was calculated from eqn. (8)

$$E_r = -0.906 - \frac{0.0591}{2} \log a_{H_2O}$$

where a_{H_2O} was evaluated as shown in Appendix 4A. The value of the reversible electrode potential was found to be - 0.9065V.

Mechanistic Considerations - from the mechanistic and charge acceptance studies and also from the literature information it seems that the solid state-dissolution precipitation mechanism describes the electrode reactions most satisfactorily. The mechanism can be described as follows. During discharge (oxidation), a film of CdO is first formed on the surface of Cd, followed by the diffusion of Cd^{++} through the CdO lattice, into the electrode-solution interface, where Cd^{++} reacts with the OH^- to form a soluble complex of the form $Cd(OH)_3^-$. This complex then precipitates as $Cd(OH)_2$ on the surface of the CdO layer. In addition, CdO continuously dissolves and enters in the above mentioned reactions to form $Cd(OH)_2$. The charge transfer reaction

$$Cd \longrightarrow Cd^{++} + 2e^- \qquad (48)$$

is fast in comparison to the rate of transfer of Cd^{++} through the solid phase. A schematic representation of the discharge reaction is given in Fig. 49a. During charge (reduction), $Cd(OH)_2$ reacts with OH^- to form the soluble complex $Cd(OH)_3^-$ which then dissociates to give Cd^{++}. The cadmium ions are first transferred through the solution-electrode interface, then through the solid CdO phase and finally are reduced to form Cd sponge. The charge reaction is schematically represented in Fig. 49 b. In support of the above proposed mechanism the following experimental evidence is presented.

From the results of the potential sweep experiments given in Fig. 26, the values of the diffusion coefficients of Cd^{++} during both the oxidation and reduction reactions were calculated using the semi-infinite diffusion model. Detailed calculations are shown in Appendix 5. The diffusion coefficients of Cd^{++} during the oxidation and reduction reactions were found to be 3.8×10^{-10} cm^2/sec and 1.2×10^{-10} cm^2/sec, respectively. Both diffusion coefficients are in the order of 10^{-10} cm^2/sec, indicating diffusion through a solid phase and implying that during reduction and oxidation diffusion occurs probably through the same solid phase. During reduction, two peaks are observed on the current-potential curves of Fig. 26, suggesting the reduction of two different active materials, CdO and $Cd(OH)_2$. The former occurring at a potential

a) DISCHARGE - OXIDATION

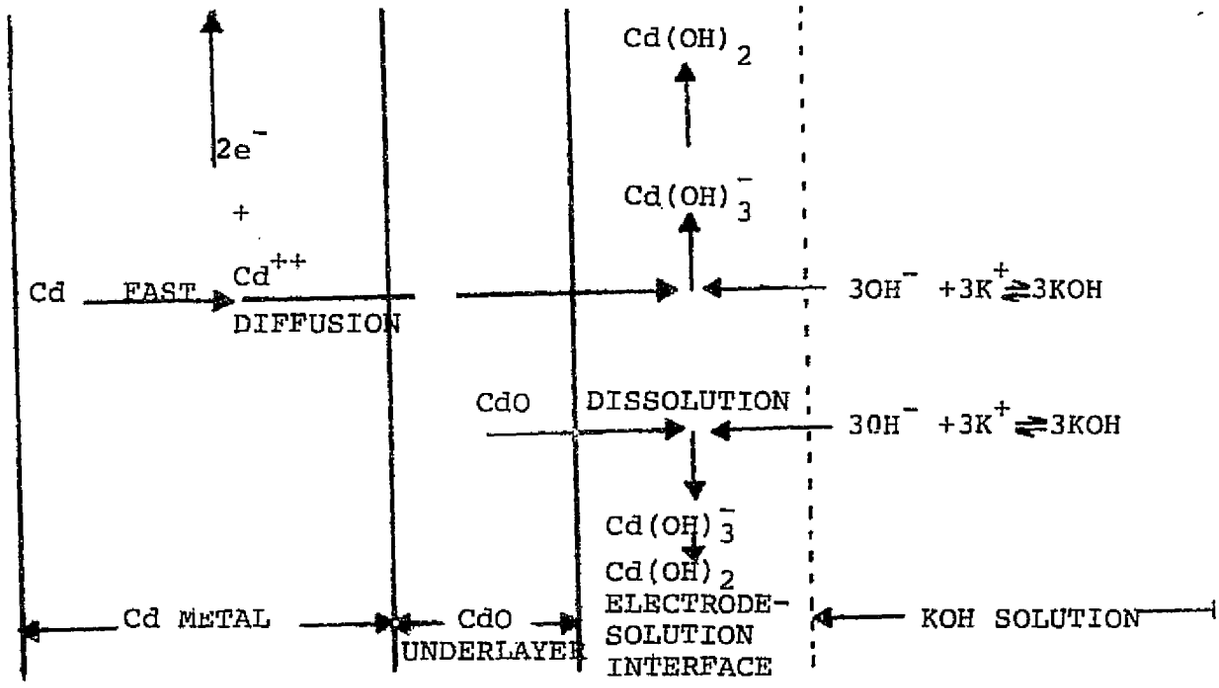

b) CHARGE - REDUCTION

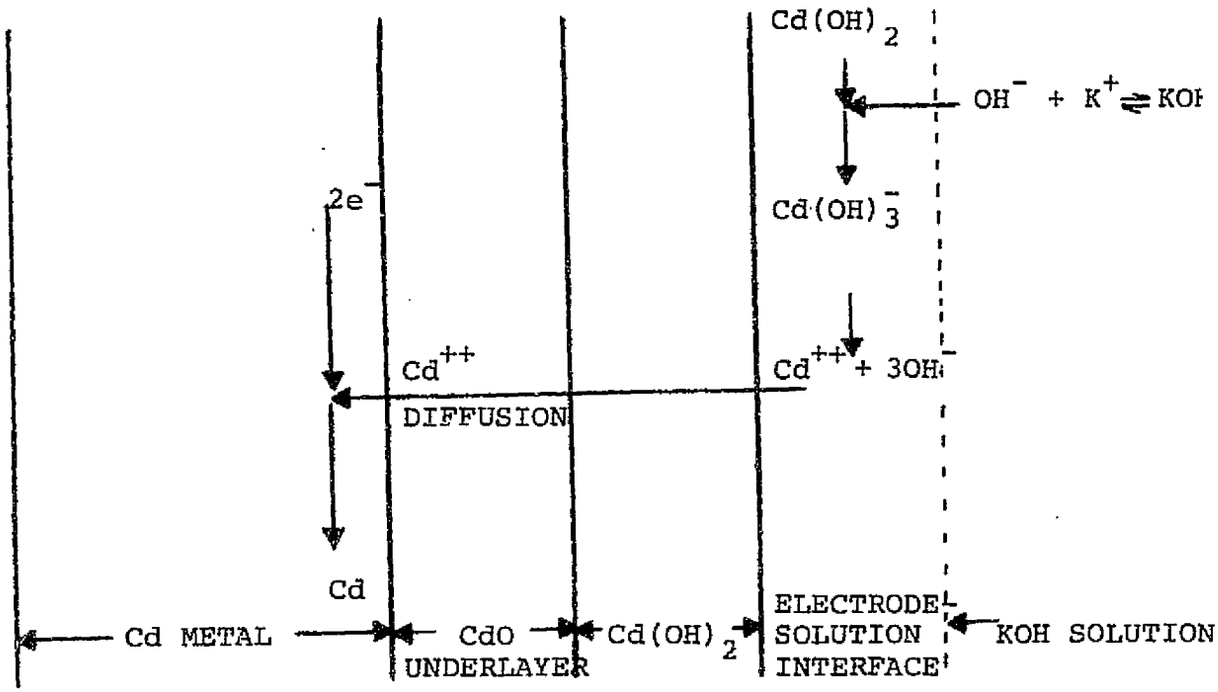

Figure 49 a) and b). Mechanism of the reactions occurring at the Cd-electrode

approximately 50mV less cathodic than the latter.

From the limiting current measurements as shown in Fig. 20, the effect of rotation speed on the value of the limiting current does not seem to be significant. However, when the results are compared to those of the Ni-electrode, the influence in this case appears to be greater. This is in agreement with the proposed mechanism, since there is a transport of Cd^{++} through a liquid phase in addition to that through a solid phase. For the cathodic reaction a small increase in the absolute value of the limiting current is observed with increase of rotation speed, thus exhibiting a behavior consistent with the proposed mechanism. During the anodic reaction, however, a decrease in the value of the limiting current is observed with increase of rotation speed. This could be attributed to the complexity of the oxidation reaction, which has two different products, CdO and $Cd(OH)_2$, the former undergoing continuous dissolution and the latter formed through a soluble intermediate. Hence, the composition of the oxidized active material is a critical factor for the value of the limiting current. Under a particular set of experimental conditions, this composition could be altered which in turn would cause a shift in the limiting current.

In summary, experimental results on the current-potential behavior of the Cd-electrode during cyclic sweep and limiting current measurements, are consistent with the

proposed electrode reaction mechanism.

Charge Acceptance Measurements - from d-c charging experiments given in Table 6, a decrease of charging efficiency is noticed with increase of charging current and time. These losses could be attributed mostly to gas evolution, which can be explained in terms of the passivation of the electrode during oxidation. Therefore when reduced, during the subsequent cycle, less A-hr are needed as compared to the previous one. As a result gas will evolve if the A-hr supply is kept constant throughout all the cycles. Increase in charge acceptance with increase in charging current and time, suggests that even after gas evolution is initiated, the current efficiency for the reduction of the oxidized species is greater than zero, resulting in accumulation of charge. In addition, faster charging rates were found to increase the charge acceptance of the electrode. This would not have been observed if the electrode reaction was controlled by the dissolution-precipitation mechanism. It is well established that smaller crystals of the active material have greater ability to react than larger ones. Therefore, if the crystal size of Cd is decreased, a greater charge acceptance is expected. For systems described by the dissolution-precipitation mechanism, a decrease of charge acceptance was reported, by Okinaha (43), with increase of charging rate, due to the formation of large Cd crystals.

From the theories of crystallization (41), the above mentioned observation could be explained as follows. There are two energy thresholds, one - of nucleation, and the other - of the interphase, the former being higher than the latter. The nucleation threshold energy is the energy necessary for the species to undergo nucleation, while the interphase threshold energy is the required energy for the species to cross the interphase. For the dissolution-precipitation mechanism, crystallization occurs at the solid-liquid interphase. An increase in charging rate will cause an increase in the concentration of Cd^{++} at the solid-liquid interphase, which in turn increases the interphase threshold energy, thus decreasing the amount of energy available for nucleation. As a result crystal growth will be favored over nucleation and the crystals formed will be larger. In the case of the solid state-dissolution-precipitation mechanism, the crystallization of Cd occurs at a solid-solid interphase. At fast charging rates it was established that the thickness of the CdO layer decreases, which resulted in a decrease of the interphase threshold energy. Therefore more energy is available for nucleation and nucleation will be favored over crystal growth, resulting in smaller crystals with better charge acceptance. A summary of the effect of charging rate on crystal size for both mechanisms is schematically represented in Fig. 50. The

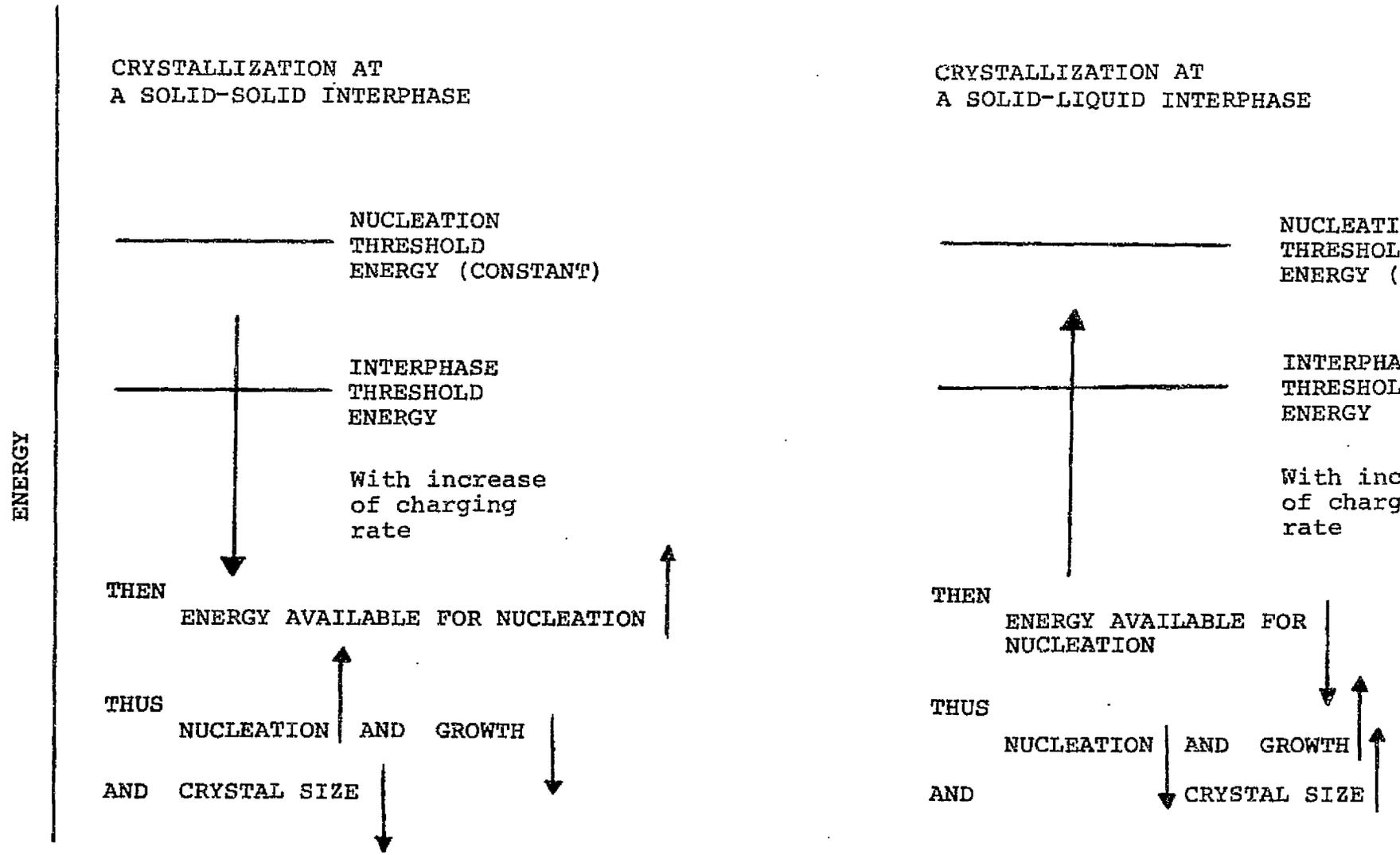

Figure 50. Effect of charging rate on crystal size for crystallization at a solid-solid interphase and a solid-liquid interphase

experimental findings from this work correspond to the effects expected during crystallization at a solid-solid interphase.

The charge acceptance under p-c charging conditions was compared to that under d-c charging conditions and expressed as a ratio in Tables 7 and 8. In general an increase of charge acceptance is observed with increase of duty cycle and instantaneous current density. This could be due to the fact that during the off period of the current, self-discharge takes place, thus reducing the electrode capacity. At shorter duty cycles (e.g. 0.1 and 0.25) the losses due to self-discharge are greater as compared to those for longer duty cycles. As a result, the charge acceptance at duty cycles of 0.1 and 0.25 (50Hz frequency and 5mA instantaneous current) is smaller than that under d-c charging conditions. In support to this effect, self-discharge measurements are presented for various duty cycles and are summarized in Table 9. It is seen that the net charge, supplied to the system during one complete cycle of the pulse current, decreases with a decrease in duty cycle and increases with an increase in instantaneous current. In addition, an increase of charging rate was found to cause an increase in charge acceptance (cf. Tables 7 and 8) which is consistent with the observations under d-c conditions. The amount of charge accumulated during the eighth cycle was compared

to that during the first cycle and represented in terms of a percentage of the initial charge, as shown in Table 19. In general a decrease in percent of charge accumulated is observed with increase of duty cycle and instantaneous pulse current, implying that losses due to gas evolution are greater at longer duty cycles. This is consistent with the theoretical development of the effect of pulsed current on concentration overpotential. Comparing these results with the ones for Ni-electrode (cf. Table 18), the effect was found to be more pronounced for the Cd-electrode, since according to the proposed mechanisms, the reaction at the Cd-electrode exhibits a greater dependence on mass transfer through a liquid phase than that at the Ni-electrode. Since the charge acceptance was found to increase, while the percent of charge accumulated decreased, with an increase in duty cycle and instantaneous pulsed current, it appears that mass transfer is not the only aspect of the system affected by p c charging. The kinetics of the reaction could also be influenced through structural modifications and the formation of a different type of active material. The value of the overpotential during the discharge reaction was calculated in the same way as for the Ni-electrode, and plotted versus fraction of capacity discharged, as shown in Fig. 51. The variation of overpotential with p-c characteristics suggests that the composition of the active material formed on

Table 19

Cd-electrode, per cent of initial charge accumulated during the eight cycle under d-c and p-c charging conditions

Experiment #	Q_1%	Q_2%
C1	73.40	86.70
C7	100.00	100.00
C8	57.40	78.70
C10	50.00	75.00
C11	84.00	92.00
C12	49.40	74.70
C14	46.60	73.30
C15	79.05	92.02
C16	60.00	80.00
C18	61.20	80.60
C19	100.00	100.00
C20	76.00	88.00

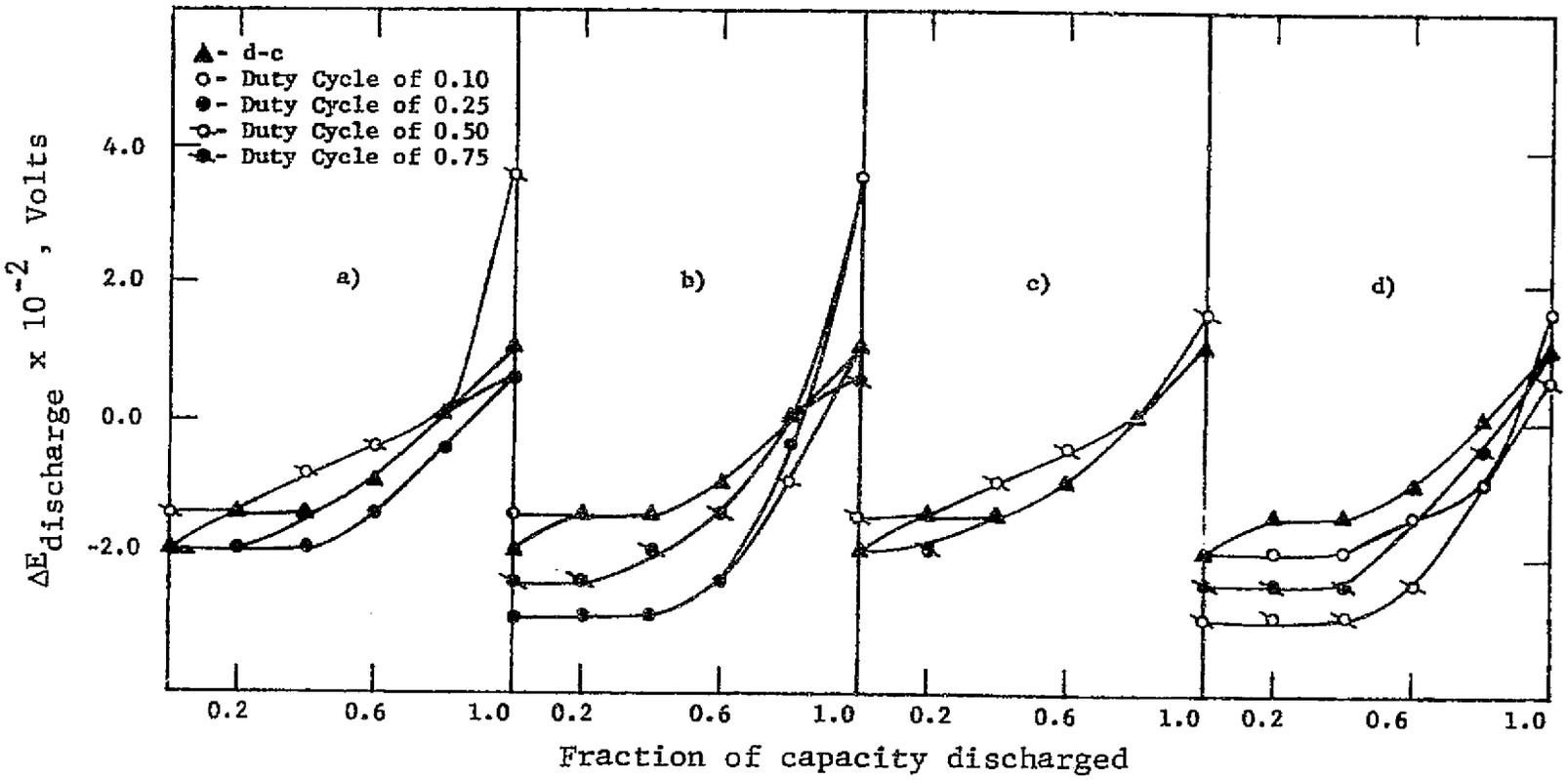

Figure 51. A plot of $\Delta E_{discharge}$ vs. fraction of capacity discharged for the Cd-electrode

discharge, depends on the type of pulsed current used during charge. The charge acceptance exhibited a maximum when charged with 10mA instantaneous p-c, duty cycle of 0.5 and a frequency of 50 Hz, while a minimum was obtained for a charging current of 5mA instantaneous p-c, duty cycle of 0.1 and frequency of 50 Hz. These are the same conditions under which the Ni-electrode showed a maximum and a minimum, respectively, in the charge acceptance values.

Structural Studies - from SEM pictures of the surface of a charged Cd-electrode as shown in Figs. 31-35, effect of p-c charging on surface morphology is evident. Under d-c charging conditions, the surface showed random orientation, while under p-c charging conditions preferred orientation with a more uniform surface was observed. In addition, the crystal size was found to decrease with decrease of duty cycle and increase of instantaneous pulse current. This is due to the fact that at shorter duty cycles, the effect of p-c on concentration overpotential is more pronounced. Thus the driving force (i.e. the concentration gradient) for crystallization is smaller, which in turn causes the formation of smaller crystals at slow charging rates. At slow charging rates, crystal growth is favored, with the reaction mechanism under consideration, a smaller driving force under crystal growth control will cause the formation of smaller

crystals. An increase of instantaneous p-c for a given duty cycle will result in fast charging rates. According to the crystallization analysis presented in Fig. 50, smaller crystals will be formed. Therefore the observations from the SEM pictures are consistent with the proposed mechanisms and interpretations of the system behavior. In addition from SEM pictures of greater magnification at 10000X and 30000X as shown in Figs. 36, 37 and Figs. 38, 39 respectively, the presence of two other phases is observed. One of them is in the form of lighter color crystals of smaller size showing lesser adherence to the surface. The amount of this crystalline material appeared to be a function of p-c characteristics. It was found to increase at decreasing duty cycle and also to be present in samples charged with d-c. Comparing these observations with charge acceptance measurements, a decrease in charge acceptance was found with an increase of the amount of the material under consideration. Based on this fact and also on the effect of self-discharge during shorter duty cycles, it is most likely that this material is $Cd(OH)_2$. The other material is of considerably smaller size, in some cases having the appearance of a thin dispersed film of droplets adhered to the Cd crystals. During SEM measurements, samples containing this substance exhibited poor conductivity. The amount as well as the appearance of the material were

found to be affected by the charging current. It was present in small quantities in samples charged with d-c. For samples charged with p-c, the amount of the material was found to increase with a decrease in duty cycle. At longer duty cycles it was present in the form of a dispersed film of small droplets. With a decrease of duty cycle, the droplets seemed to become larger and at a value of $\frac{\theta_1}{\theta} = 0.1$, they appeared as small crystals. For a Cd-electrode charged at 10mA instantaneous p-c, 0.5 duty cycle and 50Hz frequency, this substance was not present. Comparing this with charge acceptance measurements, the electrode giving maximum charge acceptance did not show the presence of the dispersed film, while that having minimum charge acceptance showed a significant amount of this substance mostly in the form of small crystals. Even though this material could not be identified, it seems to be less conductive than Cd and $Cd(OH)_2$ which hinders the discharge reaction or possibly passivates the charge reaction.

TEM pictures of two electrodes charged under 5mA d-c and a p-c of 5mA instantaneous current, 0.5 duty cycle and 50Hz frequency, showed in both samples, the presence of two phases a small and a large grain phase as shown in Fig. 40. For the electrode charged with d-c, a homogeneous small grain phase was seen on and near the surface. The appearance of another phase, of considerably larger grain

size was observed with scans away from the surface. For the electrode charged with p-c, the small grained phase was found not only near the surface but also in areas removed from it. The information thus provided could not be interpreted either qualitatively or quantitatively, due to the uncertainties involved in the experimental technique used. Hence, these results were inconclusive.

X-ray diffraction measurements were taken from surface scans of Cd-electrodes charged under d-c and a variety of p-c conditions as shown in Figs. 41-45. The presence of both Cd and $Cd(OH)_2$ was observed for all samples. This confirms that the small crystalline material as shown in the SEM pictures is $Cd(OH)_2$. The variation of the intensities of Cd and $Cd(OH)_2$ peaks suggests that the relative amounts of these two substances vary with the charging conditions. However, the exact dependence on duty cycle and instantaneous current could not be defined, since the diffraction patterns are affected by the orientation of the substrate, and their quantitative representation could lead to erroneous results. In order to avoid the substrate influence, X-ray diffraction by the powder method was conducted. The patterns thus obtained provided very little information due to the high level of background noise. A typical example is given in Fig. 46.

In summary, under the experimental conditions used in this work, the solid state-dissolution-precipitation mechanism seems to describe the Cd-electrode reactions satisfactorily, with the rate controlling step being Cd^{++} transfer through both a solid (CdO) and a liquid (electrode-solution interface) phases. The cause of passivation on discharge is the formation of CdO layer. The effect of p-c charging on charge acceptance is relatively small. It is nevertheless more pronounced than that in the case of Ni-electrode. This is due to the fact that the reactions at the Cd-electrode show a greater dependence on mass transfer through a liquid phase.

This dependence also causes variations in the crystal size of the active material with duty cycle and charging rate. The kinetics of the reaction seem to be influenced as well, since there is evidence, from SEM pictures, for the formation of a different material on the electrode surface. In addition, self-discharge becomes important for shorter duty cycles, causing a decrease of charge acceptance.

C. Reduction of Concentration Overpotential by Pulsed Current Electrolysis

The concentration overpotential of both the oxidation and reduction reactions for the ferro-ferricyanide system was measured under d-c and variety of

p-c conditions and several rotation speeds. Based on the experimental data, the reduction of concentration overpotential was calculated and compared to the theoretical values as shown in Fig. 16. From this figure good agreements were found between the experimental and theoretical results. This theoretical formulation could be of practical importance for other electrolytic processes as well. Some of the possible applications are mentioned below. If the reaction kinetics and crystallization mechanism are known for a given electrodeposition process, a pulsed current could be applied such that the crystal size and orientation will be modified to the desired specifications. In addition, a greater uniformity of the surface could be achieved. Due to the reduction of concentration overpotential, the application of some pulses could result in considerable amount of power savings. In some cases faster rates could be achieved for a given process by applying a p-c with i_p such that $(i_{p-c})_L > i_p >> (i_{d-c})_L$, without the interference of gas evolution.

VIII

CONCLUSIONS

A systematic investigation on the performance of Ni-Cd cells by pulsed current charging was conducted under a variety of well-defined charge-discharge conditions. Experiments were carried out with half cells and film electrodes. The system behavior was studied by means of charge acceptance, mechanistic and structural measurements which lead to a basic understanding of the effect of p-c on the charge acceptance of Ni and Cd half cells.

For the Ni-electrode the reversible electrode potential was calculated to be 0.3874V, while that of the Cd-electrode was - 0.9065V . These values are in good agreement with those reported in the literature (24, 33 and 38).

The reactions at the Ni-electrode were found to be represented by eqn. (46). They can be described by a solid-state mechanism as shown in Fig. 47. In this case the charge transfer reaction is fast and the rate controlling step is the diffusion of H^+ through a solid phase. The diffusion coefficients of H^+ during the oxidation and reduction reactions were calculated and found to be 5.28×10^{-10} cm^2/sec and 2.16×10^{-9} cm^2/sec, respectively. These values are in good agreement with those reported by MacArthur (34).

The transfer coefficients for both the oxidation and reduction reactions were evaluated and found to be 0.49 and 1.70 respectively. Under the experimental conditions used in this work, the solid state-dissolution precipitation mechanism was found to describe the reactions at the Cd-electrode as presented in Fig. 49. In this case the charge transfer reaction is fast and the rate controlling step is the diffusion of Cd^{++} through both a solid (CdO) and a liquid (electrode-solution interface) phase. The diffusion coefficients of Cd^{++} during the oxidation and reduction reactions were calculated and found to be 3.81×10^{-10} cm^2/sec and 1.82×10^{-10} cm^2/sec, respectively.

From d-c charge acceptance studies for the Ni-electrode, premature gas evolution during charge, was attributed to the formation of a passivating film, Ni_3O_4, during discharge. An increase in charging rate caused an increase of charge acceptance and charging efficiency, whereas the percent of charge accumulation decreased. This suggests that at fast charging rates, the improvement in the system's performance is due to either the formation of a different type of active material, or the reduction of losses from self-discharge.

Under p-c charging conditions, similar behavior was exhibited with an increase of charging rate. A reduction of mass transfer limitations was found, resulting in a postponement of gas evolution. This effect became more

pronounced with decreasing duty cycle. At duty cycles of 0.1 and 0.25 no gas evolution was observed when i_p is equal to i_{d-c}. Self-discharge proved to be a critical factor for the performance of the system. With an increase of duty cycle, losses due to self-discharge decreased, resulting in an increase of charge acceptance. The system exhibited a minimum charge acceptance at an instantaneous charging current of 5mA, a duty cycle of 0.1, a frequency of 50 Hz, and a maximum at 10mA instantaneous p-c, 0.5 duty cycle and 50 Hz frequency. The minimum is consistent with the effect of p-c on self-discharge, while the maximum suggests a possible modification in the reaction kinetics, due to either the formation of a different type of active material, or changes in the structure. SEM pictures showed that the active material, obtained under the experimental conditions of this work, is amorphous in nature and the surface morphology depends on the degree of dehydration. It is important to emphasize that the affect of p-c charging on the charge acceptance of the Ni-electrode, obtained by this study, was not of significant magnitude. In general, an increase in duty cycle and instantaneous current caused an increase in charge acceptance, whereas variation in frequency itself showed little or no effect. The performance of the system exhibited complex dependence on self-discharge and reaction kinetics.

From d-c charge acceptance studies for the Cd-electrode, premature gas evolution during charge was attributed to CdO formation during discharge. An increase of charging rate resulted in an increase of charging efficiency and charge acceptance, while the percent of charge accumulated decreased. Since crystallization of the active material during charge occurs at a solid-solid interphase, smaller crystals were formed at faster charging rates, whereby the charge acceptance of the system increased.

Under p-c charging conditions, a similar behavior was observed with an increase of charging rate. An increase of duty cycle and instantaneous p-c caused an increase in charge acceptance. Pulsed current charging was found to influence the mass transfer of the system. This effect was greater for the Cd-electrode than for the Ni-electrode which is consistent with the proposed reaction mechanism. From SEM, X-ray diffraction and charge acceptance measurements, losses due to self-discharge were found to decrease with increasing duty cycle. The system was also found to exhibit a maximum and a minimum in charge acceptance at conditions identical to those for the Ni-electrode. The appearance of a minimum is consistent with the effect of p-c on self-discharge, while that of the maximum is consistent with crystallization at fast charging rates. Under the experimental conditions used in this work, the effect of p-c charging on the charge acceptance of the Cd-electrode

was also not of a significant magnitude. However, it was greater than that for the Ni-electrode. It is apparent that the performance of the Cd-electrode shows a complex dependence on crystal size, self-discharge, type of active material formed and gas evolution during charge. All these factors are in turn functions of the charging characteristics. At slow charging rates the losses due to self-discharge become the performance determining factor, while at fast charging rates crystal size combined with the type of active material formed become the important factors.

In summary, both Ni- and Cd-electrodes show similar behavior under p-c charging, exhibiting a maximum and a minimum in charge acceptance at identical charging conditions. Their performance shows dependence on self-discharge, type of active material formed and in the case of Cd, crystal size of the active material. All these factors are functions of pulsed characteristics. Pulsed current charging was found to cause a postponement in gas evolution for both electrodes, with the effect being more pronounced in the case of Cd. These findings and the critical performance factors have practical importance in the charging of Ni-Cd cells. For instance, utilizing a p-c of optimum characteristics, an improvement in charge acceptance, a shorter charging time and a power saving could be achieved.

The effect of p-c electrolysis on the mass transfer of an electrochemical system was evaluated. A model

was developed for the reduction of concentration overpotential as a function of instantaneous current density, duty cycle and frequency. This model was experimentally verified with a ferro-ferricyanide system. Excellent agreements were obtained between the experimentally determined and theoretically calculated values. Both, duty cycle and instantaneous current density showed a very strong effect on the reduction of concentration overpotential for a given value of $a\theta$. A decrease in duty cycle and an increase in $i_p/(i_{d-c})_L$ caused an increase in the reduction of concentration overpotential. This is of practical importance for electrolytic systems, where power savings could be achieved by applying a pulse of particular characteristics.

IX.

RECOMMENDATIONS

Based on the results from this investigation, the following is a list of recommendations for further study.

1. Additional mechanistic studies on film electrodes under p-c conditions should be performed. For the Ni-electrode the anodic limiting current should be measured under p-c conditions, followed by measurements of the cathodic limiting current under d-c conditions. The value of $(i_p)_L$ for the anodic (charge) reaction has an effect on the limiting current of the cathodic (discharge) reaction. Moreover, the limiting rate of a reaction can be expressed in terms of the limiting current, leading to a prediction of the maximum charging rate. Similarly, for the Cd-electrode, the cathodic limiting current for p-c electrolysis should be measured, while the anodic limiting current should be evaluated under d-c condtions.

2. Additional structural and analytical investigations should be carried out in regard to the active material of both electrodes for quantitative evaluation of its composition.

3. Structural and analytic studies for both discharged electrodes should also be performed. This will provide information about modifications in the kinetics

and structure of the discharged material.

4. The reduction of concentration overpotential by p-c charging should be evaluated at both electrodes at various pulsed currents. This will quantify the effect of p-c on mass transfer. In addition, it will show the applicability of our theoretical calculations to real systems.

5. In contrast to the film electrodes used in this work, it is likely that mass transport limitations can play a major role in governing the behavior of sintered electrodes. If this were the case, p-c charging could have a considerably larger effect. Consequently, a systematic investigation on charge acceptance with p-c charging should be carried out with sintered plates. At short duty cycles, the reduction of mass transfer limitations is significant, however, this effect is accompanied with losses due to self-discharge. The results of a systematic study would yield information on the relative importance of these two opposing factors. Based on the results from this work, major effects are likely to be observed at large instantaneous current density, frequency within 50 and 200 Hz, and duty cycle in the range of 0.25 to 0.75.

6. Theoretical modeling should be attempted for the sintered-plate electrodes.

7. Experiments should also be performed with commercially available Ni-Cd batteries, under a set of

well selected p-c charging conditions. This will show the applicability of the findings from the half cell experiments, to real batteries.

BIBLIOGRAPHY

1. R. N. Adams, "Electrochemistry at Solid Electrodes," M. Dekker, New York, 1969.

2. G. C. Akerlof and P. Bender, J. Am. Chem. Soc. 70, 2366 (1948).

3. R. D. Armstrong, K. Edmondson and G. D. West, "The Electrochemical Behavior of Cadmium in Alkaline Solution," Electrochem. 4, 18 (1974).

4 S. Arouete, K. F. Blurton and H. G. Oswin, J. Electrochem. Soc. 116, 166 (1969).

5. J. O'M. Bockris and B. E. Conway (ed.), "Modern Aspects of Electrochemistry" 6, Plenum Press, New York, 1971.

6. J. O'M. Bockris and Z. Nagy, J. Chem. Education 50, 839 (1973).

7. J. O'M. Bockris and A. K. N. Reddy, "Modern Electrochemistry" 2, Plenum/Rosetta Edition, Plenum Press, New York, 1973.

8. H. Bode, K. Dehmelt and J. Witte, "Nickel Hydroxide Hydrate," paper presented at CITCE Meeting, Strasburg, France, 1965.

9. W. A. Boyd, "Pulse Charging Techniques for Nickel-Cadmium Batteries," paper presented at the Electrochem. Soc. Meeting, Cleveland, Ohio, October, 1971.

10. M. W. Breiter and K. Vedder, Trans. Faraday Soc. 63, 1042, 1967.

11. D. C. Briggs, "Hermetically Sealed Nickel-Cadmium Batteries for the Initial Defense Communication Satellite Program/Augmentation (IDCSP/A)," IECEC '68 Record 689001.

12. G. [illegible]. Briggs, "The Nickel Hydroxide and Related [illegible]des," Electrochem. 4, 33 (1974).

13. S. Bruckenstein, J. Electrochem. Soc. 122, 1215 (1975).

14. E. J. Casey and C. L. Gardner, J. Electrochem. Soc. 122, 851 (1975).

15. G. Charlot, J. Badoz-Lambling and B. Tremillon, "Electrochemical Reactions," Elsevier Publishing Company, Amsterdam - New York, 1962.

16. H. Y. Cheh, J. Electrochem. Soc. 118, 551 (1971).

17. H. Y. Cheh, J. Electrochem. Soc. 118, 1132 (1971).

18. H. Y. Cheh and R. D. Sard, J. Electrochem. Soc. 118, 1737 (1971).

19. D. L. Chua, "Relationship of Electrode Structures and Cell Performance in Sealed, Sintered-Type Nickel-Cadmium Button Cells During Cycling," Ph.D. Thesis, Rensselear Polytechnic Institute, Troy, New York, 1973.

20. B. E. Conway, "Theory and Principles of Electrode Processes," Ronald Press, New York, 1965.

21. P. Delahay, "New Instrumental Methods in Electrochemistry," Interscience Publishers, New York, 1954.

22. P. Delahay, "Instrumental Analysis," Macmillan, New York, 1957.

23. J. D. Dunlop and R. W. Bounds, "Adhydrode Control of Ni-Cd Battery Charging to Evaluate Charging Methods," IECEC '68 Record 689002.

24. S. U. Falk, J. Electrochem. Soc. 107, 661 (1960).

25. S. U. Falk and A. J. Salkind, "Alkaline Storage Batteries," Wiley, New York, 1969.

26. E. Gileadi, E. Kirowa-Eisner and J. Penciner, "Interfacial Electrochemistry an Experimental Approach," Addison-Wesley, Massachusetts, 1975.

27. N. N. Khoi, W. W. Smeltzer and J. D. Embury, J. Electrochem. Soc. 122, 1495 (1975).

28. F. P. Kober, J. Electrochem. Soc. 112, 1064 (1965).

29. F. P. Kober, J. Electrochem. Soc. 114, 215 (1967).

30. P. E. Lake and E. J. Casey, J. Electrochem. Soc. 105, 52 (1958).

31. W. M. Latimer and J. H. Hildebrand, "Reference Book of Inorganic Chemistry," Third Edition, Macmillan, New York, 1951.

32. V. G. Levich, "Physicochemical Hydrodynamics," Prentice Hall, Englewood Cliffs, 1968.

33. D. M. MacArthur, J. Electrochem. Soc. 117, 422 (1970).

34. D. M. MacArthur, J. Electrochem. Soc. 117, 729 (1970).

35. C. L. Mantell, "Batteries and Energy Systems," McGraw-Hill, New York, 1970.

36. L. May, "The Effect of the Electrolyte on the Open Circuit Potentials in the Nickel-Cadmium Cell," paper presented at the Goddard Space Flight Center, Greenbelt, Maryland, 1975.

37. R. S. McEwen, J. Phys. Chem. 75, 1782 (1971).

38. P. C. Milner and U. B. Thomas, "The Nickel-Cadmium Cell," Adv. Electrochem and Electrochem. Eng. (C. W. Tobias ed.) 5, 1 (1967).

39. J. S. Newman, "Electrochemical Systems," Prentice-Hall, New Jersey, 1973.

40. J. S. Newman, "Transport Processes in Electrolytic Solutions," Adv. Electrochem. and Electrochem. Eng. (C. W. Tobias ed.) 5, 87 (1967).

41. M. Ohara and R. C. Reid, "Modeling Crystal Growth Rates from Solution," Prentice-Hall, New Jersey, 1973.

42. Y. Ohinaka, J. Electrochem. Soc. 117, 289 (1970).

43. Y. Ohinaka and C. M. Whitehurst, J. Electrochem. Soc. 117, 583 (1970).

44. J. H. Sluyters, Recueil 81, 297 (1962).

45. W. M. Smit and M. D. Wijnen, Recueil 79, 5 (1960).

46. W. M. Smit and M. D. Wijnen, Recueil 79, 22 (1960).

47. R. H. Sparks, "Rapid Charging Batteries for Electric Propulsion Systems," paper presented at the Automotive Engineering Congress, Detroit, Michigan, 1972.

48. Z. Takehara, M. Kato and S. Yoshizawa, Electrochem. Acta 16, 833 (1971).

49. P. Teppema, M. Sluyters-Rehibach and J. H. Sluyters, Recueil 85, 303 (1966).

50. V. P. Tysyachnyi, O. S. Ksenzhek and L. M. Pototskaya, Electrokhimiya 8, 1692 (1972).

51. G. W. Vinal, "Storage Batteries," Wiley, New York, 1955.

52. O. C. Wagner and D. D. Williams, "Investigation of Charge Methods for Nickel-Cadmium Batteries," paper presented at the Power Sources Conference, Atlantic City, New Jersey, 1974.

53. C. P. Wales, J. Electrochem. Soc. 111, 131 (1964).

54. C. P. Wales, J. Electrochem. Soc. 113, 757 (1966).

Appendix 1

Reduction of Concentration of Overpotential by Pulsed Current Electrolysis

Theoretical Development and Calculations

Appendix 1A - Previous derivation by Cheh (16)

Consider the system sketched below:

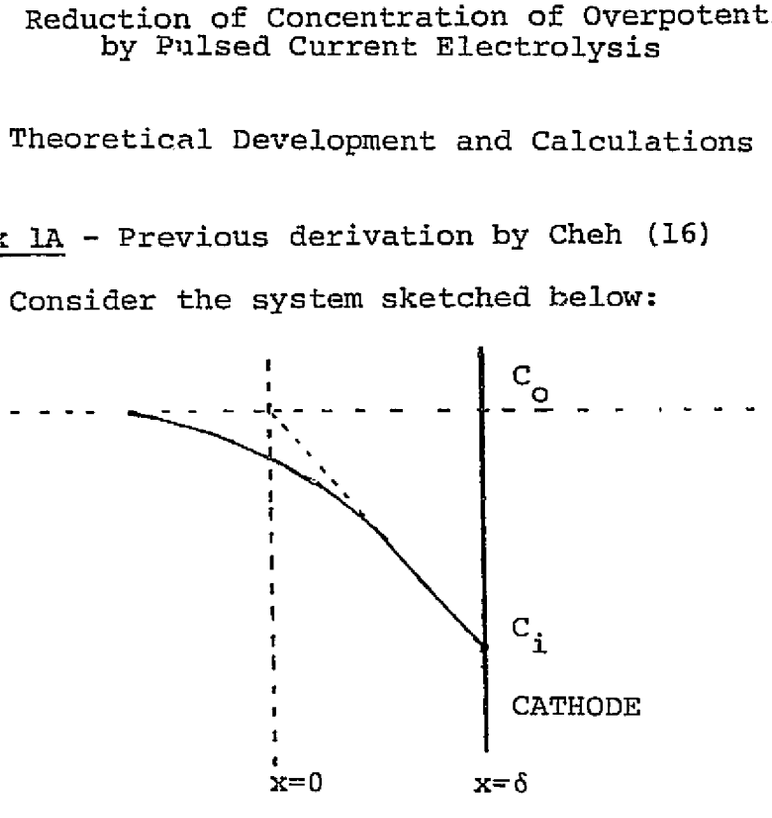

Then $$\frac{\partial C}{\partial t} = D \frac{\partial^2 C}{\partial x^2} \qquad \text{(A1)}$$

with boundary conditions:

1. $C = C_o$ @ $t = 0$, $x \geq 0$ (A2)

2. $C = C_o$ @ $t > 0$; $x = 0$ (A3)

3. $D \frac{\partial C}{\partial x} = \frac{i}{nF}$ @ $t > 0$; $x = \delta$ (A4)

When a pulsed current as shown in Fig. A1 is applied to the system, the current density in eqn. (A4) can be expressed as

during periods when the current is on

$$i = i_p \quad \text{for} \quad 0 < t \leq t_1 \; ; \; t_2 < t \leq t_3 \text{ etc.} \qquad \text{(A5)}$$

and during periods when the current is off

$$i = 0 \quad \text{for} \quad t_1 < t \leq t_2 \; ; \; t_3 < t \leq t_4 \text{ etc.} \qquad \text{(A6)}$$

the cyclic period is given by

$$\theta = \theta_1 + \theta_2 = t_2 = (t_4 - t_2) = t_6 - t_4) = \text{etc.} \qquad \text{(A7)}$$

Equation (A1), subject to the boundary conditions given by eqns. (A2) - (A6) was originally solved by Roseburgh and Miller. Based on their solution the surface concentration of the metal ion was evaluated to be

during periods when the current is on.

$$\frac{(C_i - C_o)nFD}{i_p \delta} = 1 - \frac{8}{\pi^2} \sum_{j-1}^{\infty} \frac{\exp[-(2j-1)^2 a\tau]}{(2j-1)^2} \; x$$

$$\frac{\exp[(2j-1)^2 a\theta] - \exp[(2j-1)^2 a\theta_1]}{\exp[(2j-1)^2 a\theta] - 1} - \qquad \text{(A8)}$$

$$\frac{8}{\pi^2} \sum_{j-1}^{\infty} \frac{\exp[-(2j-1)^2 at]}{(2j-1)^2} \; x$$

$$\frac{\exp[(2j-1)^2 a\theta_1] - 1}{\exp[(2j-1)^2 a\theta] - 1}$$

Figure A1. Schematic diagram of a pulsed current

where $a = \frac{\pi^2 D}{4\delta^2}$, $\tau = t - N\theta$ (A9)

during periods when the current is off

$$\frac{(C_i - C_o)FDn}{i_p \delta} = \frac{8}{\pi^2} \sum_{j=1}^{\infty} \frac{\exp[-(2j-1)^2 a\tau]}{(2j-1)^2} \times \frac{\exp[(2j-1)^2 a\theta] - \exp[(2j-1)^2 a\theta_2]}{\exp[(2j-1)^2 a\theta] - 1} -$$

$$\frac{8}{\pi^2} \sum_{j=1}^{\infty} \frac{\exp[-(2j-1)^2 a\tau]}{(2j-1)^2} \times \frac{\exp[(2j-1)^2 a\theta_1] - 1}{\exp[(2j-1)^2 a\theta] - 1} \quad \text{(A10)}$$

where $\tau = t - N\theta - \theta_1$ (A11)

Cheh (16) has shown that the transient terms in eqns. (A8) and (A10) decay rapidly and the system reaches a periodic state which is described by:

during periods when the current is on

$$\frac{(C_i - C_o)nFD}{i_p \delta} = 1 - \frac{8}{\pi^2} \sum_{j=1}^{\infty} \frac{\exp[-(2j-1)^2 a\tau]}{(2j-1)^2} \times \frac{\exp[(2j-1)^2 a\theta] - \exp[(2j-1)^2 a\theta_1]}{\exp[(2j-1)^2 a\theta] - 1} \quad \text{(A12)}$$

and during periods when the current is off

$$\frac{(C_i - C_o)nFD}{i_p \delta} = \frac{8}{\pi^2} \sum_{j=1}^{\infty} \frac{\exp[-(2j-1)^2 a\tau]}{(2j-1)^2} \times \frac{\exp[(2j-1)^2 a\theta] - \exp[(2j-1)^2 a\theta_2]}{\exp[(2j-1)^2 a\theta] - 1} \quad \text{(A13)}$$

Appendix 1B - theoretical calculations

Consider a rotating disk electrode system, with $D = 10^{-5}$ cm^2/sec, $\nu = 10^{-2}$ cm^2/sec and the electrode is rotating at 400 rpm. Then the thickness of the diffusion layer is given by

$$\delta = 1.61 \left(\frac{D}{\nu}\right)^{1/3} \left(\frac{\nu}{\omega}\right)^{1/2} \qquad \text{(A14)}$$

substituting the above values, $\delta = 0.0025$cm., a is evaluated from $a = \frac{\pi^2 D}{4\delta^2} = 3.95$. For $a\theta = 0.5$, the cycle time $\theta = 0.127$ sec. Based on eqns. (38) and (39) the instantaneous values of $(\eta_p)_c/(\eta_{d-c})_c$ were calculated for

$i_p = i_{d-c} = 0.2(i_{d-c})_L$, $0.4(i_{d-c})_L$, $0.6(i_{d-c})_L$,
$0.8(i_{d-c})_L$, $0.9(i_{d-c})_L$, $0.95(i_{d-c})_L$

$\theta_1/\theta = 0.2$, 0.4 , 0.6 , 0.8

and $a\theta = 0.5$

Results are summarized in Tables A1 - A4 and graphically represented in Figs. 2 and A2 - A4. The average reduction of concentration overpotential was evaluated by numerical intergration of Figs. 2 and A2 - A4. Results are summarized in Table A5 and graphically represented in Fig. 3.

Table A1

Instantaneous values of the $(\eta_p)_c/(\eta_{d-c})_c$ calculated from eqns. (38) and (39) for $\theta_1/\theta = 0.2$ and $a\theta = 0.5$

$a\tau$	$(\eta_p)_c/(\eta_{d-c})_c$ Instantaneous Value					
	0	.02	.04	.06	.08	.10 0
$1/(i_{d-c})_L$						
.2	.120727	.212571	.249683	.277840	.301387	.322011
.4	.106925	.190339	.224575	.250762	.272806	.292223
.6	.909682	.163307	.193632	.217041	.236896	.254500
.8	.069836	.127338	.151811	.170894	.187225	.201816

Table A1 (continued)

	$(\eta_p)_c/(\eta_{d-c})_c$ Instantaneous Values				
$a\tau$	.08	.16	.24	.32	.40
$1/i_{d-c})_L$					
.2	.193826	.164689	.146229	.132251	.120727
.4	.173166	.144627	.129909	.117299	.106925
.6	.148211	.125032	.110521	.099620	.090682
.8	.115261	.096847	.085397	.076834	.069836

Table A2

Instantaneous values of the $(\eta_p)_c/(\eta_{d-c})_c$ calculated from eqns. (38) and (39) for $\theta_1/\theta = 0.4$ and $a\theta = 0.5$

$a\tau$	$(\eta_p)_c/(\eta_{d-c})_c$ Instantaneous value					
	0	.04	.08	.12	.16	.20
$1/(i_{d-c})_L$						0
.2	.259938	.386384	.433532	.468120	.520821	.520821
.4	.234091	.353505	.399061	.432856	.460747	.484980
.6	.202117	.310796	.353410	.385465	.412219	.435690
.8	.158705	.249227	.285928	.314037	.337848	.359014

Table 2 (continued)

	$(\eta_p)_c/(\eta_{d-c})_c$ Instantaneous value				
a_T	.06	.12	.18	.24	.30
$1/(i_{d-c})_L$					
.2	.377086	.333578	.303411	.279763	.369948
.4	.395163	.303159	.274707	.252558	.234019
.6	.303066	.264463	.238614	.218654	.202117
.8	.359014	.210122	.188644	.172216	.158705

Table A3

Instantaneous values of the $(\eta_p)_c/(\eta_{d-c})_c$ calculated from eqns. (38) and (39) for $\theta_1/\theta = 0.6$ and $a\theta = 0.5$

$a\tau$	0	$(\eta_p)_c/(\eta_{d-c})_c$ Instantaneous value .06	.12	.18	.24	.30 0
$1/(i_{d-c})_L$						
.2	.424031	.568679	.615174	.647523	.673199	.694943
.4	.389837	.532999	.580301	.613600	.640266	.663015
.6	.344724	.482849	.530192	.564081	.591567	.615273
.8	.278387	.402380	.447132	.479988	.507181	.531051

Table A3 (continued)

	$(\eta_p)_c/(\eta_{d-c})_c$ Instantaneous value				
$a\tau$	.04	.08	.12	.16	.20
$1/(i_{d-c})_L$					
.2	.559620	.511133	.476213	.448043	.424031
.4	.523859	.475340	.440810	.413200	.389834
.6	.473804	.426327	.393067	.366773	.344724
.8	.393972	.350539	.320769	.297592	.278387

Table A4

Instantaneous values of the $(\eta_p)_c/(\eta_{d-c})_c$ calculated from eqns. (38) and (39) for $\theta_1/\theta = 0.8$ and $a\theta = 0.5$

$a\tau$	0	$(\eta_p)_c/(\eta_{d-c})_c$ Instantaneous value .08	.16	.24	.32	.40 0
$1/(i_{d-c})_L$						
.2	.627527	.768943	.802301	.823678	.839993	.853538
.4	.592978	.741615	.777667	.800980	.818886	.833828
.6	.543038	.699101	.738617	.764554	.784686	.801630
.8	.459502	.618914	.662441	.691844	.715160	.735136

Table A4 (continued)

	$(\eta_{p\ c}/(\eta_{d-c})_c$ Instantaneous value				
$a\tau$	.02	.04	.06	.08	.10
$1/(i_{d-c})_L$					
.2	.747726	.706271	.675300	.649709	.627527
.4	.718888	.674928	.642457	.615862	.592978
.6	.674544	.627783	.593841	.566400	.543038
.8	.592579	.543811	.509453	.482263	.459502

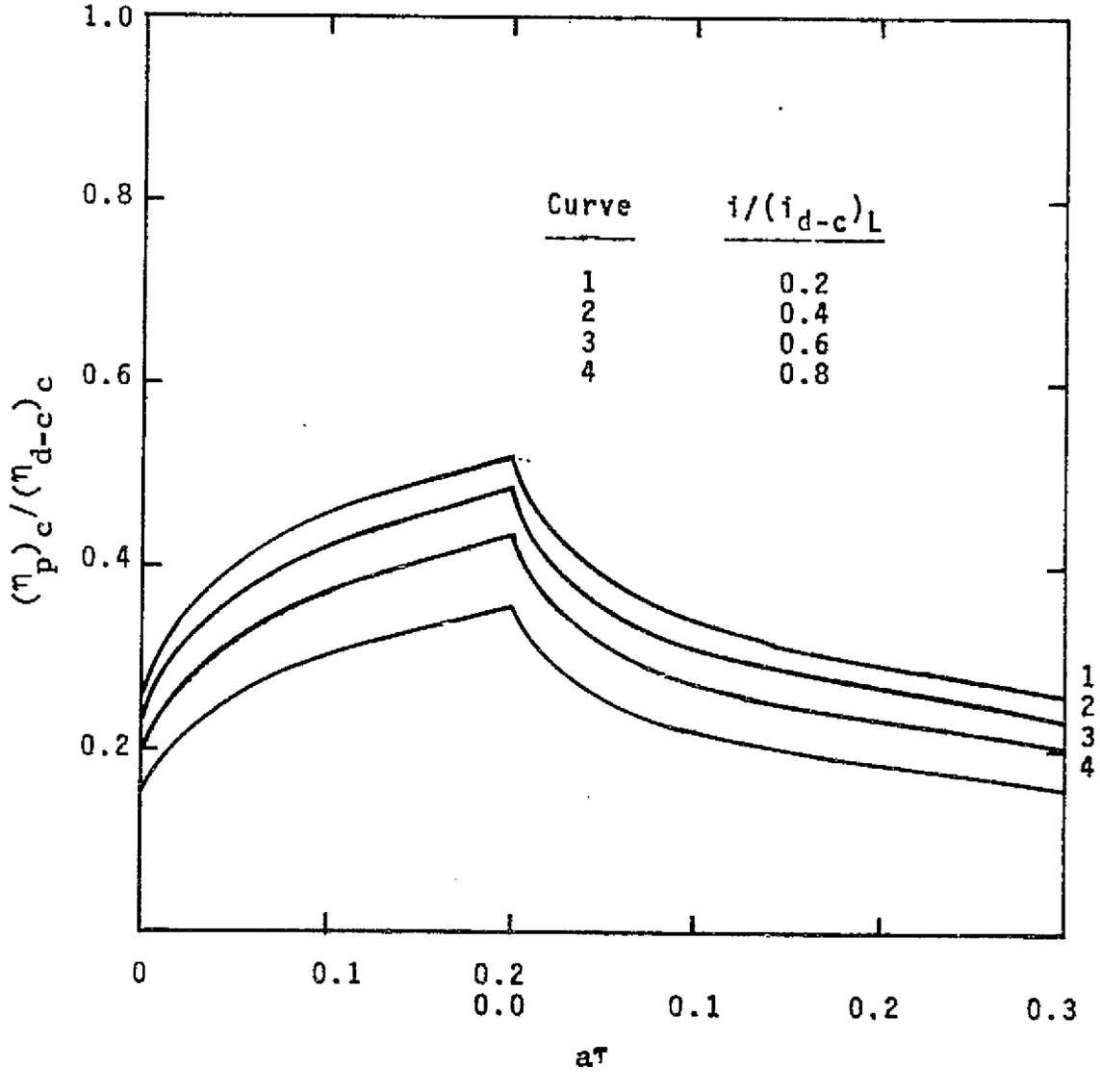

Figure A2. Instantaneous values of $(\eta_p)_c/(\eta_{d-c})_c$ during one complete cycle of the applied p-c, with a duty cycle of 0.4 and $a\theta$ of 0.5

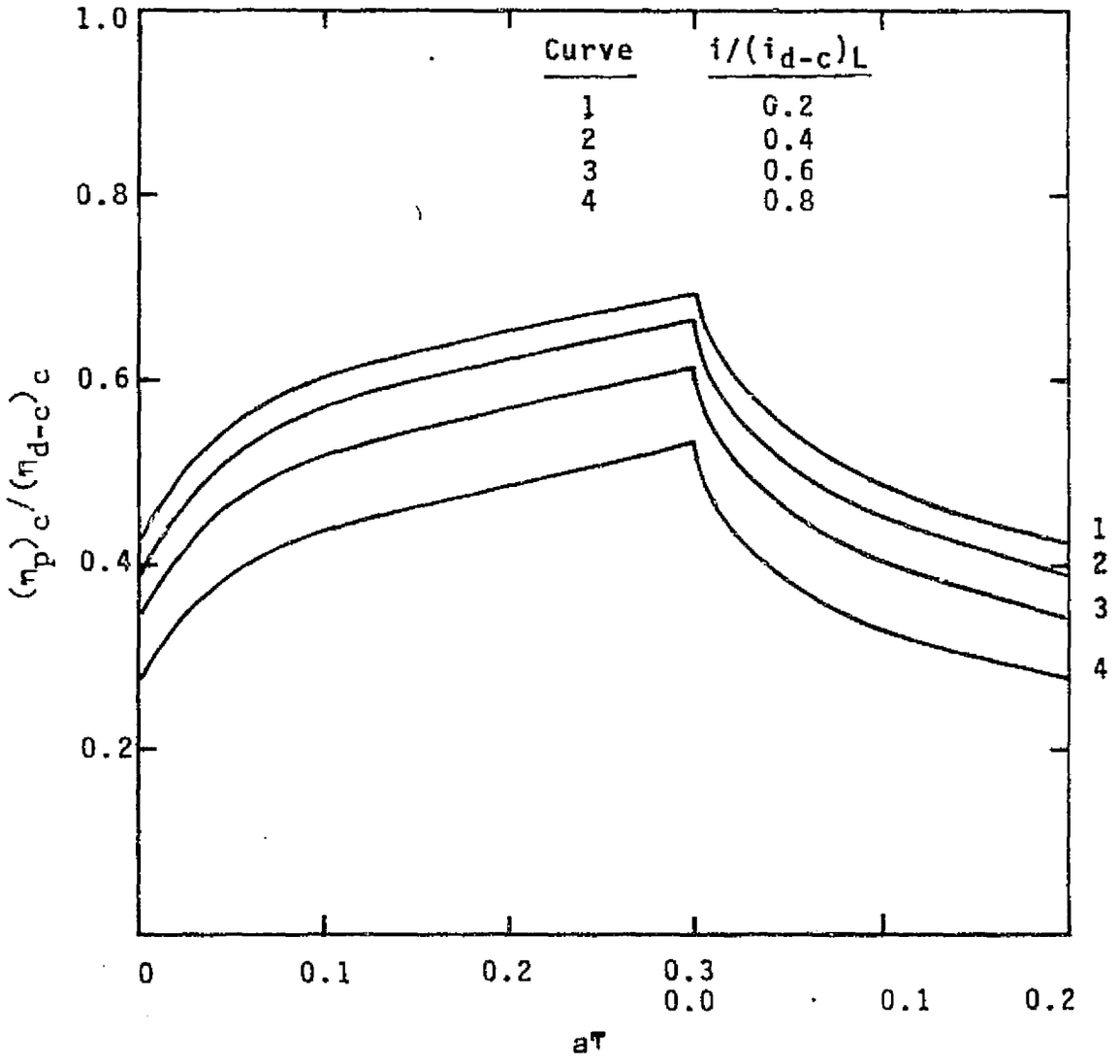

Figure A3. Instantaneous values of $(\eta_p)_c/(\eta_{d-c})_c$ during one complete cycle of the applied p-c, with a duty cycle of 0.6 and aθ of 0.5

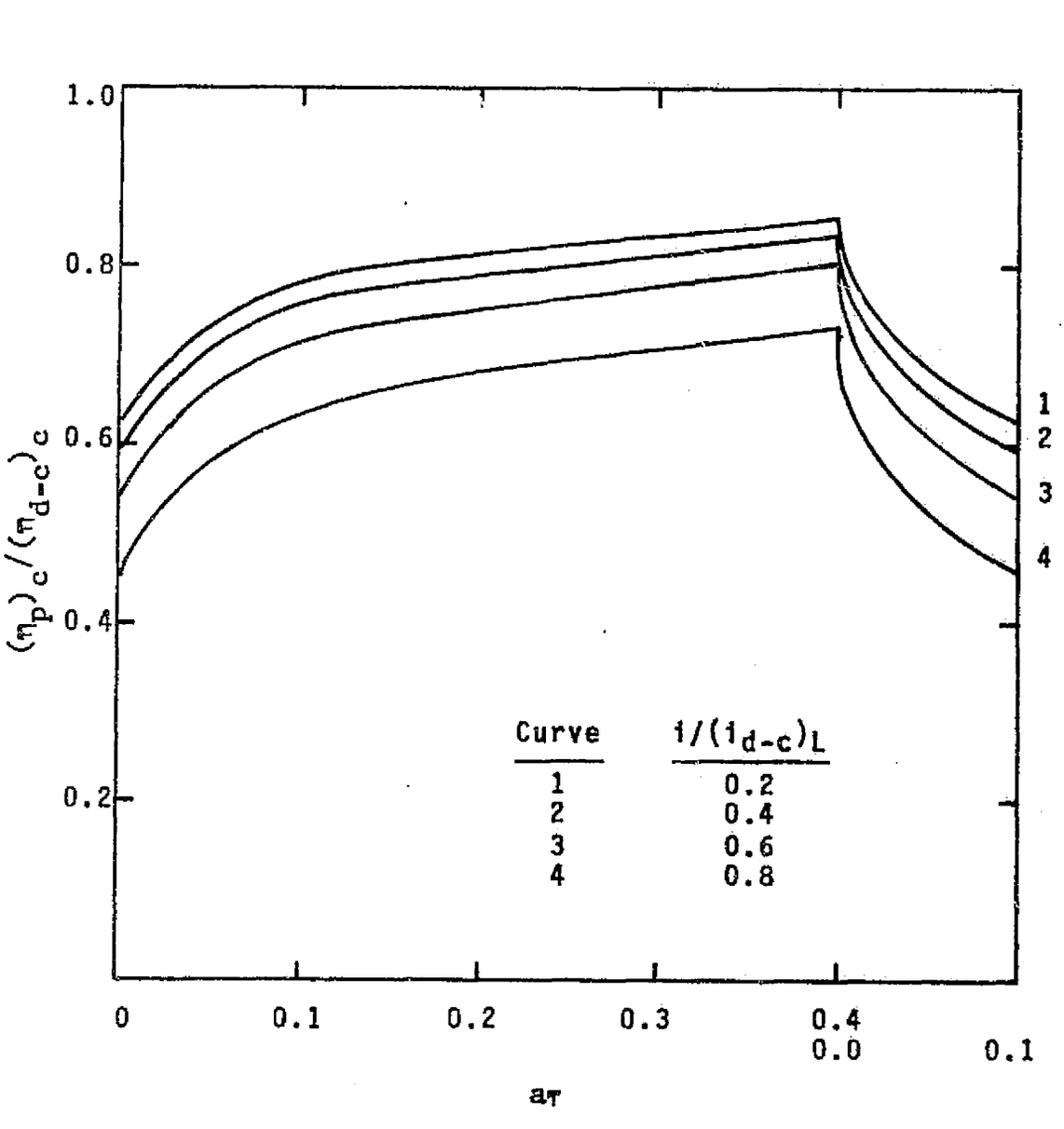

Figure A4. Instantaneous values of $(\eta_p)_c/(\eta_{d-c})_c$ during one complete cycle of the applied p-c, with a duty cycle of 0.8 and $a\theta$ of 0.5

Table A5

Average value of the reduction of concentration overpotential for $a\theta=0.5$

$[(\eta_p)_{c/}(\eta_{d-c})_c]$ average				
$\frac{\theta_1/\theta}{i/(i_{d-c})_L}$	.2	.4	.6	.8
.2	.185	.375	.573	.779
.4	.166	.344	.538	.754
.6	.142	.303	.490	.714
.8	.111	.243	.411	.637

Appendix 2

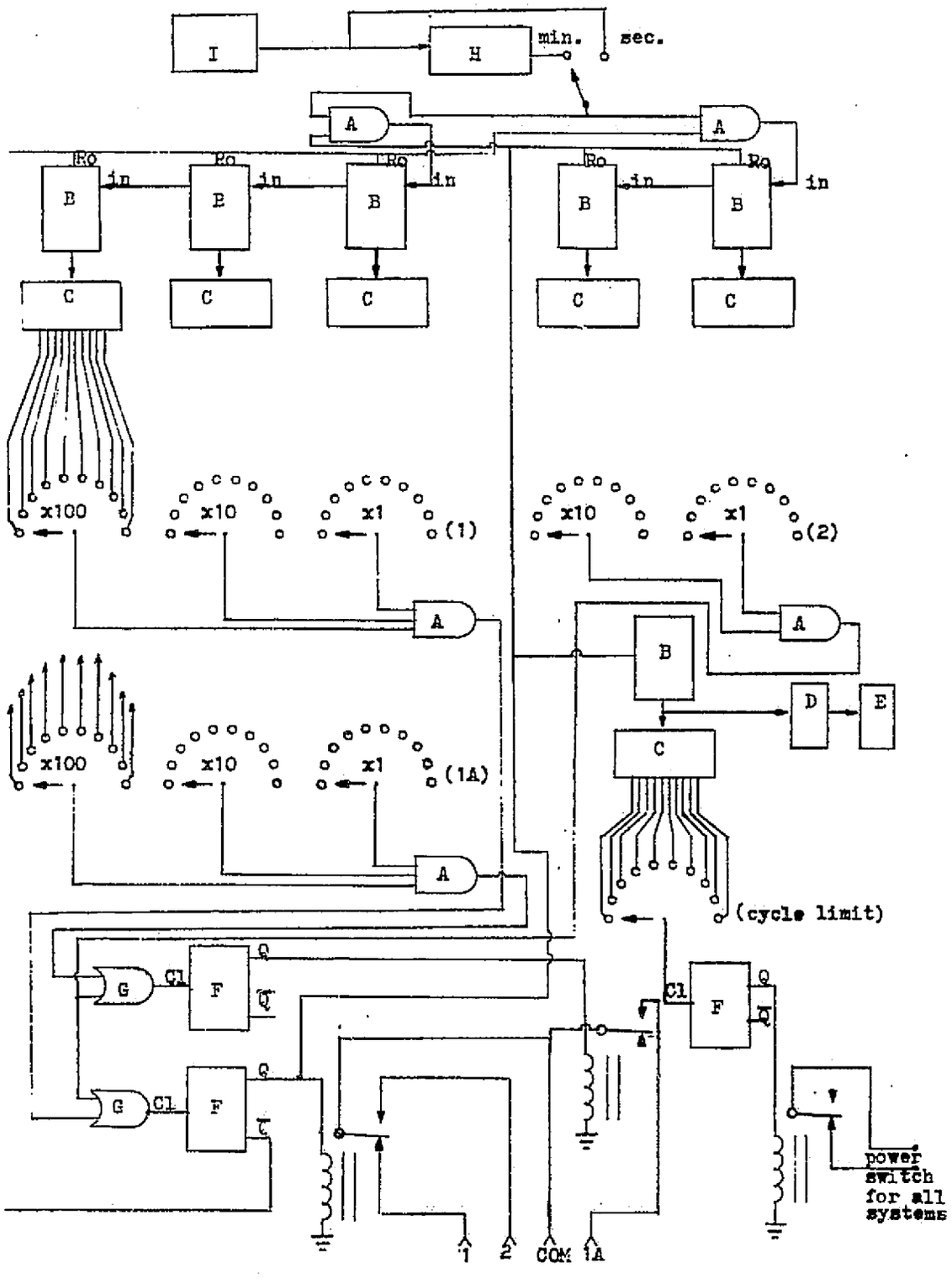

Figure A5. a) Schematic diagram of the electronic circuit used in the Time Control unit

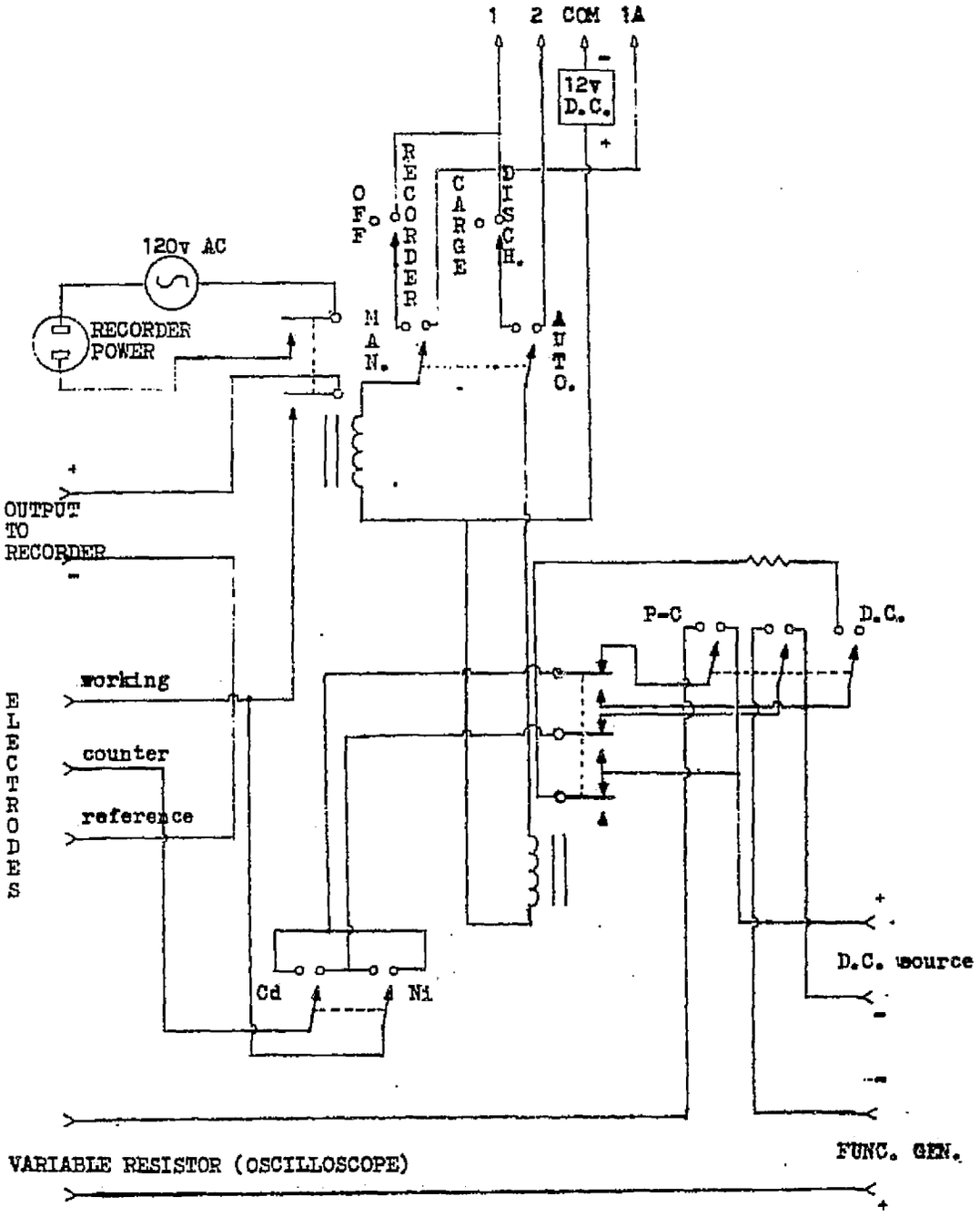

Figure A5. b) Schematic diagram of the electronic circuit used for the Operations Control unit

Appendix 3

Reduction of Concentration Overpotential by Pulsed Current Electrolysis with the Ferro-Ferricyanide System

From d-c experiments, the value of the potential of the working electrode with respect to the reference was recorded for each applied current at the various rotation speeds. Results are summarized in Tables A6 - A11 and graphically represented in Fig. 12. From these tables the value of the overpotential was evaluated from

$$\eta = E_{measured} - E_{rev} \qquad (A15)$$

results are summarized in Tables A6 - A11 and graphically represented in Fig. 13.

The diffusion coefficient can be evaluated from eqn. (24) as presented by Newman:

$$i_L = \frac{0.62048nF\ Sc^{-2/3}\nu^{1/2}\omega^{1/2}C_o}{1 + a\ Sc^{-1/3} + bSc^{-2/3}}$$

let $$0.62048nF\,\nu^{1/2}\,\omega^{1/2}\,Co_L^{-1} = A \qquad (A16)$$

then $$A^{-1} = Sc^{2/3} + a\ Sc^{1/3} + b \qquad (A17)$$

or $$A^{-1} = \left(\frac{\nu}{D}\right)^{2/3} + a\ \left(\frac{\nu}{D}\right)^{1/3} + b \qquad (A18)$$

let $$D^{-1/3} = x \qquad D = x^{-3} \qquad (A19)$$

Table A6

Ferro-ferricyanide system overpotential under d-c conditions and 400 rpm

i mA	i mA/cm^2	η Volts	V Volts
0.05	0.1085	0.0055	0.22
0.10	0.2170	0.0125	0.227
0.15	0.3255	0.0195	0.234
0.20	0.434	0.0285	0.243
0.25	0.5425	0.0375	0.252
0.30	0.651	0.0495	0.264
0.35	0.7595	0.0685	0.283
0.38	0.8246	0.0885	0.303
0.40	0.8681	0.340	0.1255
-0.1	-0.2170	-0.0145	0.200
-0.2	-0.434	-0.0275	0.187
-0.3	-0.651	-0.0445	0.170
-0.35	-0.7595	-0.0595	0.155
-0.40	-0.8681	-0.0775	0.1370

Table A7

Ferro-ferricyanide system overpotential under d-c conditions and 915 rpm

i mA	i mA/cm^2	η Volts	V Volts
0.1	0.217	0.006	0.218
0.2	0.434	0.016	0.228
0.3	0.651	0.027	0.239
0.4	0.8681	0.039	0.251
0.45	0.9765	0.047	0.259
0.50	1.0851	0.060	0.272
0.55	1.1936	0.076	0.288
-0.1	-0.217	-0.011	0.201
-0.2	-0.434	-0.021	0.191
-0.3	-0.651	-0.030	0.182
-0.4	-0.8681	-0.04	0.172
-0.5	-1.0851	-0.053	0.159
-0.6	-1.3021	-0.085	0.127

Table A8

Ferro-ferricyanide system, overpotential under d-c conditions and 1610 rpm

i mA	i mA/cm^2	η Volts	V Volts
0.1	0.217	0.009	0.201
0.2	0.434	0.017	0.209
0.3	0.651	0.024	0.216
0.4	0.8681	0.028	0.220
0.5	1.0851	0.038	0.230
0.6	1.3021	0.048	0.240
0.7	1.5191	0.068	0.260
-0.1	-0.217	-0.004	0.188
-0.2	-0.434	-0.013	0.179
-0.3	-0.651	-0.016	0.176
-0.4	-0.8681	-0.027	0.168
-0.5	-1.0851	-0.032	0.160
-0.6	-1.3021	-0.041	0.151
-0.7	-1.5191	-0.055	0.137

Table A9

Ferro-ferricyanide system, overpotential under d-c conditions and 2500 rpm

i mA	i mA/cm^2	η Volts	V Volts
0.1	0.217	0.01	0.200
0.2	0.434	0.015	0.205
0.3	0.651	0.025	0.215
0.4	0.8681	0.032	0.222
0.5	1.0851	0.040	0.230
0.6	1.3021	0.044	0.234
0.7	1.5191	0.052	0.242
0.8	1.7361	0.063	0.253
0.9	1.9531	0.081	0.271
-0.1	-0.217	-0.005	0.185
-0.2	-0.434	-0.009	0.181
-0.3	-0.651	-0.011	0.179
-0.4	-0.9765	-0.013	0.177
-0.5	-1.0851	-0.015	0.175
-0.6	-1.3021	-0.021	0.169
-0.7	-1.5191	-0.03	0.160
-0.8	-1.7361	-0.04	0.150
-0.9	-1.9531	-0.059	0.131

Table A10

Ferro-ferricyanide system, overpotential under d-c conditions and 3600 rpm

i mA	i mA/cm^2	η Volts	V Volts
0.5	1.0851	0.026	0.233
0.9	1.9531	0.054	0.261
1.0	2.1701	0.063	0.270
1.1	2.3871	0.084	0.291
1.2	2.6042	0.134	0.341
-0.1	-0.217	-0.002	0.205
-0.2	-0.434	-0.007	0.200
-0.5	-1.0851	-0.021	0.186
-1.0	-2.1701	-0.060	0.147
-1.1	-2.3871	-0.062	0.145
-1.2	-2.6042	-0.073	0.134

Table A11

Ferro-ferricyanide system, overpotential under d-c conditions and 4950 rpm

i mA	i mA/cm^2	η Volts	V Volts
0.5	1.0851	0.021	0.236
1.0	2.1701	0.049	0.264
1.4	3.0382	0.145	0.360
-0.5	-1.0851	-0.019	0.196
-1.0	-2.1701	-0.042	0.173
-1.5	-3.2552	-0.092	0.123

Substituting in eqn. (A18)

$$A^{-1} = \nu^{2/3} x^2 + a \nu^{1/3} x + b \qquad \text{(A20)}$$

Solving the quadratic equation for x

$$x = - \frac{a\nu^{1/3}}{2\nu^{2/3}} + \frac{\nu^{1/3}}{\nu^{2/3}} \left[\frac{a^2}{4} - (b - A^{-1}) \right]^{1/2} \qquad \text{(A21)}$$

or

$$D = \nu \left[- \frac{a}{2} + \left(\frac{a^2}{4} - b + A^{-1} \right)^{1/2} \right]^{-3} \qquad \text{(A22)}$$

where $a = 0.298$

and

$b = 0.14514$

From Table 10 and eqns. (A16) and (A22) the value of D for each rotation speed was calculated for both the anodic and cathodic reactions, results are summarized in Table 11.

The diffusion coefficient can also be calculated from a plot of i_L vs. $\omega^{1/2}$. From eqn. (24), the slope of this line is represented by

$$\text{Slope} = \frac{0.62048\ n\ F\ Sc^{-2/3}\ \nu^{1/2}\ C_o}{1 + a Sc^{-1/3} + b Sc^{-2/3}} \qquad \text{(A23)}$$

or $$\frac{0.0179629}{\text{Slope}} = Sc^{2/3} + a\ Sc^{1/3} + b \qquad \text{(A24)}$$

Approaching the solution of this equation as for eqn. (A17) the diffusion coefficient is given by:

$$D = 0.01\ [-0.149 + (\frac{0.0179629}{\text{Slope}} - 0.122939)^{1/2}]^{-3} \qquad \text{(A25)}$$

From Fig. 14, the slopes of the oxidation and reduction reactions were found to be 0.1364×10^{-3} and 0.1556×10^{-3} respectively. Substituting these values in eqn. (A25)

$$(D_{ox})_{slope} = 6.8912 \times 10^{-6} \text{cm}^2/\text{sec}$$

$$(D_{red})_{slope} = 8.4206 \times 10^{-6} \text{cm}^2/\text{sec}$$

To evaluate the exchange current density the following derivations are performed.

$$i = i_o \frac{i_{L_A} - i}{i_{L_A}} \exp[\frac{\alpha nF}{RT}\eta] - \frac{i_{L_C} - i}{i_{L_C}} \exp[\frac{-(1-\alpha)nF}{RT}\eta] \qquad \text{(A26)}$$

expanding the exponential in terms of Taylor series up to the third term (good approximation since η is very small)

$$i = i_o [(\frac{i_{L_A} - i}{i_{L_A}})[1 + \frac{\alpha nF}{RT}\eta + \frac{1}{2}(\frac{\alpha nF}{RT}\eta)^2] - (\frac{i_{L_C} - i}{i_{L_C}}) [1 - \frac{(1-\alpha)nF}{RT}\eta + \frac{1}{2}(\frac{(1-\alpha)nF}{RT}\eta)]] \qquad \text{(A27)}$$

Rearranging eqn. (A27) becomes

$$i = i_o [\frac{nF}{RT}\eta + \frac{(2\alpha-1)}{2}(\frac{nF}{RT})^2\eta^2 + (\frac{i}{i_{L_A}} - \frac{i}{i_{L_C}})(1 + \frac{\alpha nF}{RT}\eta) - \frac{i}{2i_{L_A}}(\frac{\alpha nF}{RT})^2\eta^2 + \frac{i}{i_{L_C}}(\frac{nF}{RT}\eta + \frac{1}{2}(\frac{(1-\alpha)nF}{RT})^2\eta^2)] \qquad \text{(A28)}$$

Differentiating eqn. (A28) with respect to η as $\eta \to 0$, thus $i \to 0$ the following is obtained

$$\left(\frac{di}{d\eta}\right)_{\eta\to 0} = i_o\left(\frac{nF}{RT} + \frac{i_{LA} - i_{LC}}{i_{LA} i_{LC}} \left(\frac{di}{d\eta}\right)_{\eta\to 0}\right) \qquad \text{(A29)}$$

$$\text{or} \quad i_o = \frac{\left(\frac{di}{d\eta}\right)_{\eta\to o}}{\frac{nF}{RT} + \left(\frac{1}{i_{LC}} - \frac{1}{i_{LA}}\right)\left(\frac{di}{d\eta}\right)_{\eta\to 0}} \qquad \text{(A30)}$$

From Fig. 13, Table 10, and eqn. (A30) the values of i_o were evaluated at each rotation speed, and are tabulated in Table 12. The average value of the exchange current density was thus obtained to be $i_{o\ Avg.} = 5.733 \quad mA/cm^2$

To determine the value of the activation overpotential calculations were performed based on

$$i = i_o\left(\frac{nF}{RT}\eta_a\right) \qquad \text{(A31)}$$

The values of i were calculated for arbitrary values of η_a using $i_o = 5.733 \quad mA/cm^2$. Results are summarized in Table A12 and graphically represented in Fig. 13. From Fig. 13 it follows that the experimental conditions used so far are within the limits of mass transfer controlled region. In addition the values of η_c at a given current and rotation speed can be evaluated from

$$\eta = \eta_c + \eta_a \qquad \text{(A32)}$$

Table A12

Activation overpotential for the ferro-ferricyanide system calculated from eqn. (A31) and exchange current density of 5.733 mA/cm^2

η_a Volts	i mA/cm^2
0.01	2.233
0.02	4.466
0.03	6.700
0.04	8.933
0.05	11.166
0.07	15.632
0.09	20.098
0.11	24.565

The transfer coefficient can be evaluated from

$$i = i_o \left[\exp\left(\frac{\alpha nF}{RT}\eta\right) - \exp\left(-\frac{(1-\alpha)nF}{RT}\eta\right)\right] \qquad (A33)$$

rearranging

$$i = i_o \left(\exp\frac{\alpha nF}{RT}\eta\right) \left[1 - \exp\left(-\frac{nF}{RT}\eta\right)\right] \qquad (A34)$$

taking the natural logarithm of eqn. (A34)

$$\ln i = \ln i_o + \ln\left[1 - \exp\left(-\frac{nF}{RT}\eta\right)\right] + \frac{\alpha nF}{RT}\eta \qquad (A35)$$

or

$$\ln \frac{i}{1-\exp\left(-\frac{nF}{RT}\eta\right)} = \ln i_o + \frac{\alpha nF}{RT}\eta \qquad (A36)$$

From eqn. (A36), a plot of $\ln \dfrac{i}{1 - \exp\left(-\frac{nF}{RT}\eta\right)}$ vs. η

will give a straight line with a slope of $\frac{\alpha nF}{RT}$, from which the value of α can be calculated. From Fig. 13, the values of $\ln \dfrac{i}{1 - \exp\left(-\frac{nF}{RT}\eta\right)}$ were calculated for 400 rpm.

Results are summarized in Table A13 and Fig. 15.
From Fig. 15, the slopes of the amodic and cathodic reactions were found to be 6.1224 and 31.6279 respectively.
The transfer coefficients were then calculated from

$$\alpha = \frac{\text{Slope}}{\left(\frac{nF}{RT}\right)} \qquad (A37)$$

and were found to be $\alpha_A = 0.1572$ and $\alpha_C = 0.8119$.

Table A13

Values of $\ln \frac{i}{1-\exp(-\frac{nF}{RT}\eta)}$ for the ferro-ferricyanide system at 400 rpm

	i mA/cm^2	η Volts	$\frac{i}{1-\exp(-\frac{nF}{RT}\eta)}$	$\ln \frac{i}{1-\exp(-\frac{nF}{RT}\eta)}$
Anodic	0.1085	0.0055	0.56261	-0.5751
	0.2170	0.0125	0.5629	-0.5746
	0.434	0.0285	0.6473	-0.435
	0.651	0.0495	0.7618	-0.2721
	0.8246	0.0885	0.8517	-0.1605
	0.8681	0.340	0.8681	-0.1414
Cathodic	-0.2170	-0.0145	0.28584	-1.2523
	-0.434	-0.0275	0.2262	-1.4865
	-0.651	-0.0445	0.1397	-1.9683
	-0.7595	-0.0595	0.08298	-2.4892
	-0.8681	-0.0775	0.04459	-3.1103

From the experimental data obtained under d-c electrolysis, the conditions for p-c electrolysis were determined in the following manner. First the thickness of the diffusion layer was evaluated at each rotation speed from

$$\delta = \frac{DCnF}{i_L} \tag{A38}$$

Substituting for i_L with eqn. (24)

$$\delta = \frac{[1 + a\,Sc^{-1/3} + b\,Sc^{-2/3}]D}{0.62048\,Sc^{-2/3}\,\nu^{1/2}\,\omega^{1/2}} \tag{A39}$$

The values of δ thus obtained were then used for calculating a from

$$a = \frac{\pi^2 D}{4\delta^2}$$

The values of a were used for evaluating θ such that $a\theta = 0.5$ (A40). Table A14 summarizes δ and θ at each rotation speed.

For p-c electrolysis duty cycle and instantaneous current density were chosen to be such that

$\frac{\theta_1}{\theta}$ = 0.2, 0.4, 0.6, 0.8 and

$\frac{i_p}{(i_{d-c})_L}$ = 0.2, 0.4, 0.6, 0.8. Based on these and on Table A14, the experimental conditions were determined and summarized in Table 1.

Table A14

Values of the diffusion layer thickness and cycle time for the ferro-ferricyanide system at six rotation speeds

	ω rpm	ω-1/2 (rad/sec) 1/2	δ cm	a	θ m sec
Anodic D=6.8912 * 10^{-6} cm^2/sec	400	6.4721	$2.2599 * 10^{-3}$	3.3293	150
	915	9.7887	$1.4942 * 10^{-3}$	7.6158	65.6
	1610	12.9846	$1.1264 * 10^{-3}$	13.4014	37.3
	2500	16.1802	$0.90397 * 10^{-3}$	20.8078	24.03
	3600	19.4163	$0.75331 * 10^{-3}$	29.9631	16.69
	4950	22.7676	$0.64243 * 10^{-3}$	41.1986	12.14
Cathodic D=8.4206 * 10^{-6} cm^2/sec	400	6.4721	$2.4207 * 10^{-3}$	3.5457	141
	915	9.7887	$1.6005 * 10^{-3}$	8.1109	61.6
	1610	12.9846	$1.2066 * 10^{-3}$	14.27106	35.04
	2500	16.1802	$0.96828 * 10^{-3}$	22.1606	22.56
	3600	19.4163	$0.80689 * 10^{-3}$	31.9120	15.67
	4950	22.7676	$0.68813 * 10^{-3}$	43.8775	11.40

Appendix 4

Ni-electrode

Appendix 4A - Thermodynamics

The mean ionic activity coefficient for KOH was evaluated from an expression derived by Akerlof and Bader

(2) $$\log \gamma\pm = \frac{u\sqrt{m}}{1+\sqrt{2m}} + Bm + Cm^2 + Dm^3 + Em^4 \qquad (A41)$$

where

$$B = 6.629 \times 10^{-2} + 6.135 \times 10^{-4}t - 1.1018 \times 10^{-5}t^2 + 4.096 \times 10^{-8}t^3 \qquad (A42)$$

$$C = 1.0909 \times 10^{-2} - 1.7108 \times 10^{-4}t + 1.6895 \times 10^{-6}t^2 - 7.969 \times 10^{-9}t^3 \qquad (A43)$$

$$D = -7.351 \times 10^{-4} + 9.973 \times 10^{-6}t - 9.347 \times 10^{-8}t^2 + 6.215 \times 10^{-10}t^3 \qquad (A44)$$

$$E = 1.5502 \times 10^{-5} - 1.980 \times 10^{-7}t + 1.8424 \times 10^{-9}t^2 - 1.764 \times 10^{-11}t^3 \qquad (A45)$$

$u = 0.506$ @ $T = 25°C$

and $m = 6.548$ for a 6.0M KOH solution

Solving these equations $\gamma\pm = 0.983046$

then a_{KOH} was calculated from eqn. (42)
and found to be 41.434778.

In order to calculate a_{H_2O}, the following was derived.

From the Gibbs-Duhem equation

$$N_{KOH} d\ln a_{KOH} = - N_{H_2O} d\ln a_{H_2O} \quad (A46)$$

$$d \ln a_{KOH} = - \frac{N_{H_2O}}{N_{KOH}} d \ln a_{H_2O} \quad (A47)$$

but $$\frac{N_{H_2O} \times M.W._{H_2O}}{N_{KOH} \times 1000} = \frac{1}{m} \quad (A48)$$

then $$d \ln a_{KOH} = - \frac{1000}{m \times M.W_{H_2O}} d \ln a_{H_2O}$$

or $$d \ln a_{KOH} = - \frac{55.50825}{m} d \ln a_{H_2O}$$

$$d \ln a_{H_2O} = - \frac{m}{55.50825} d \ln a_{KOH} \quad (A49)$$

Therefore a numerical integration of the above eqn. (A49) will give the value of $\ln a_{H_2O}$. Choosing limits of integration between m = 0.01 where $a_{H_2O} = 1$ and m = 6.548, value of $\ln a_{KOH}$ were obtained for various m within the above range and are given in Table A15. From this table a plot of $\frac{m}{55.5082}$ vs. $\ln a_{KOH}$ was prepared as shown in Fig. A6. This curve was numerically integrated by using the Simpson rule with 10 intervals. The activity of water thus calculated was found to be $a_{H_2O} = 1.041258$.

Table A15

Values of the activity coefficient and the activity of KOH solution for various molal concentrations

m	$\frac{m}{55.50825}$	$\gamma\pm$	a_{KOH}	$\ln a_{KOH}$
0.01	0.00018	0.91035	0.00083	-9.3982
1	0.018015	1.133745	1.285378	0.251023
2	0.036031	1.396635	7.802357	2.054426
3	0.054046	1.426685	18.318871	2.907932
4	0.07206	1.305193	27.25646	3.305291
5	0.090077	1.147734	32.9323	3.494455
6	0.108092	1.024793	37.80722	3.6325
6.548	0.11796	0.983046	41.434778	3.7241

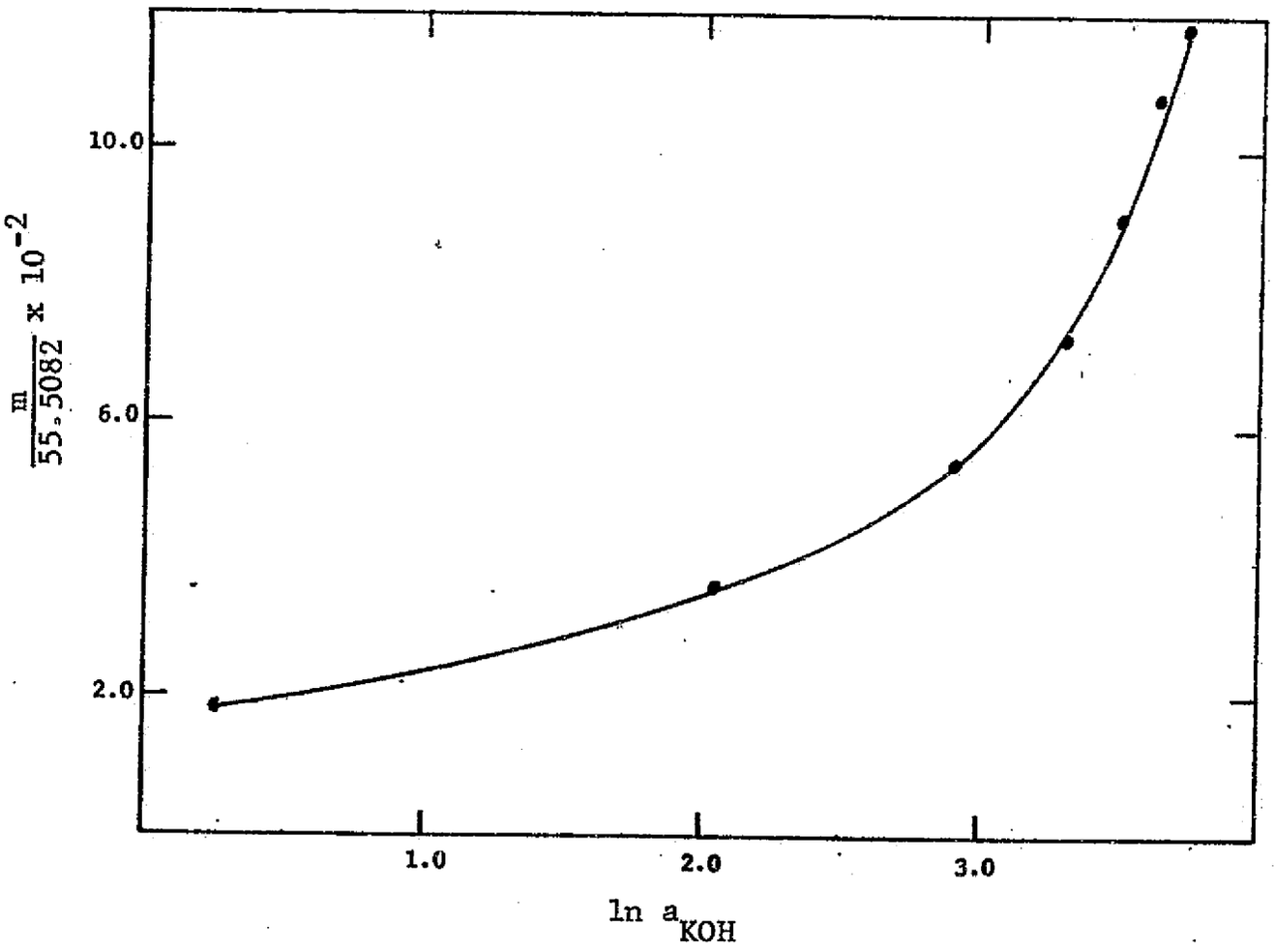

Figure A6. A plot used for evaluating the activity of H_2O in a 6.0 M KOH solution

Substituting the values of a_{H_2O} and a_{KOH} in eqn. (6), the reversible electrode potential was calculated.

$$E_r = 0.3874 \text{ V}$$

Appendix 4B

From eqn. (25) the value of the diffusion coefficient can be evaluated from the slope of a plot of i_p vs. $v^{1/2}$. For both the anodic and cathodic reactions the variation of i_p with $v^{1/2}$ is graphically represented in Fig. A7. From this figure the slopes for the anodic and cathodic reactions were evaluated and found to be 0.207 and 0.420 respectively. The diffusion coefficients were then calculated from

$$D = \frac{\text{Slope}}{A\, C_o \times 2.7 \times 10^5} \qquad \text{(A50)}$$

where $C_o = \frac{\rho}{M.W}$,

$$\rho = 2.5 \text{ gm/cm}^3$$

and

$$M.W = 104.71 \text{ gm/mole}$$

both the density and molecular weight of $\alpha - Ni(OH)_2$ were used. The values of the diffusion coefficients were calculated in the above given manner and resulted in $D_{ox} = 5.28 \times 10^{-10} \text{cm}^2/\text{sec}$ and $D_{red} = 2.16 \times 10^{-9} \text{cm}^2/\text{sec}$.

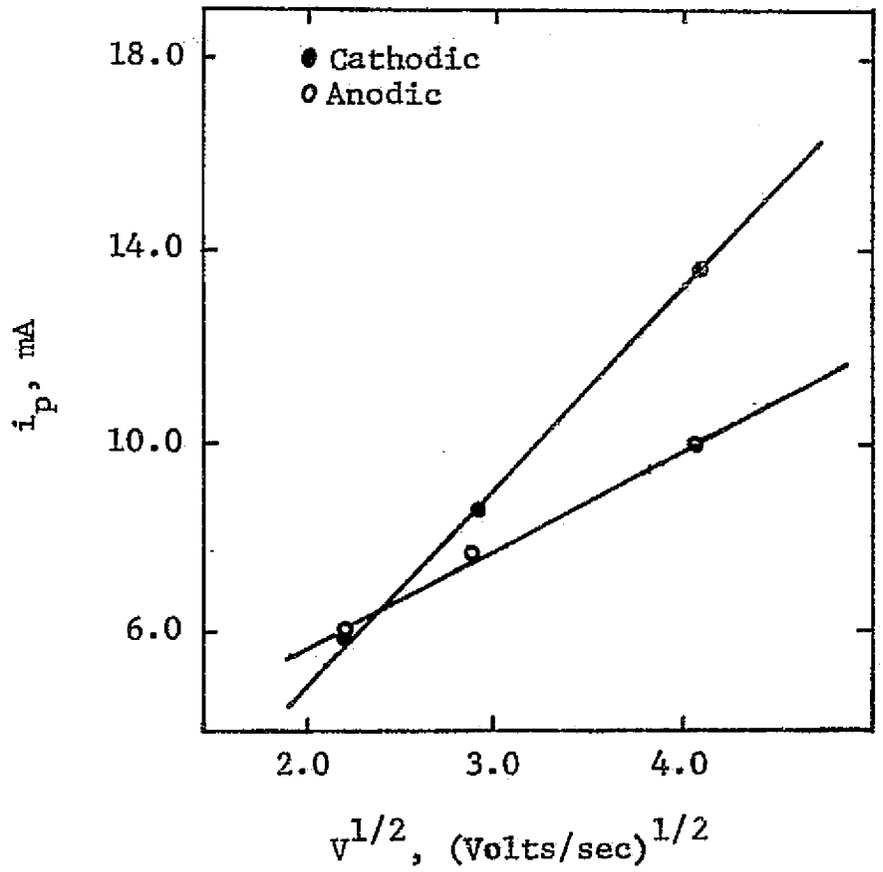

Figure A7. A plot of i_p vs. $V^{1/2}$ for the Ni-electrode

From eqn. (27), the Taffel slope can be evaluated from the slope of a plot of E_p vs. log V. The value of the Taffel slope can further be used for calculating the transfer coefficients. From Fig. 22 a plot of E_p vs. log V for both the anodic and cathodic reactions was prepared as shown in Fig. A8. The slopes of the lines for the oxidation and reduction reactions were found to be 0.0607 and - 0.01654 respectively. The Taffel slopes were calculated from b_{ox} = slope x 2 = 0.1214 and b_{red} = - slope x 2 = 0.03308. The transfer coefficients were then evaluated from

$$\alpha = 2.303 \frac{RT}{nFb} \qquad \text{(A51)}$$

and resulted in $\alpha_{ox} = 0.49$ and $\alpha_{red} = 1.70$

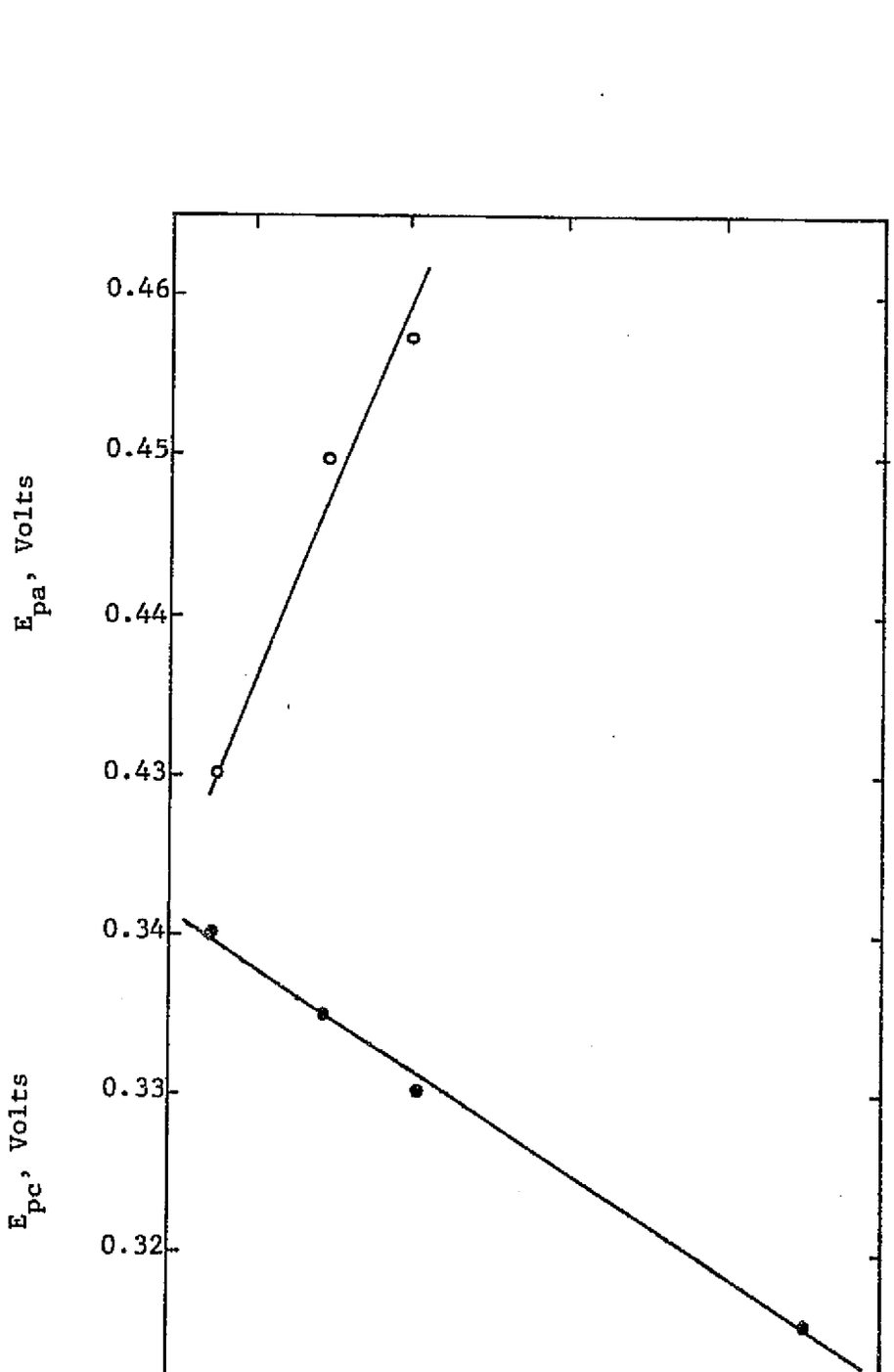

Figure A8. A plot of E_p vs. log V for the Ni-electrode

Appendix 5

Cd-electrode

The diffusion coefficient of Cd^{++} through the solid CdO phase was evaluated for both the reduction and oxidation reactions from eqn. (25). Where C_o was calculated from

$C = \frac{\rho CdO}{M.W_{CdO}}$. Assuming CdO to appear in amorphous form,

$\rho_{CdO} = 6.95$ gm/cm^2 and M.W. = 128.41 gm/mole

then $D_{ox} = 3.81 \times 10^{-10}$ cm^2/sec and

$D_{red} = 1.82 \times 10^{-10}$ cm^2/sec.

APPENDIX 6

Definition of Terms from the Battery Field Used in the Present Work

Sintered Plate	porous, sintered plaque into which the active material is impregnated
Pocket Electrode	nickel-plated, cold-rolled, perforated steel ribbon, whose pockets are filled with active material
Film Electrode	the active material is electrolitically precipitated on the surface of a thin metal sheet
Faded Cell	a cell which can not meet the minimum capacity requirements after recharge
Degradation Effect	loss of capacity
Memory Effect	after successive cycles of constant shallow depth of discharge, the cell assumes the demanded capacity, thus loses all of its extra capacity
Charge Efficiency	a ratio between the Ahr applied to the cell during charge and the Ahr obtained from the cell on discharge
Duty Cycle	a ratio between the duration of the on period of a pulse and the duration of one complete cycle of a pulsed current

NOMENCLATURE

A	area
a	a diffusion parameter, $a = \pi^2 D/4\delta^2$
a_{KOH}	activity of KOH electrolyte
a_{H_2O}	activity of water
b	Tafel slope
C	concentration
C_i	concentration of the reacting species at the electrode-solution interface
C_o	concentration of the reacting species in the bulk of the solution
D	diffusion coefficient
E	electrode potential
$E_{1/2}$	half-wave potential
E_o	standard electrode potential
E_r	reversible electrode potential
F	Faraday's constant
i	current
i_o	exchange current density
i_p	instantaneous pulsed current
k	reaction rate constant
M.W.	molecular weight
m	molality
N	number of cycles of current already passed
n	number of electrons transfered in an electrochemical reaction

Q_1	fraction of charge accumulated during the eight cycle, assuming current efficiency for oxidation of Ni to be 0% after gas evolution begins
Q_2	fraction of charge accumulated during the eight cycle, assuming current efficiency for oxidation of Ni to be 50% after gas evolution begins
R	gas constant
Sc	Schmidt number
T	temperature
t	time
V	sweep rate
α	transfer coefficient
$\gamma\pm$	mean activity coefficient
δ	diffusion layer thickness
ν	kinematic viscosity of a solution
ω	rotation speed
θ	duration of one complete cycle
θ_1	duration of the on period of a pulse
θ_2	duration of the off period of a pulse
τ	a time parameter
η	overpotential
η_a	activation overpotential
η_c	concentration overpotential
$(\eta_p)_c$	concentration overpotential under p-c conditions
$(\eta_{d-c})_c$	concentration overpotential under d-c conditions

Subscripts:	A,a	anodic
	C,c	cathodic
	a	activation
	L	limiting
	p	peak